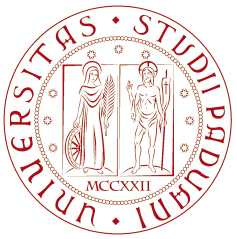

Università degli Studi di Padova

Department of Information Engineering

University of Padova

Aalto University
School of Engineering

Master's Degree in Engineering of Automation

Master's Thesis

Position Control and Overall Efficiency of Electro-Hydraulic System

Author: Carlo Bonato

Supervisor: Prof. Matti Juhala
Advisor: Prof. Alessandro Beghi
Instructor: D.Sc. Tatiana Minav

07/04/2014

Abstract

In this thesis a novel approach to electro-hydraulic systems is investigated from both position control and efficiency point of view. The Direct Driven Hydraulic (DDH) approach consists in employing a servo motor to directly control the pump speed, implementing flow control without the usage of conventional valves. The main advantages of this technique are: compactness and theoretical higher efficiency; smoothness and precision of the movements; potential energy regeneration; sensorless approach.

The research process begins with modelling of the electro-hydraulic system. The pumps leakage flow is also modelled and the model parameters are identified by means of dedicated empirical measurements. For the sensorless approach, a pressure estimation function is implemented. Practical tests are carried out for analysing control precision and evaluating efficiency of single components and overall system. Possible potential energy recovery is discussed.

The thesis work reveals the possibility of a considerable control precision, in the scope of mobile working machines applications. Moreover the leakage flow prediction proves to be precise, while the pressure estimation functions needs to be improved in case of highly variable payload. The efficiency evaluation is strongly affected by pump dimensioning error, nonetheless the results remain comparable to the ones of a common hydraulic system. This outcome confirms the chance of improving efficiency with proper sizing.

Based on the results, a rule for the system design is obtained, further studies on the pressure estimation function are recommended. Efficiency tests with more accurately dimensioned system are suggested.

Keywords

direct driven hydraulics (DDH), drive, efficiency, hydraulics, leakage model, non-road mobile machinery (NRMM), position control, servomotor.

Abstract

Nella presente tesi viene studiato un approccio innovativo ai sistemi elettro-idraulici, in merito sia al controllo di posizione sia all'efficienza. L'approccio Direct Driven Hydraulics (DDH) consiste nell'utilizzo di un motore servo per il controllo diretto della velocità di rotazione delle pompe idrauliche, in modo da realizzare controllo di flusso senza l'impiego delle classiche valvole. I principali vantaggi di questa strategia sono: dimensione ridotta e maggiore efficienza teorica; fluidità e precisione dei movimenti; rigenerazione dell'energia potenziale; approccio sensorless.

Il processo di ricerca inizia con la modellizzazione del sistema elettro-idraulico. Il flusso delle perdite nelle pompe viene inoltre modellizzato e i parametri del modello vengono identificati per mezzo di un esperimento dedicato. Al fine di realizzare la strategia sensorless, una funzione di stima della pressione è definita. Per valutare la precisione del controllo e l'efficienza dei singoli componenti e del sistema globale, specifiche misurazioni vengono svolte. L'eventuale recupero di energia potenziale viene discusso.

Il lavoro di tesi dimostra la possibilità di ottenere considerevole precisione, nell'ambito delle macchine da lavoro mobili. Inoltre la predizione del flusso delle perdite si dimostra affidabile, mentre la funzione di stima della pressione necessita di ulteriore raffinamento nel caso di carico rapidamente variabile. L'efficienza misurata è influenzata da un errore di dimensionamento delle pompe, tuttavia i risultati sono comparabili con quelli ottenibili in un sistema idraulico convenzionale. Ciò conferma la possibilità di ottenere elevata efficienza tramite accurato dimensionamento.

Basandosi sui risultati, si ricava una regola di progetto per sistemi DDH. Si raccomandano ulteriori approfondimenti sulla funzione di stima della pressione. Si suggeriscono test di efficienza impiegando un sitema dimensionato più accuratamente.

Parole chiave

controllo di posizione, direct driven hydraulics (DDH), drive, efficienza, idraulica, modello delle perdite, motore servo, non-road mobile machinery (NRMM).

Acknowledgements

The intention of summing up a quarter of a century in a single page is doomed to fail, especially when the feeling is to have received much more than what was given. Thus, I beg for pardon to everyone who will be left out.

I would like to thank my team in Aalto University, particularly: my supervisor Prof. Matti Juhala for his constant willingness; Eng. Panu Sainio for giving me the chance to use his laboratory and to get plenty of ideas from our talks; my advisor D.Sc. Tatiana Minav for the priceless help and assistance which she dedicated me every single day during the thesis process; Eng. Antti Sinkkonen for, too often, sorting out my problems and giving me a different point of view about hydraulics issues. From the Italian side, I truly appreciate the support of my supervisor, Prof. Alessandro Beghi, for his availability for any issue related to thesis work and deadlines.

Precious thanks go to my office mates Arto, Antti, Juha and Lauri for all the answers and the ideas, for the nice times we shared together, for letting me get to know what Finnish culture is and, especially, for the chicken.

I manifest my sincere thankfulness to both my EILC and erasmus groups, for sharing the exciting and the difficult moments, for becoming my family and for letting me understand that no-one is ever alone. In particular I thank my friends Libor, Nico, Nicola and Ruben and my flatmates, Ignacio and Tammo, because they made the difference between a stay and a life.

A lot of people indelibly marked my university life. All my gratitude goes to my fellows Marco and Federico for everything we shared, to Cristian for teaching me the dedication and a many other things, to Giovanni for the constance with which he endured my company, to Alessandro, Alessandro, Fabiano and Stefano for their daily commitment to build the amazing *ST*. Thanks to my flatmates Simone, Marco, Roberto and Omar for all the unforgettable moments. Thanks to my dear Alice, I am glad to have shared part of this journey with you; all we had, will always remain.

Intimate thanks to Alessandro, Filippo, Irene, Veronica and Lucio, who made bearable the way to maturity. The *tripod* does not fall down.

I am very thankful to my lifetime friends from my Negrisia, together we grew. Especially Veronica, you were always able to find a *shrimp* way out from any life issue; the members of the thriving company *Officine C.C.*: Gabriele, Eros and Marco, examples of stable unbiased authentic friendship.

I am extravagantly grateful to my dearest Magdaléna, for unveiling each day a new step in my staircase to happiness. Let us climb it hand in hand.

At last, I want to express my deep gratitude to my whole family. My relatives have always been a source of disinterested love, a shining example of family life and a model to follow. My parents, Marina and Pio, have always educated, supported and pushed me into the right direction. Try to take this work as an evidence of all the good you have done to me. My siblings Ariel and Gioele, have often given me a reason to smile and work every day. My beloved brother Leo, my model and my best friend. Your life is my life.

CARLO BONATO

Contents

Nomenclature

Latin Alphabet

A_1	area of the piston head 1	m^2
A_2	area of the piston head 2	m^2
A_c	piston head area	m^2
A_r	area occupied by the piston rod on the piston head 2	m^2
A_{sec}	area of a boom section	m^2
B_1	arm of the application point of the first segment's mass force	m
B_2	arm of the application point of the second segment's mass force	m
B_c	arm of the application point of the piston force	m
B_d	viscous damping coefficient of the pump	$(N \cdot s)/m$
B_l	arm of the application point of the load's mass force	m
B_v	viscous damping coefficient of the load	$(N \cdot s)/m$
C_{ec}	external leakage coefficient of the cylinder	$m^3/s/Pa$
C_{ep}	external leakage coefficient	$m^3/s/Pa$
C_f	internal friction coefficient	$-$
C_{ic}	internal or cross-port leakage coefficient of the cylinder	$m^3/s/Pa$
C_{ip}	internal leakage coefficient	$m^3/s/Pa$
C_s	slip coefficient	$m^3/s/Pa$
$C_{s,i}$	reduced slip coefficient	$-$
d_1	diameter of the piston head 1	m
D_1	displacement of pump 1	cm^3/rev
d_2	diameter of the piston head 2	m
D_2	displacement of pump 2	cm^3/rev
D_p	volumetric displacement of a pump	m^3/rad
d_r	diameter of the piston rod	m
E_{avg}	average position error during the cycle	cm

$E^{\%}_{\text{avg}}$	average percent position error, compared to the piston full stroke	%
E_{fin}	final position error at the end of cycle	cm
$E^{\%}_{\text{fin}}$	final percent position error, compared to the piston full stroke	%
E_{ele}	electric energy at motor terminals	J
$E_{\text{h,1,f}}$	hydraulic energy in line 1, in free-fall condition and measurement condition	J
$E_{\text{h,1,m}}$	hydraulic energy in line 1, in measurement condition	J
$E_{\text{h,1}}$	hydraulic energy in line 1	J
$E_{\text{h,2}}$	hydraulic energy in line 2	J
E_{load}	mechanical energy imparted to the load in order to overcome the free-fall speed	J
F_a	arbitrary additional force on piston	N
F_{b1}	force generated by the second segment's mass	N
F_{b2}	force generated by the first segment's mass	N
F_c	force generated on the load at the piston's rod	N
F_c	force generated or developed by the piston	N
$F_{\text{c,avg}}$	average force acting on the piston during the motion	N
F_g	force generated or developed by the piston	N
F_l	force generated by the load's mass	N
g	gravitational constant	$N(m/kg)^2$
h	height of the crane from basement to joint	m
$I_1,\ I_2,\ I_3$	phase currents	A
K_c	current scaling factor for the drive	A
K_e	voltage constant of the electric motor	V/rpm
K_l	load spring gradient	N/m
K_t	torque constant of the electric motor	Nm/A
l	length of the crane's boom	m
m	mass of a single weight	kg
m_{b1}	mass of the first boom segment	kg
m_{b2}	mass of the second boom segment	kg
m_{ch}	mass of the supporting chain	kg
m_h	mass of the weights holder	kg

m_l	total mass of the payload	kg
m_t	total mass of the load referred to piston	kg
p_1	pressure in pump forward chamber	pA
p_2	pressure in pump return chamber	pA
p_L	pressure difference across the pump lines	pA
$p_{1,\mathrm{f}}$	pressure in line 1, in free-fall condition	pA
$p_{1,\mathrm{m}}$	pressure in line 1, in measurement condition	pA
$p_{\mathrm{c,avg}}$	average pressure in chamber 1 during the motion	pA
$P_{\mathrm{h},1}$	hydraulic power in line 1	W
$P_{\mathrm{h},2}$	hydraulic power in line 2	W
P_{hyd}	hydraulic power delivered by the pump	W
P_{load}	work performed by the additional force only, on the load.	
p_{max}	pressure obtained in maximum torque condition	pA
P_{mec}	mechanical power at the pump/motor shaft	W
P_{out}	power output of the cylinder, i.e. power acting on the load	W
P_{pot}	work performed by the gravitational force only, on the load	W
$P_{\mathrm{pot+load}}$	work performed by the sum of gravitational force and additional force, on the load	W
$Q_{1,\mathrm{f}}$	flow in line 1, in free-fall condition	m^3/s
$Q_{1,\mathrm{m}}$	flow in line 1, in measurement condition	m^3/s
Q_1	forward flow to pump	m^3/s
Q_2	return flow from pump	m^3/s
Q_{ec}	cylinder external leakage flow	m^3/s
Q_{ep}	externbal leakage flow	m^3/s
Q_{ic}	cylinder internal leakage flow	m^3/s
Q_{ip}	internal leakage flow	m^3/s
Q_L	flow through the pump = input flow of the cylinder	m^3/s
Q_L	load flow of a pump	m^3/s
Q_s	slip flow (total leakage flow)	m^3/s
R_1	resistance of voltage divider resistor 1	Ω
R_2	resistance of voltage divider resistor 2	Ω
R_A	ratio between the piston head areas	$-$
R_D	displacement ratio between the pumps	$-$
s_p	stroke of the piston	m

s_{rpm}	speed reading of the drive	rpm
T_d	damping torque of the pump	Nm
t_f	free-fall time	s
T_f	friction torque of the pump	Nm
T_{fs}	full-swing of torque scale for the drive	Nm
t_m	measured time	s
T_m	torque at the motor shaft	Nm
T_{Nm}	torque reading of the drive	Nm
T_p	torque at the pump shaft	Nm
T_p	torque at the pump shaft	Nm
T_s	seal torque	N
V_{boom}	volume of the boom	m^3
$V_{\text{in,d}}$	voltage input of the voltage divider	V
$V_{\text{out,d}}$	voltage output of the voltage divider	V
$V_{\text{out,speed}}$	voltage output of the speed signal of the drive	V
$V_{\text{out,torque}}$	voltage output of the torque signal of the drive	V
V_{01}	initial volume of cylinder's forward chamber	m^3
V_{02}	initial volume of cylinder's return chamber	m^3
V_0	dead volume of a cylinder's chamber	m^3
V_1	volume of cylinder forward chamber	m^3
$V_1,\ V_2,\ V_3$	phase voltages	V
V_2	volume of cylinder return chamber	m^3
V_{IH}	high voltage level of the board's digital inputs	V
V_{IL}	low voltage level of the board's digital inputs	V
$V_{OH,e}$	high voltage level of the encoder signals	V
V_{OH}	high voltage level of the board's digital outputs	V
$V_{OL,e}$	low voltage level of the encoder signals	V
V_{OL}	low voltage level of the board's digital outputs	V
V_c	volume of a cylinder's chamber	m^3
V_h	high threshold voltage of the relays	V
V_l	low threshold voltage of the relays	V
V_r	rated coil voltage of the relays	V
x_0	initial position of the piston	m
x_c	piston position	m
$\dot{x}_c$	velocity of the cylinder's piston	m/s

Greek Alphabet

α, β, γ	angles of boom's joints	$\circ$
β	effective bulk modulus of the system	Pa
$\Delta E_{\mathrm{h,1}}$	hydraulic energy differential in line 1	J
ΔE_{pot}	variation of load potential energy	J
ΔQ_s	slip flow increment rate	m^3/s^2
$\eta_{\mathrm{cyl,down}}$	efficiency of the hydraulic cylinder during lowering	%
$\eta_{\mathrm{cyl,up}}$	efficiency of the hydraulic cylinder during lifting	%
$\eta_{\ \mathrm{gain}}$	product of the efficiencies for the lifting and lowering motion	%
$\eta_{\mathrm{mot,down}}$	efficiency of the electric motor	%
$\eta_{\mathrm{mot,up}}$	efficiency of the electric motor during lifting	%
$\eta_{\mathrm{pumps,down}}$	efficiency of pumps and distribution line during lowering	%
$\eta_{\mathrm{pumps,up}}$	efficiency of pumps and distribution line during lifting	%
$\eta_{\mathrm{tot,down}}$	overall efficiency during lowering	%
$\eta_{\mathrm{tot,up}}$	overall efficiency during lifting	%
μ	absolute viscosity of the fluid	$Pa \cdot s$
ρ	oil density	kg/m^3
ρ_s	mass density of common steel	kg/m^3
$\dot{\theta}_p$	pump shaft speed	rad/s

Abbreviations

NRMM	Non-road mobile machinery
AC	Alternating Current
ADC	Analog to Digital Converter
DC	Direct Current
DDH	Direct Driven Hydraulics
e.g.	exempli gratia
EHS	Electric Hydraulic System
i.e.	id est
I/O	input/output
LMS	Least Mean Squares
NRMM	Non-Road Mobile Machinery
Pr	drive's parameter
PWM	Pulse Width Modulation
RMS	Root Mean Square
rpm	rounds per minute

Chapter 1

Introduction and Literature Review

Non-road mobile working machines (NRMM) are fundamental means of production in modern industry. They are employed in various fields and for different purposes, such as mining, forest harvesting, harbour work, manufacturing and construction. This study concentrates on the investigation of position control, efficiency and application possibilities of a novel approach to NRMM.

The common thread, in all these dissimilar NRMM applications, is the need of high power delivery in a contained space. For this sake, hydraulic actuation has shown to be, and still remains, the most effective choice. One of the strongest features of hydraulics is its straightforward capability of working as a force transformer [1]. The hydraulic power amplification, depending on the cross-sectional areas of the piston, guarantees the possibility to generate very high power factor in reduced spaces [2]. Moreover hydraulic actuators work in a simple manner and can be used to transmit, produce and store fluid power [2]. Actually, they use *nearly incompressible* fluid which results in a greater, more efficient and consistent work or power output [3]. This is due to the fact that hydraulic fluid molecules are able to resist compression under heavy load hence minimal energy loss is experienced and work applied is directly transferred to the actuating surfaces. Moreover, hydraulic fluid operates very well in harsh environments, demanding productive cycles and heavy working applications [2].

Hydraulic systems have disadvantages as well. A higher constructional weight is required in order to guarantee structural integrity in condition

of heavy loads, with addition of side components such as hydraulic lines, reservoirs, filters, valve blocks and so on [4]. Furthermore, hydraulic fluid is susceptible to contaminations and foreign object damage, because of its polluting nature [5],[6]; this turns out also in a health risk for users [7],[8]. Other drawbacks are losses, such as friction and leakage [9] and the protection against rust, corrosion and dirt is required [2]. Even considering these issues, the attempt to produce equal forces by means of magnetic fields has been unfruitful, so far. That because, with magnetic actuation, it would be needed 10-100 times as much axial stress in order to compete with a normal hydraulic system [1]. In practice, hydraulic systems remain the most functional implementation, also for the future [10].

Once the oil hydraulic is chosen for working machines, the power supplying has to be considered. Machinery is often diesel operated, but trends towards diesel-electric hybrid and fully electric operated machines are arising [11]. Some of the issues which push technology in this direction are the constantly growing cost of mineral fuels, the air pollution derived from their employment and efficiency of diesel motors, which is usually sensibly lower than the electric counterpart [12]. For what concerns the environmental awareness, in the latest decades regulations for harmful exhaust gases for diesel powered equipment became more and more strict [13],[14]. In order to improve the efficiency, moreover, energy consumption and regeneration must be considered, especially in heavy working machines [15]. For this reason hybrid technologies are the main trend of industry and research facilities [16].

In this framework, tendency towards clean and compact electro-hydraulic systems, which deliver powerful, linear movement with valve-controlled or pump-controlled implementation, is observed in industry. They aim to fulfil the requirements for small size-to-power ratio, low pollution and energy efficiency, by means of lowering losses and introducing energy recovery [17].

The most widely applied systems are valve - controlled, but they present few relevant drawbacks, such as throttled pressure loss [18], lower efficiency [19], cavitation [19], serious heat generation [2], non-linear modelling complexity [20] and difficult size reduction [20]. In recent investigations the pump-controlled electro-hydraulic servo systems directly driven by servo motor (DDH) have appeared. These systems have the chance to overcome some of the traditional hydraulic systems disadvantages. In the fact, pump-controlled systems appear more compact, more reliability and highly efficient [17].

Various applications of DDH design strategy can be found in recent literature. In [21] the direct drive approach is implemented by means of an electric motor controlling a variable displacement pump. The flow control is handled by a variable displacement pump and an accumulator is used to absorb and buffer the pressure pulses. The actuation system is employed to control an emulsion pump and the energy regeneration capabilities in various working conditions are analysed.

In [22] and [23], direct electric drive control implementations are proposed in order to control a forklift with single-acting cylinder (Fig. 1.1). The results show relevant energy saving capabilities, thanks to the potential energy recovery strategy implemented. Trend toward DDH appears also in the pump innovation analysis carried out in [24], in which the stress is on throttling losses elimination and compactness enhancement.

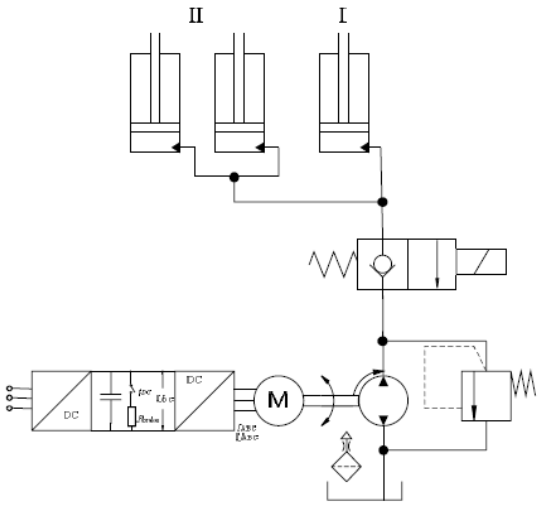

Figure 1.1: Forklift control with DDH [23]

An example of DDH system in which flow control is implemented directly regulating the servo motor speed is found in [25] (Fig. 1.2).

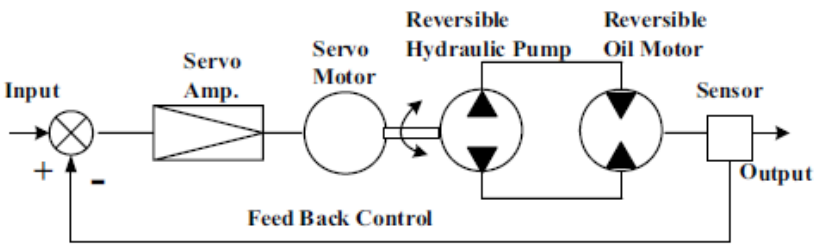

Figure 1.2: Rudder roll stabilization EHS servo control [25]

The article outlines a novel approach to rudder roll stabilization and employs the DDH strategy - actually called *Electric Hydraulic System* (EHS) in the paper - in order to reduce power consumption, size of the system and piping complexity. It turns out in operative noise lowering as well.

The DDH approach, with switched reluctance servo motor, appears again in [26], [27] and [28] (Fig. 1.3), where the system is applied to a hydraulic press.

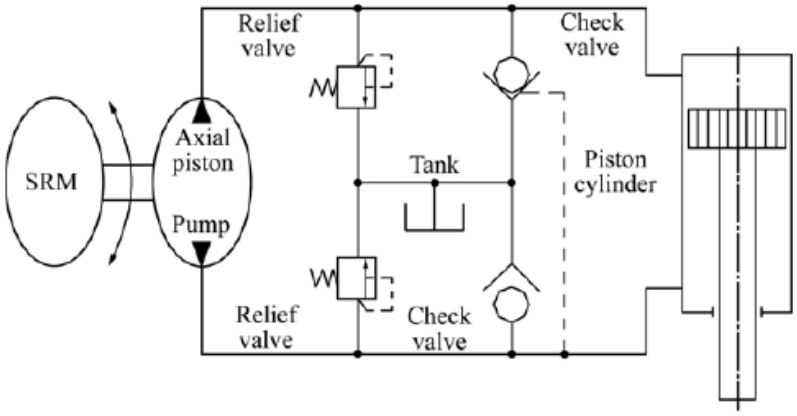

Figure 1.3: Direct drive hydraulic press [26]

Furthermore, taking advantage of the servo motor control, other aims can be achieved. The servo motor control allows wide speed regulation range, high accuracy and smooth movement, since the motor motion profiles could be finely tuned and adjusted depending on the particular system. Moreover, the energy savings are remarkable [25], because the rotation, and consequent power consumption of the motor, starts only when a movement is required, in a on-demand strategy.

In this work, particularly, the DDH strategy is applied to a crane, actuated by a double - acting hydraulic cylinder. The flow control is implemented regulating the speed of a servo motor which directly controls two reversible pumps, which share the same axle. The resulting system has compactness properties, prompt and controllable response and high power output, thanks to the cylinder.

The objectives of this study are: to define a position control for automated applications and to evaluate the achievable precision; to understand and model the sources of losses; to evaluate the system overall efficiency and the possibilities of energy recovery. The work concerns mainly three different engineering fields: electric engineering, hydraulics and control systems.

1.1 Scope of the work

The aim of this Master's thesis is to evaluate the application possibilities of a novel hydraulic system, analysing both automated position control precision and system efficiency. The work focuses on employing fixed displacement hydraulic motors, implementing the control strategy as flow control obtained with variable speed servo motor, instead of the common and less efficient valve control or the more complex variable displacement pump control. The study suggests an implementation of the control strategy oriented to obtain smooth and efficient movements, taking advantage of the servo drive capabilities. The energy evaluation is based on the analysis of the system efficiency and on the possibility of recovering a certain amount of potential energy. The thesis consist on modelling the system, providing and implementing a suitable control strategy, evaluating its performances and the resulting energy balance.

1.2 Scientific contributions

This thesis contains a system engineering study of an electro-hydraulic crane, focused on the applicable control strategy and on the efficiency of the components. The main scientific contributions follow:

- Accurate modelling of novel electro-hydraulic system, with consideration for the main sources of losses.
- Analysis and estimation of the leakage flow.
- Study of the applicability in conditions of unpredictable variable load.
- Flow control strategy implementation, based on variable speed servo motor.
- Definition of a sensorless control strategy, basing on a pressure estimation function, obtainable from motor's feedback.
- Efficiency evaluation of each system component and of overall system.
- Energy recovery possibilities and theoretical cycle efficiency.

1.2.1 List of publications

The publications concerning this work are:

1. Bonato C., Minav T.A, Sainio P., Pietola M., "Position control of direct driven hydraulic drive", FPNI proceedings, June 2014 (under review)

2. Minav T.A, Bonato C., Sainio P., Pietola M., "Direct driven hydraulic drive", IFK proceedings, March 2014

3. Minav T.A, Bonato C., Sainio P., Pietola M., "Efficiency Direct driven hydraulic drive for Non-road mobile working machines", ICEM proceedings, September 2014 (under review)

1.3 Outline of the work

The contents of this thesis are divided into the following 6 chapters.

Chapter 2: Description of the setup employed. The main features, ratings and parameters of the components are outlined.

Chapter 3: Theoretical electro-hydraulic modelling of the system. The control equations are derived, the leakage modelling and the pressure estimation curve are described. The load is modelled from a physical point of view. At last, the efficiency equations are calculated and explained.

Chapter 4: Description of the control strategy implementation. Control logic and employed software (PowerTools, LabView) are explained. A brief report of Matlab calculations for efficiency is given.

Chapter 5: Main results concerning both control performance and efficiency. The numerical outcomes of measurements are listed and analysed.

Chapter 6: Conclusions from the work. The main findings are summed up. Potential applications and advise for future development are discussed.

Chapter 2

Description of the System

In the following chapter an accurate description of the test setup is given. The reader is made aware of the system structure and of its main characteristics. The final aim is to be able to understand all the following procedures in which the hardware is involved and, also, to make the system completely reproducible. When the thesis project started, the main structure of the setup was already built in the automotive laboratory of Aalto University. Therefore, the sections of this chapter concerning this topic will be merely descriptive. The whole control interface, the wirings of sensors, input/output signals and acquisition systems, instead, were implemented as part of this thesis work. For this reason the sections concerning control part will be more exhaustive.

For further information, references to user manuals and datasheets will be given for each component.

A picture of the mechanical system employed for this research is shown in Fig. 2.1, while its schematic description can be found in Fig. 2.2.

2.1 Setup Overview

First of all, some naming conventions for the various components of the system will be stated. They will make the descriptions quicker and help an easier understanding of the topic. These names will be kept for the whole document. The reader is advised to compare the given names with the system parts reported in Fig. 2.2.

Figure 2.1: Setup employed

Chamber 1 - Chamber 2 According to the convention suggested by [29], the ensemble of each pump outlet volume, tube volume and piston side volume will be named as chamber.

Pump 1 - Pump 2 The two hydraulic machines employed (described in Section 2.4) will be called pumps.

Sensors The four pressure sensors employed will be referred with the names stated in Fig. 2.2. In the chambers the sensors reveal the pressure built by the pumps (Sensor Pump 1, Sensor Pump 2). Otherwise in the tank line the sensors (Sensor Tank 1, Sensor Tank 2) always read atmosphere pressure, in this application. The height sensors reads the real position of the piston.

Line 1 - Line 2 These labels will address the two hydraulic macro-structures, each composed by inlet tube, pump, outlet tube and pressure sensors.

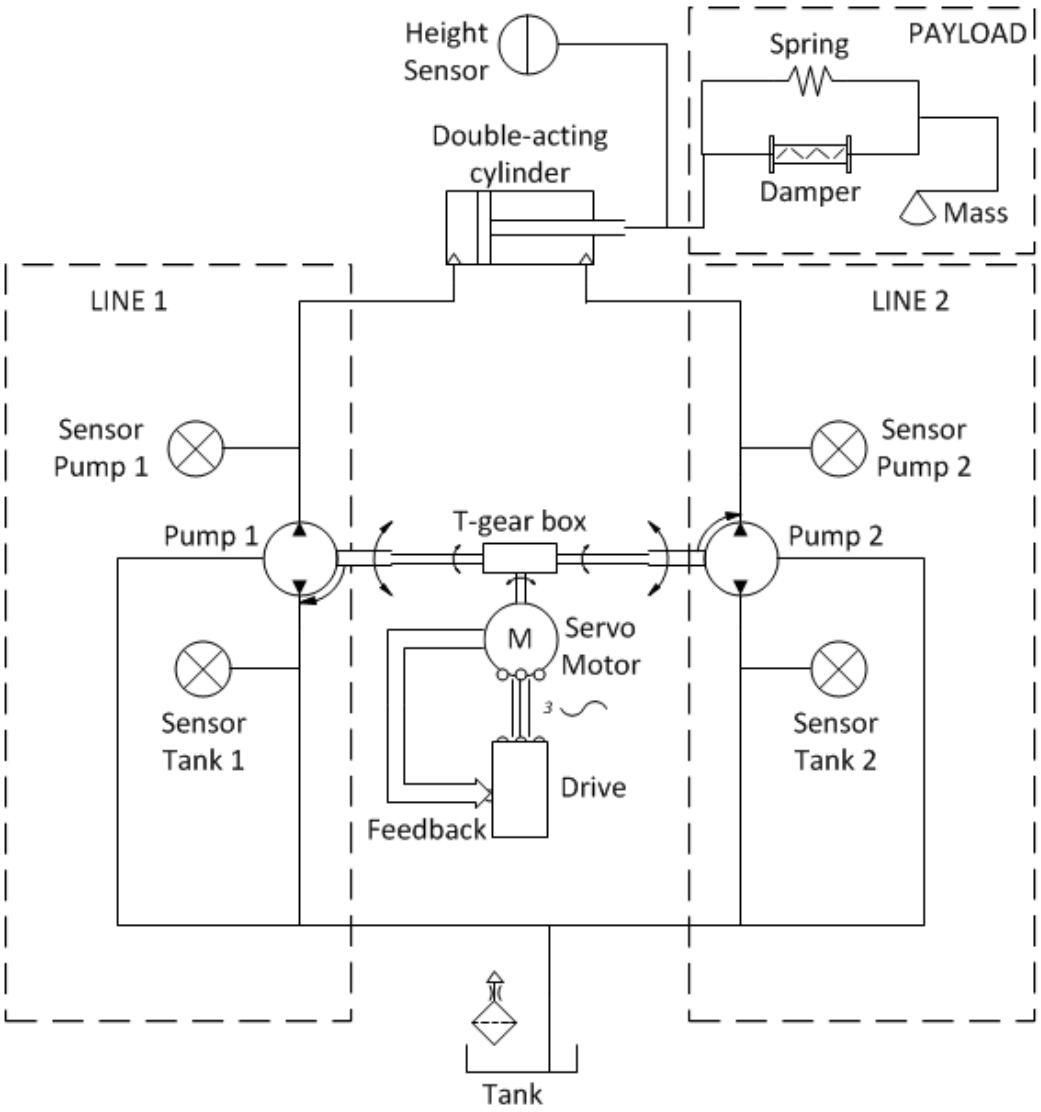

Figure 2.2: Schematic of the system (for naming conventions refer to page 2.1)

Let us now proceed with the description of the components. The electric drive converts three-phase AC power supply from the power line and controls the three-phase AC servo motor. The shaft angular speed is its control quantity, that means it is forced to follow the reference given by the drive, by means of closed-loop PID control. Actually the motor gives as feedback the real readings for angular position of the shaft, through the in-built encoder, and the active current output, which can be directly converted to obtain the amount of torque generated at the shaft. The shaft rotation is delivered to the pumps by means of a mechanical T-shaped gearbox with fixed ratio (1,5:1) so that the two pumps are constantly rotating at the same speed, but in opposite direction. The provided torque splits between the two shafts basing

on the amount of resistance to the movement required by each hydraulic line. Each pump, while rotating delivers to the hydraulic line a certain amount of oil flow, from tank to cylinder or in the other way round. For example, during lifting movement, pump 1 rotates clockwise and the oil flows from the tank through the tube up to the cylinder, while the pump 2 works in opposite direction, generating oil flow from cylinder to tank.

During the lifting movement, the force generated by the pressure built in chamber 1, acting on the first piston head, must be higher than the one induced by the payload, in order to let the piston move. During the lowering movement, instead, the pressure in chamber 1 slows down the free-fall of the load, obtaining a controlled lowering motion. During both the movements, pump 2 is supposed to work together with the first one, accompanying it.

The final aim of pump 2 would be to give to the system the possibility to deliver power in the way down as well. In fact, the setup is implemented as a test bench for different future applications. For example, in a non-road mobile working machine (NRMM), such as a mine loader, during a working cycle could be required not only the ability of lifting and lowering weights, but also the capability to generate force from up to down, typically for digging the soil. In that scope, the stiff reference chamber would be the second one and pump 1 would operate accompanying the movement.

Concerning the sensors, the system has been equipped with four pressure sensors to keep the pressure checked both in the chambers and in the discharging pipe to the tank. For the application studied in this thesis work, only the 2 transducers in the pumps side will be used, while the other 2 remain available for future application. For example, a hydraulic closed-loop setup in which the whole system is supposed to work under pressure. The tank line would be kept under pressure as well, actually replacing the tank with a hydraulic accumulator.

Moreover, a height sensor for the cylinder's piston movement was installed. The sensor, a wire incremental encoder, gives continually the actual position of the piston during every movement. The sensors were used for programming and testing purpose only. Actually, the final aim is not to use them for the control strategy, taking advantage only of the information coming from the motor feedback.

As an interface between the hardware system and the control software, a USB acquisition board was employed (see Section 2.8). The board has

the capability to read some analog and digital inputs and to write on digital outputs. Its purpose is both to convoy the information obtained from the pressure transducers, from the wire encoder, from the outputs of the drive and to write on the digital inputs of the drive to actuate particular control strategies which will be explained in Section 4.2. It's interesting to notice that 2 particular conditioning system had to be done: a voltage divider to make the encoder output readable by the board and a relays system to amplify the digital outputs of the board, to make them sensible for the drive. These devices will be properly described in Section 2.8.

As can be seen in the schematic (Fig. 2.2), the payload is modelled by second order system with the presence of mass, damper and spring.

2.2 Electric Drive

The electric drive employed for the test setup is Emerson Control Techniques Unidrive SP1406. Its complete description can be found in the manuals [30], [31] and a picture is shown in Fig. 2.3.

In this section, the main characteristics of the drive will be listed, starting from the ratings, which are shown in Tab. 2.1.

Normal Duty			Heavy Duty		
Maximus continuous output current, $[A]$	Nominal power at 400V, $[kW]$	Motor power at 460V, $[kW]$	Maximus continuous output current, $[A]$	Nominal power at 400V, $[kW]$	Motor power at 460V, $[kW]$
11	5,5	5,5	9,5	4,0	5,5

Table 2.1: 400V drive ratings ($380V$ to $480V \pm 10\%$)

The employed drive can be used in three different operating modes: Open-Loop mode, Closed Loop vector mode and Servo mode. To pursue the final aim, it is necessary to use the **Servo mode**, in which the drive directly controls the speed of the motor using the feedback device to ensure the rotor speed is exactly as demanded. In effect the motor feedback, speed and direct current, is going to be the only useful information in the control strategy applied. For the research process, the speed is taken as control quantity and

Figure 2.3: Emerson Control Techniques Unidrive SP1406

the torque (obtained from the direct current) is used to obtain additional knowledge about the system status.

2.2.1 Parameters and Control Connections

The tuning of the drive's behaviour is obtained by setting the drive's parameters. Although some of the parameters are fundamental for the thesis process, in fact, an accurate description of them could result cumbersome in this early part of the work. Mainly for this reason it was decided to dedicate the Appendix A.1 to this aim, the reader is advised either to go quickly through it, or to consult it on need.

Another fundamental feature of the drive is the presence of connections which make it accessible and allow to get information from it. The previous reasoning over the parameters remains valid, thus the reader is addressed to Appendix (A.2) for a brief explanation of the useful connections.

2.2.2 Scales I/O

The input/output terminals get and give information from and to the outside world, in particular these terminals are supposed to communicate with the NI USB Board (Section 2.8). For practical purposes it is necessary to keep in consideration type, scale and amplitude of these signals. On the one hand to avoid physical problems (such as: signals too weak to be read, signals too strong can damage the system), on the other hand to be able to convert properly voltage or current outputs to significant physical quantities.

From the physical point of view, the voltage operating mode is chosen for this setup because the wirings are sufficiently short not to generate a sensible voltage drop which could influence the accuracy of the readings. The analog ports of the drive are designed to give as output voltage values in the range $[-10 : 10]$ V, which means perfect match with the ratings of the NI USB board. Otherwise the digital input ports of the drive work in the range $[0 : 24]$ V (where 0 V is the logic 0 and 24 V is the logic 1), while the NI board writes digital outputs in the range $[0 : 5]$ V. To overcome this difference a relay for each digital line has to be used, their implementation is explained in the next paragraph (Par. 2.2.3).

As it comes to the conversions, it is necessary to understand properly the scales of the analog outputs to obtain precise readings of the quantities. The procedure finalized to obtain the right conversions, the parameters involved and the interesting results, which will be referred in the software implementation (Chap. 4), are described in Appendix A.3.

2.2.3 Relays

As previously remarked in this section, the presence of relays employed as an interface between the output of the NI USB board and the Drive digital input terminals appears to be necessary. To this aim *Omron G6J-2FL-Y* signal relays have been chosen, for an exhaustive description, ratings and characteristics the reader is addressed to the manufacturer's datasheet [32]. The main features of these relays are the coil voltage (rated $V_r = 5V$ with threshold $V_l = 0,1 \cdot V_r$ and $V_h = 0,75 \cdot V_r$) and the contact rated voltage (up to 30 A), which make these devices the optimal choice for the system. In Fig. 2.4, an excerpt from the datasheet is shown.

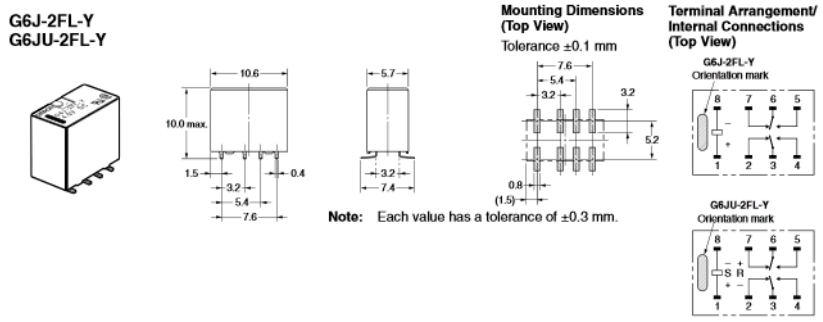

Figure 2.4: Employed relay type (Omron [32])

2.2.4 Drive Software

A basic control software is provided by Emerson: *PowerTools*. This tool is needed to communicate with the drive, download user programs in it, access and modify the system variables, shape the control signals for the movement, assign input and outputs to internal variables, implement a *Selector* for the digital inputs, define simple control strategies and set home position. This software is not powerful enough (for example it can't integrate the speed) to manage the position control of an hydraulic system. Therefore, it is used for configuration of the device and for low level commands (such as move up, move down, stop, move home). The high level part of the control strategy is handled by LabView (Section 4.2).

The main characteristic of the PowerTools configuration employed and their settings will be outlined in Section 4.1, along with the explanation of user program for the control logic.

2.3 Electric Motor

The chosen motor for this setup is Emerson Control Techniques Unimotor FM115 U2C300 VACAA115190, its exhaustive description can be found in the datasheet [33] and a picture is shown in Fig. 2.5.

Stall torque, $[Nm]$	Peak torque, $[Nm]$	Rated torque, $[N]$	Rated speed, $[rpm]$	Max speed, $[rpm]$	Stall current, $[A]$	Rated power, $[kW]$	Drive VPWM, $[VAC]$
9,4	37,6	8,1	3000	4800	5,9	2,54	380/480

Table 2.2: Motor ratings

Unimotor FM is a high performance brushless permanent magnet AC servo motor, matched to use for Control Techniques drives. The ratings for this particular model are shown in Tab. 2.2.

Other relevant parameters of the employed motor are:

$$K_t = 1,6 \text{ Nm/A} \tag{2.1}$$

$$K_e = 9,8 \cdot 10^{-2} \text{ V/rpm} \tag{2.2}$$

where: K_t is the torque constant of the motor (i.e., torque in Nm per Ampere of torque producing current); K_e is the voltage constant, i.e., ratio between RMS line to line voltage produced by the motor and the speed, in V/rpm.

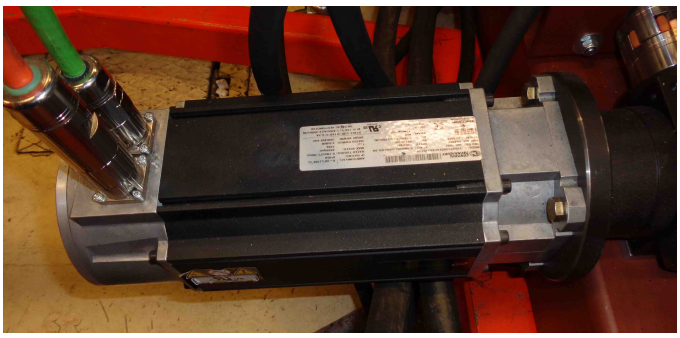

Figure 2.5: Emerson Control Techniques Umimotor FM115

As can be seen in Fig. 2.5, on the motor side opposite to the mechanical shaft, there are two electric connectors: one is the power plug which carries the AC three-phase PWM supply from the drive; the other one is the signal plug, which carries low-voltage power supply for the encoder and gets its feedback.

In this particular model of servo motor, the feedback device fitted is an *incremental encoder* with 4096 pulses per revolution and 5 V dc supply voltage. This device uses an optical disc. The position is determined by counting steps or pulses, 2 sequences of pulses in quadrature are used so the direction sensing may be determined. A marker pulse occurs once per revolution and is used to zero the position count. The encoder also provides commutation signals, which are required to determine the absolute position during the motor phasing test. Positional information is non absolute - i.e. position is lost when the drive is powered down.

2.4 Hydraulic Motors

The employed hydraulic reversible motors are Vivoil XV-2M/14 and XV-2M/22 with external drainage, a picture is given in Fig. 2.6. For their complete description the reader is addressed to the manufacturer's datasheet [34].

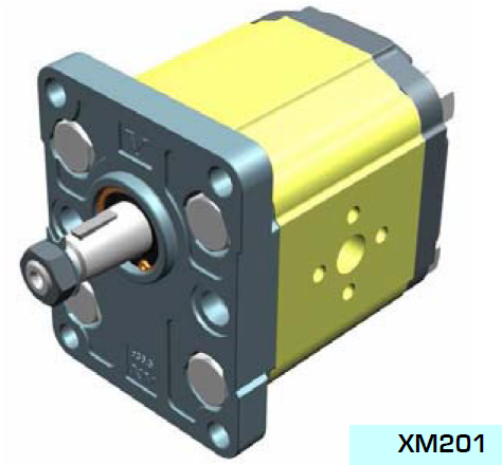

Figure 2.6: Vivoil XV series

A reversible motor is a device which can operate both as a motor (generating mechanical energy as shaft rotation from oil flow) and as pump (delivering hydraulic flow from shaft rotation). It can also rotate in both the counterclockwise and clockwise directions. In this application the motors are used as pumps during the lifting movement and as controlled motors during the lowering one. Moreover, these hydraulic machines need to be capable of rotating in both the directions since the T-shaped gearbox imposes opposite rotation to them. In effect while one delivers oil to the chamber, the other one must suck oil from the other side, in order to produce a harmonic movement of the actuator.

From this former description, it is easy to understand how in this particular application the role of the reversible motors employed is a mixture of motoring and pumping in each cycle. For this reason, in the following, these hydraulic devices will be referred as **pumps** (according to the conventions stated in the beginning of Section 2.1). In the case the motor classification will be needed, the reason will be carefully explained for each particular case.

Two different pumps are used for the setup, these devices behave in identical way and have the same characteristics, the only difference between them

is the displacement. For line 1 the bigger one is installed (22,8 cm^3/rev), while for line 2 the smaller one (14,4 cm^3/rev). This inequality between the two lines is due to the different head areas of the piston. Actually, as it will be explained extensively in the next section (Section 2.5), the employed cylinder presents asymmetry between head areas. This asymmetrical configuration must be preserved in the sizing of the pumps as well (this assumption will be explained and demonstrated in Chap. 3).

Anyway, it is worth deducing the ratio between displacements, since it is going to be a fundamental value in the forthcoming discussions:

$$R_D = \frac{D_2}{D_1} \simeq 0,63 = 63\% \tag{2.3}$$

where R_D is the ratio between pump displacements, D_1 is the displacement of pump 1, D_2 is the displacement of pump 2.

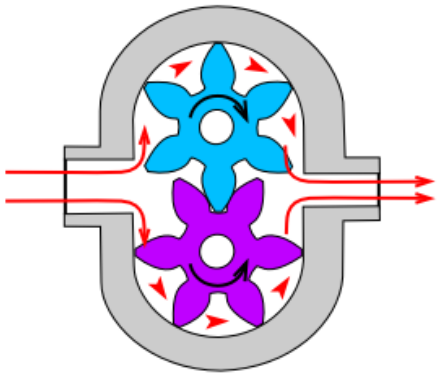

Figure 2.7: Example of an external gear pump

As a last remark, relevant construction characteristics of these hydraulic machines and their installation will be outlined. They are external gear pumps, which means the oil is convoyed from the inlet to the outlet by means of two meshed gears (Fig. 2.7). The flow could go from tank line to piston chamber or the other way round, depending on the particular movement. Even though close tolerances are held between the housing and the gear side, some clearance is needed to allow the movement. Therefore, as any other hydraulic machine, they are bound to have a certain amount of leakage, which is convoyed towards the drainage and discharged back into the tank.

2.5 Cylinder

The setup is equipped with a Pikapaja MIRO C-10-60/30x400 A-55 hydraulic cylinder used as actuator for the crane, its extensive description can be found in the datasheet (in Finnish) [35] and a picture is shown in Fig. 2.8.

Figure 2.8: Hydraulic Cylinder MIRO C-10-60

The device is a common double-acting cylinder, which means it has two chambers separated by the piston head. Each chamber is fed by its own orifice and the sealing of the piston head is supposed to be highly reliable in order to neglect the leakage between chambers.

It is worth noticing, as previously outlined, that the head areas are different in the two sides of the piston. From the datasheet:

$$d_1 = 0,060 \text{ m} , \tag{2.4}$$

$$d_r = 0,030 \text{ m} , \tag{2.5}$$

$$s_p = 0,400 \text{ m} , \tag{2.6}$$

where d_1 is the piston head diameter (side 1), d_r is the rod diameter and s_p is the stroke.

From values (2.4) and (2.5), it is easy to derive the areas. The second head surface is obtained as a difference between the whole area and the one occupied by the rod:

$$A_1 = \pi \cdot \left(\frac{d_1}{2}\right)^2 = 2,8274 \cdot 10^{-3}\ m^2 \tag{2.7}$$

$$A_r = \pi \cdot \left(\frac{d_r}{2}\right)^2 = 7,0686 \cdot 10^{-4}\ m^2 \tag{2.8}$$

$$A_2 = A_1 - A_r = 2,1205 \cdot 10^{-3}\ m^2 \tag{2.9}$$

where A_1 is piston head area side 1, A_r is piston rod area, A_1 is piston head area side 2.

Finally, the ratio between head areas R_A is calculated as:

$$R_A = \frac{A_2}{A_1} \simeq 0,75 = 75\% \tag{2.10}$$

2.6 Sensors

In this section all the sensors employed in the system are described and their function is outlined.

2.6.1 Pressure Transducers

The chosen pressure transducers are Gems 3100R 0400S (Fig. 2.9), for further details refer to the datasheet [36].

Figure 2.9: Pressure Transducer Gems 3100R

This kind of sensor takes advantage of a thin film of semiconductor, deposed by sputtering, which, when a certain pressure is applied, modifies its geometry (strain). The strain in semiconductor thin films causes variation

of electrical resistivity, this phenomenon is detected as piezoresistive effect. All in all, the transducer works as strain gauge, measuring the resistivity opposed to the supply current, it gives a precise and repeatable measure of the applied pressure.

Those particular sensors are designed to bear pressures in the range $[0 : 400]$ bar, giving as an output a voltage value in the range $[0 : 5]$ Volts, which varies with the gradient of resistance. The output suits perfectly the range of NI USB board analog inputs (which can be set to ± 5 V, while the maximum amplitude is ± 10 V) and does not need to be attenuated nor amplified. The pressure scale of the sensors is slightly oversized, in this application, peaks of pressure not higher than 105 bar are observed indeed, but still sufficiently precise for the purpose.

It is worth remarking, these sensors were employed in order to evaluate the system efficiency, to collect data for improving the quality of control logic and to keep system behaviour under observation. But then, the final goal is to define a control which does not take advantage of the pressure values information, which means they would not be needed in a real application.

2.6.2 Height sensor

A SIKO SGI3500 wire-actuated encoder is installed to serve as a sensor for the piston displacement. This sensor is composed by the wire SGI drum (datasheet [37]), coupled with the SIKO IV58M incremental encoder (datasheet [38]). A picture of the complete sensor is given in Fig. 2.10a.

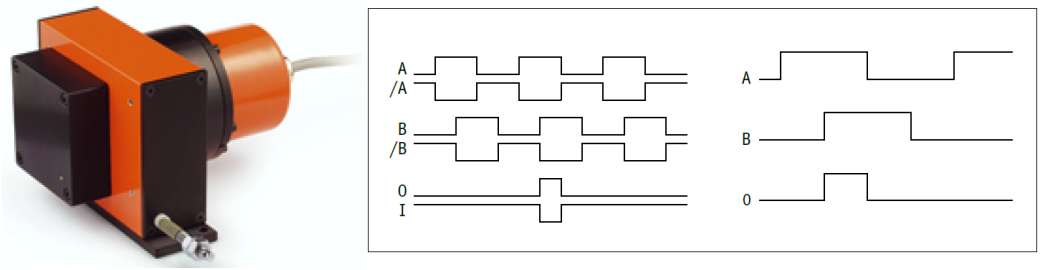

(a) Height sensor (b) Digital output signals

Figure 2.10: Wire-actuated encoder SIKO SGI3500

The main housing of the sensor is fastened against the cylinder barrel, while the terminal of its wire is fixed to the piston rod-end head. A stainless steel cable is wound up around the drum inside the housing. When the piston

moves, the cable unwinds following the movement, that causes the rotation of the drum. The drum is tied to the encoder flange, an optical disc, whose holes generates 3 different digital signals: A, B and 0 (Fig. 2.10b). This particular encoder has a resolution of 2560 pulses/revolution, that means signals A and B rise 2560 times per revolution, while 0 rises one time per revolution, it is called *marker* since it is used as a reference to define the zero position.

A and B are called quadrature outputs, as they are 90 degrees out of phase. This feature is fundamental to understand the direction of the movement: either A rises first, so the drum is spinning clockwise and the piston is moving forth; or B rises first, so the drum is spinning counter-clockwise and the piston is moving back.

To translate the train of pulses into an angular position measure a counter is needed, in this application NI USB-6210 board internal counter is used (Section 2.8). Finally, considering the drum circumference it is easy to transfer the angular measure in a linear one. For this particular encoder the **linear resolution** is 10 pulses/mm.

It is worth noticing that the output digital signals of the encoder have threshold levels $V_{OL,e} = O,5$ V and $V_{OH,e} = 29,2$ V, that means these signals must be attenuated in order to make them compatible with the board specifications ($V_{IL} = O$ V and $V_{IH} = 5$ V (see Section 2.8). Therefore, it is necessary to implement a voltage divider (Fig. 2.11a) with the same characteristics for each of the three channels. The task is accomplished by means of three couples of resistors, with $R_2 = 120\ k\Omega$ and $R_1 = 24\ k\Omega$. In effect, following the theoretical scheme in Fig. 2.11b, the resulting voltage for the high level is:

$$V_{\text{out,d}} = \frac{R_1}{R_1 + R_2} \cdot V_{\text{in,d}} \simeq 4,87\ V \tag{2.11}$$

Likewise for the pressure sensors, the height sensor has its role during control logic set up, efficiency measurements and observation of system behaviour. On the contrary, in the final stages the control technique is supposed to set the position neglecting encoder's information.

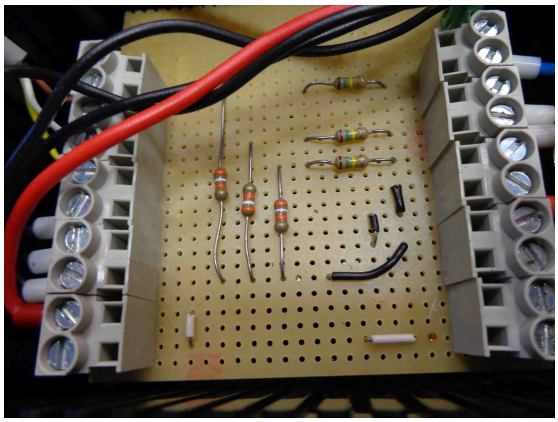

(a) Implementation

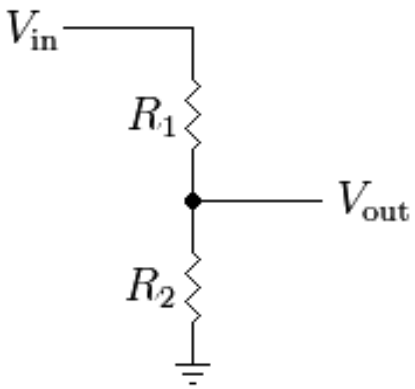

(b) Scheme

Figure 2.11: Voltage divider

2.7 Mechanical T-shaped gearbox

For the aim of delivering the motion generated by the electric motor to the hydraulic pumps shafts, a MS-Graessner P-90-FL fixed-teeth T-shaped gearbox was employed (Fig. 2.12). An exhaustive description can be found in the datasheet [39].

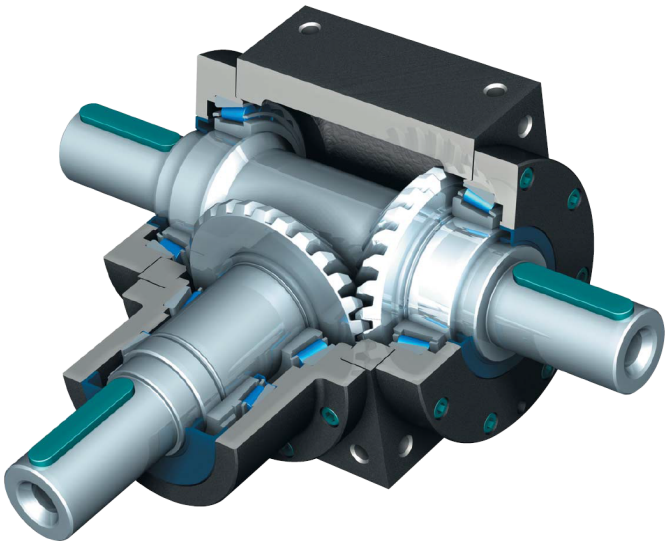

Figure 2.12: Mechanical T-shaped gear

Its behaviour is straightforward: the gear delivers the motion reducing the module of the speed of one third (transmission ratio 1,5:1) and inverting the direction on each pump shaft.

Regarding the power efficiency, the declared efficiency of the gearbox is 98%. This value is confirmed by an accepted rule of thumbs in engineering: it

is assumed a loss of 1% efficiency each 90° turn in a mechanical shaft. Hence, across this work, it will be hypothesized that the sum of the mechanical energy transferred to the two pump shaft be roughly around 98% of the power measured at the electric motor shaft.

2.8 NI USB Board

The employed board is Nation Instruments NI USB-6210, its detailed specifications can be found in the datasheet [40] and for further explanation about the board capabilities and behaviour refer to the user manual [41]. A picture is given in Fig. 2.13.

Figure 2.13: NI USB-6220 board

The main purpose of the board is to link the real system with the control part. It actually convoys each output from the setup sensors and from the drive, samples them and get readings of their values. Furthermore, by means of its digital outputs delivers control signals to drive inputs, allowing the control strategy implementation.

The main specifications and a wiring scheme can be found in App. B.

2.9 Crane

The main structure of the setup is a Masters Craneworks Vestas FC 1100 small crane (see Fig. 2.1 at page 8). The height from base to joint is $1,55$ m, while the boom length is $l = 1,67$ m. An accurate analysis and modelling will be given in Section 3.1.

Chapter 3

Theoretical Model

In the present chapter, the employed system model is precisely described and analysed. The theory followed in order to model the hydro-mechanical part is mainly taken from Merritt's work [29]. Other contributions, regarding leakage modelling and efficiency, are obtained from Wilsons' work: [42],[43] and [44].

The employed system can be modelled as a pump-controlled hydraulic double-acting linear actuator. Pumps and motors are used to convert mechanical energy into hydraulic energy and vice versa, respectively. These machines may be divided in *hydrodynamic* or *positive displacement*. Hydrodynamic machines are not suited for control purposes.

According to [29], in positive displacement machines, fluid passes through the inlet into a chamber which expands the volume and fills it with fluid. The volume expansion causes a shaft rotation in a motor, in contrast to a pump where volume expansion is caused by shaft rotation. The volume of trapped fluid is sealed from the inlet by some mechanical means and then transported to the outlet side where it is discharged. A succession of small volumes of fluid transported in this manner gives a fairly uniform flow. Thus a positive or definite amount of fluid is displaced through the machine per unit of shaft revolution. Positive displacement machines are quite efficient and find extensive use in control systems.

The pumps employed for the test setup are positive fixed-displacement machines, therefore, they will be modelled according to this description. Moreover, these machines are *continuous travel devices* (in detail *external gear pumps*), which means they have a lever mechanism (gear radius) to which the shaft torque is applied; a mechanical element (gear's meshed part)

to convert this force from shaft torque into flow and build pressure; some method to seal inlet from outlet (gear coupling); some method of porting fluid to the mechanical elements on which the pressure acts (hoses).

The cylinder used for the test setup, in contrast, is a *limited travel device*, since it is linear and there is not any flow between inlet and outlet (besides the leakage one). In this kind of devices the inlet flow is used to build pressure which acts on the piston head in order to contrast the force generated by the load and produce movement. The modelling and basic description of these machines is usually more straightforward and they are characterized by a high efficiency.

3.1 Electro-hydraulic and Mechanical Model

In order to obtain a global model for the system, it is necessary to start modelling each component, first with its ideal description and then adding the corrections to consider non-idealities. At a later stage these models will be linked by a relation considering the system construction and taking advantage of the continuity equations for hydraulics.

For this particular setup, the whole system will be modelled as a pump controlled cylinder, in which the pumps have constant displacement but the flow control is achieved varying the input speed at the shaft. This kind of system, compared to the valve controlled type, has the advantage of a high theoretical efficiency, but it is often characterized by a slower response (motor start-up); requirement of a servo motor to control the flow; necessity of close coupling of pumps and actuator [29]. These requirements and characteristics will be kept in consideration during the modelling stage and their influence on the system will be described.

3.1.1 Ideal Pump and Cylinder Analysis

An ideal pump or motor is defined as having no power losses due to friction and leakages and, consequently, has an efficiency of 100%. Although this is certainly not true in practice, hydraulic machines are quite efficient, and system design is often based on ideal machines [29] and non-idealities are added in a later phase, upon need.

Consider an ideal hydraulic pump. The mechanical power input P_{mec} is:

$$P_{\text{mec}} = T_p \dot{\theta}_p \tag{3.1}$$

where: T_p is the torque at the pump shaft and $\dot{\theta}_p$ is the pump shaft speed. The hydraulic power output (P_{hyd}) is:

$$P_{\text{hyd}} = p_L Q_L \tag{3.2}$$

where p_L is the pressure difference across the pump lines and Q_L is flow through the pump. Because the pump is assumed to be ideal, the equations (3.1) and (3.2) can be equated to yield:

$$T_p = \frac{Q_L}{\dot{\theta}_p} p_L \tag{3.3}$$

Now, by definition, the volumetric displacement (D_p) is:

$$D_p = \frac{Q_L}{\dot{\theta}_p} \tag{3.4}$$

Finally, by substitution of (3.4) in (3.3):

$$T_p = D_p p_L \tag{3.5}$$

which is the fundamental relation for an ideal pump (or motor, swapping input and output). Only one parameter (D_p) is required to define the ideal machine, and this quantity is also the single most important parameter for practical machines. This analysis also holds for the ideal motor, except that the power flow is reversed, that is, hydraulic power is transformed in mechanical power.

Hydraulic Cylinder A similar analysis can be made for an ideal cylinder. The piston area is the parameter analogous to the displacement of a rotary device. In particular, in order to calculate the power acting on the load (P_{out}):

$$P_{\text{out}} = F_c \dot{x}_c \tag{3.6}$$

where F_c is the force generated at the piston rod and $\dot{x}_c$ is the velocity of the piston.

Since the cylinder is assumed to be ideal, power input (3.2) can be equated to power output (3.6) to yield:

$$F_c = \frac{Q_L}{\dot{x}_c} p_L \tag{3.7}$$

Now, the volume of the cylinder's chamber (V_c) is:

$$V_c = V_0 + A_c x_c \tag{3.8}$$

where: V_0 is the dead volume of the cylinder's chamber, A_c is the piston head area and x_c is the piston position.
Its variation corresponds to the input flow (Q_L):

$$Q_L = \frac{V_c}{dt} = A_c \dot{x}_c \tag{3.9}$$

Then, by substitution of (3.9) in (3.7):

$$F_c = A_c p_L \tag{3.10}$$

which is the fundamental relation for an ideal cylinder. As previously stated, the parameter A_c plays the same role as D_p for the ideal pump. Only difference is that the piston, by its nature of linear actuator, is defined also by the length of the maximum movement (stroke of the piston), while this is absent in a rotary machine.

3.1.2 Practical Pump and Cylinder Analysis

Leakage flow and friction are the sources of losses in hydraulic machines. In this section these losses will be examined and included in the analysis of steady state performance. Consider the schematic of the gear pump in Fig. 3.1. It is apparent that two type of losses can exist: *internal or cross-port leakage* between the lines and *external leakage* from each pump chamber, past the gears, to the case drain. Because all mating clearances are intentionally made small to reduce the losses, these leakage flows are laminar [43].

The internal leakage (Q_{ip}) is proportional to motor pressure difference, while the external leakage (Q_{ep}) in each chamber is proportional to the particular chamber pressure (assuming negligible drain pressure), and they can

be written as:

$$Q_{ip} = C_{ip} p_L \tag{3.11}$$

$$Q_{ep1} = C_{ep} p_1 \tag{3.12}$$

$$Q_{ep2} = C_{ep} p_2 \tag{3.13}$$

where $p_L =$ $p_1 - p_2 =$ pressure difference across pump,
$C_{ip} =$ internal leakage coefficient,
$C_{ep} =$ external leakage coefficient,
$p_1 =$ pressure in forward chamber,
$p_2 =$ pressure in return chamber.

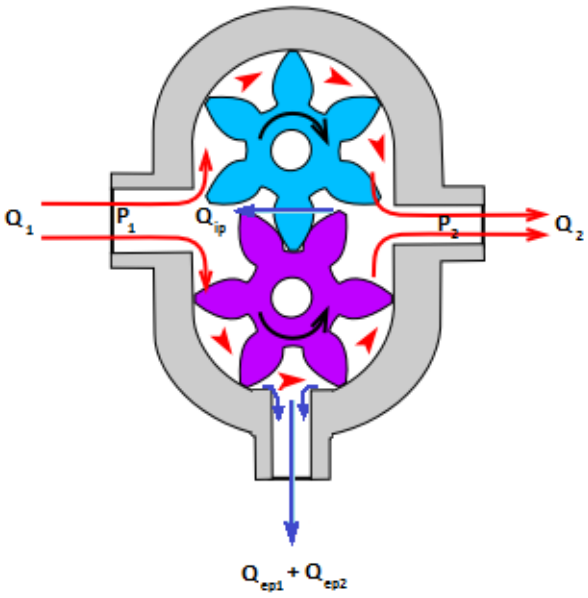

Figure 3.1: Schematic diagram of a gear pump

The steady-state continuity equations for the pump chambers are:

$$Q_1 - C_{ep} p_1 - C_{ip}(p_1 - p_2) - D_p \dot{\theta}_p = 0 \tag{3.14}$$

$$D_p \dot{\theta}_p + C_{ip}(p_1 - p_2) - C_{ep} p_2 - Q_2 = 0 \tag{3.15}$$

where $D_p =$ ideal volumetric displacement of the pump,
$\dot{\theta}_p =$ pump shaft speed,
$Q_1 =$ forward flow to pump,
$Q_2 =$ return flow from pump

These two equations completely describe the flows in the pump. If leakage coefficients are zero then $Q_1 = Q_2 = D_p\dot{\theta}_p$, which is the result for the ideal pump.

Subtracting (3.15) from (3.14) yields

$$Q_L = D_p\dot{\theta}_p + \left(C_{ip} + \frac{C_{ep}}{2}\right) p_L \tag{3.16}$$

where by definition

$$Q_L = \frac{Q_1 + Q_2}{2} \tag{3.17}$$

The quantity Q_L, commonly called *load flow*, represents the average quantity of the flows in the two pump lines; Q_L equals the flow in each line only if external leakage is zero. The concept of load flow is useful because it reduces two flow equations to a single equation which relates load flow to pump pressure and speed only. Moreover, it clearly shows that external leakage acts like internal leakage as far as pressure difference is concerned.

The description can be further simplified because in the employed control strategy, the input pump line is assumed to be at atmosphere pressure (being connected directly to the tank), which means $p_1 = 0$ and $p_L = -p_2$. With this simplification the continuity equations (3.15) and(3.14) become:

$$Q_1 + C_{ip}p_2 - D_p\dot{\theta}_p = 0 \tag{3.18}$$

$$D_p\dot{\theta}_p - (C_{ip} + C_{ep})p_2 - Q_2 = 0 \tag{3.19}$$

And the load flow (3.16):

$$Q_L = D_p\dot{\theta}_p + \left(C_{ip} - \frac{C_{ep}}{2}\right) p_2 \tag{3.20}$$

These results permit to describe the pump behaviour through one pressure and the speed only. Moreover, it is noticeable that the leakage flow depends only on the pressurised chamber of the pump, through the leakage coefficients. Therefore it is possible to define the *slip flow* (Q_s) and the *slip coefficient* (C_s):

$$Q_s = (C_{ip} + C_{ep})\, p_2 = C_s p_2 \tag{3.21}$$

Q_s represents the total flow which decreases the ideal flow at pump outlet, because of all the leakage effects. In this way it is possible to summarize

the effect of the leakage with one parameter. A deeper description of this parameter and its derivation will be given in Section 3.2.

Hydraulic Cylinder As far as the hydraulic cylinder is concerned, a practical analysis of it must include the effects of the leakage flow. For this type of power element, the leakage is due to the seals. There are *external leakage* (Q_{ec}), around the rod, and *internal leakage* (Q_{ic}), around the piston head, between the chambers. According to the schematic in Fig. 3.2, applying the continuity equation to each piston chamber yields:

$$Q_1 - C_{ic}(p_1 - p_2) = \frac{dV_1}{dt} + \frac{V_1}{\beta}\frac{dp_1}{dt} \tag{3.22}$$

$$C_{ic}(p_1 - p_2) - C_{ec}p_2 - Q_2 = \frac{dV_2}{dt} + \frac{V_2}{\beta}\frac{dp_2}{dt} \tag{3.23}$$

where
C_{ic} = internal or cross-port leakage coefficient of the cylinder,
C_{ec} = external leakage coefficient of the cylinder,
β = effective bulk modulus of the system (Section 3.5),
p_1, p_2 = pressure in forward and return chamber,
Q_1, Q_2 = flow in forward and return chamber,
V_1, V_2 = volume of forward and return chamber,
t = time.

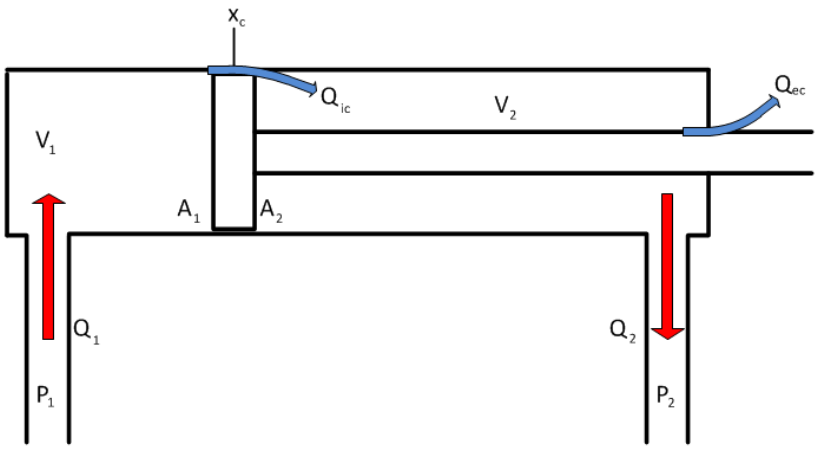

Figure 3.2: Schematic diagram of a double-acting cylinder

At right hand of continuity equation, there are two terms. The first one keeps in consideration the volume variations due to the displacement of the piston, while the second term concerns the pressure variations due to the

elasticity of the system. This phenomenon will be illustrated in Section 3.5. In the following, the external leakage for the cylinder will be always assumed to be zero, since its amount is negligible.

The volumes of the cylinder chambers may be written:

$$V_1 = V_{01} + A_1 x_c \tag{3.24}$$

$$V_2 = V_{02} - A_2 x_c \tag{3.25}$$

where A_1, A_2 = piston heads areas,
x_c = displacement of the piston,
V_{01} = initial volume of the forward chamber,
V_{02} = initial volume of the return chamber.

Replacing the volume expressions in the continuity equations and neglecting the external leakage yields:

$$Q_1 - C_{ic}(p_1 - p_2) = A_1 \frac{x_c}{dt} + \left(\frac{V_{01} + A_1 x_c}{\beta} \right) \frac{dp_1}{dt} \tag{3.26}$$

$$C_{ic}(p_1 - p_2) - Q_2 = -A_2 \frac{x_c}{dt} + \left(\frac{V_{02} - A_2 x_c}{\beta} \right) \frac{dp_2}{dt} \tag{3.27}$$

Equations (3.26) and (3.27) completely describes the hydraulic behaviour of double-acting cylinder.

3.1.3 Joint Model for the System

After modelling the single components it is necessary to built a model for the whole system. In this section the equations previously outlined will be unified in a common description. The derivation will be carried out according to the symbols depicted in Fig. 3.3.

The continuity equations for the cylinder (3.26) and (3.27) remain valid. The flows Q_1 and Q_2 are delivered by the pumps, therefore, their description is obtained in (3.14) and (3.15), and can be replaced in the equations. For pump 1 the inlet pressure is zero (tank line), while for pump 2 the outlet pressure is zero. Remarking that $\dot{\theta}_p$ is forced to be the same because of the

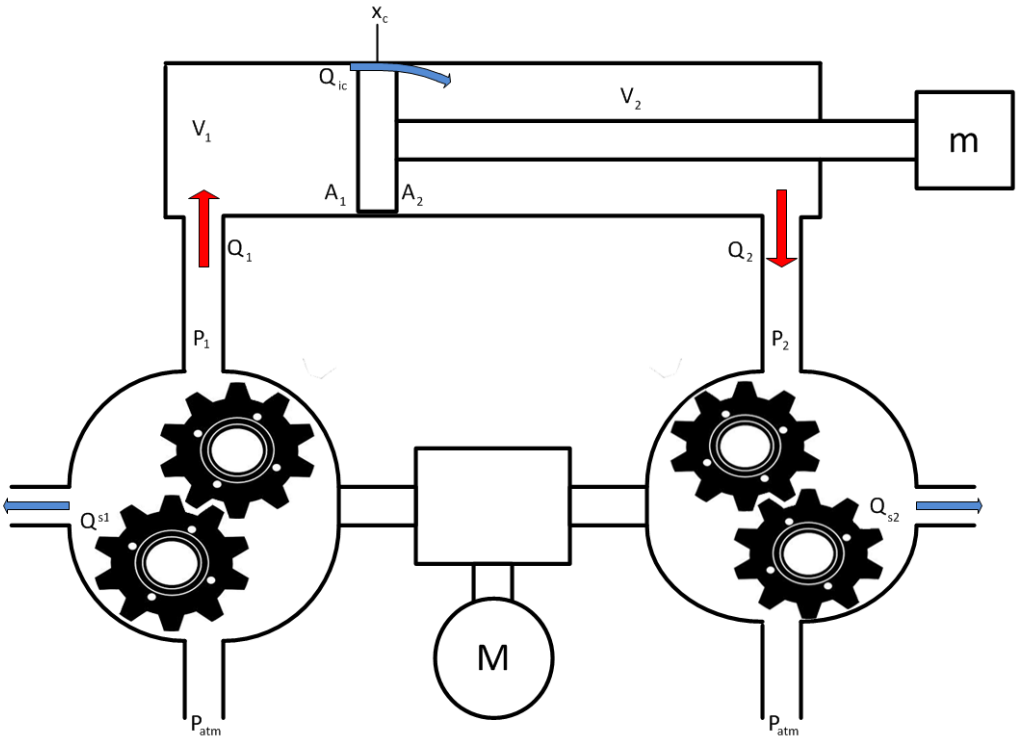

Figure 3.3: Schematic diagram of the whole system

gear box, yields:

$$D_{p1}\dot{\theta}_p - C_{s1}p_1 - C_{ic}(p_1 - p_2) = A_1\frac{x_c}{dt} + \left(\frac{V_{01} + A_1 x_c}{\beta}\right)\frac{dp_1}{dt} \tag{3.28}$$

$$C_{ic}(p_1 - p_2) - C_{s2}p_2 - D_{p2}\dot{\theta}_p = -A_2\frac{x_c}{dt} + \left(\frac{V_{02} - A_2 x_c}{\beta}\right)\frac{dp_2}{dt} \tag{3.29}$$

Equations (3.28) and (3.29) model the hydraulic behaviour of the global system. It is now necessary to build a proper model of the leakage flow, in order to completely define the left hand terms of the equation, and of the load, so that the relation between pressure and force acting on the piston rod can be found. In the following Section the model of the leakage will be derived, while in Section 3.3 the payload will be discussed.

3.2 Leakage Model

In this section, the leakage flow is analysed for one of the hydraulic lines of the system. In particular, from (3.28), it is apparent that two terms are mostly relevant for the description of leakage flow: slip flow of the pump and

cross-chamber flow of the cylinder.

As a first simplification, the internal leakage flow of the cylinder will be neglected. This assumption is acceptable because, as stated in [2], the overall efficiency of this linear actuator is mainly influenced by frictional losses encountered by the piston and rod during its stroke. As a matter of fact, the common approach to overall efficiency for linear actuators does not even keep in consideration the leakage, but only the torque efficiency.

Moreover, the leakage coefficient of the pump will be evaluated empirically, which implies the effect of the cylinder leakage will be fairly included in the total leakage. For these reasons, the continuity equation for side 1 (3.28) can be written as:

$$D_{p1}\dot{\theta}_p - C_{s1}p_1 = A_1\frac{x_c}{dt} + \left(\frac{V_{01} + A_1 x_c}{\beta}\right)\frac{dp_1}{dt} \tag{3.30}$$

Let us proceed in the analysis of the pump leakage; for this purpose [29] gives a first very basic model of it. The slip flow is usually laminar and, therefore, inversely proportional to the viscosity [29]. Test results also indicate that the slip flow is related to motor displacement. Hence:

$$Q_s = C_s p = C_{s,i}\frac{D_m}{\mu}p \tag{3.31}$$

where $C_{s,i} =$ reduced slip coefficient,
$\mu =$ absolute viscosity of the fluid.

Once the constant contributions to the slip coefficient are separated, it is necessary to understand which are the variables influencing the leakage in a gear pump. Interesting and detailed analysis of the topic is carried out in [45]. Where the author analyses the effects of operating conditions, such as pressures, speeds and oil temperatures, on the leakage flow characteristic for various type of gear pumps. An even more detailed internal leakage model, specialized for exterior meshing gear pumps, can be found in [46]. In this work the different causes of flow losses are divided and particularized for the sake of obtaining a mathematical model of the global flow. The results of the previously introduced articles ([45] and [46]) are at the basis of the following leakage flow modelling.

Speed In [45], tests were carried out at different temperatures and for different pumps. The results show that the flow losses are almost independent from the operating speed. Therefore, shaft speed will be excluded from the leakage modelling.

Temperature The slip flow (Q_s) increases with the raising oil temperature (T_o), since the viscosity reduces, and with the increasing pressure differential across pump lines (for this implementation it is equal to p_1 sine the pump inlet is kept to atmosphere pressure) [45]. However, the changing rates ΔQ_s are nearly equal for all oil temperatures. Which means, when the temperature increases, the viscosity of the oil decreases and, being under the fraction sign, forces the Q_s vs. p_1 characteristic to raise, without sensible modifications. For this particular work, the oil temperature was checked to be constant, in order not to consider this phenomenon. Nonetheless, according to these results, if in future investigations the temperature variation would be considered, it could be simple to add them to the model.

Pressure The operating pressure is taken as the key parameter in order to model the slip flow. As already stated, Q_s is proportional to p_1. Nevertheless, the increasing rate of the flow (ΔQ_s) is not directly proportional to the increasing pressure p_1, it actually becomes smaller and smaller when the pressure raises. For this last reason, the desired slip coefficient has to behave in the same manner; i.e., it must depend on some powers of the pressure in a way which assures that it slowly decreases with the raising pressure. In other words, even if Q_s becomes more relevant as p_1 raises, its variation becomes smaller for high pressures. Otherwise, the slip flow could become critically high, even comparable with the delivered flow.

Finally, the first model (3.31) can be extendend by the more general one given in [45]. It is composed by four terms, depending on up to the third power of p_1, i.e.:

$$Q_s = \frac{C_a}{\mu} p_1 + \frac{C_b}{\mu} p_1^2 + \frac{C_c}{\sqrt{\rho}} p_1^{1/2} + \frac{C_d}{\sqrt{\rho}} p_1^{3/2} \tag{3.32}$$

where C_a, C_b, C_c, C_d = coefficients from geometry of the pump,
μ = viscosity of the oil,
ρ = density of the oil.

3.2.1 Slip Coefficient Derivation

In order to identify the parameters involved in the leakage description (3.32), it was decided to follow the empirical way, setting up a dedicated experiment. The procedure consists in lifting the piston at different heights, locking the motor shaft and keeping the load in the decided position. In this situation, the load starts its slow drop due the effect of the losses. An estimation of the slip coefficient is deducible, by means of pressure readings and observation of drop speed. In the fact, imposing zero shaft speed and assuming the pressure almost constant, the continuity equation (3.30), after reordering of the terms, yields the slip coefficient:

$$C_s = -\frac{A_1}{p_1}\dot{x}_c \tag{3.33}$$

Once enough data is obtained, the coefficient derivation can be carried out by curve fitting of the results. An example of the data fitting is depicted in Fig. 3.4.

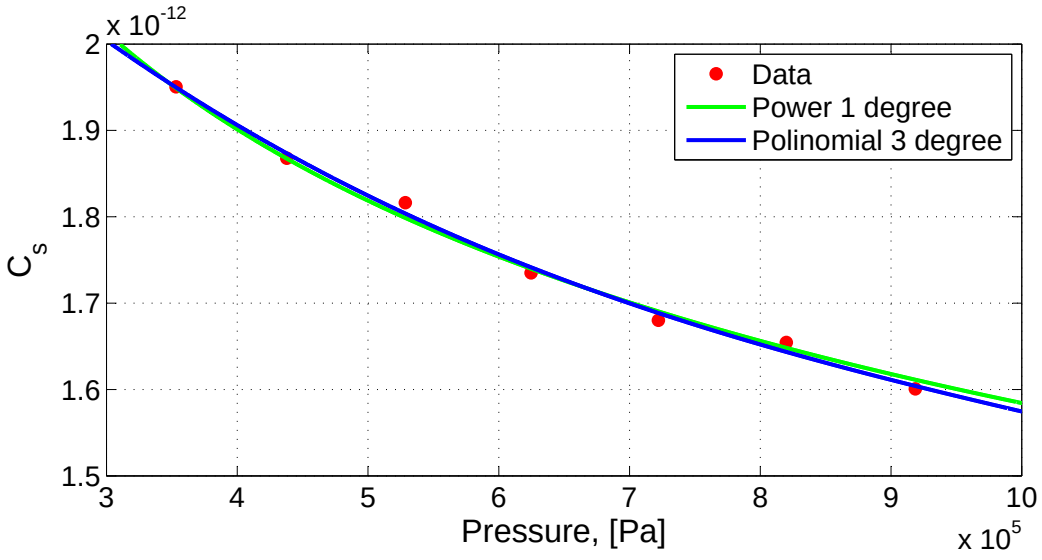

Figure 3.4: Graphics of the two curves fitted

In practice, the model (3.32) results quite cumbersome and hardly applicable, for this reason the first guess is to fit the results with a **third order polynomial curve** in p_1 (blue curve in Fig. 3.4), which is supposed to fit the data slightly simplifying the model. The curve equation follows:

$$C_s = a_1 p_1^3 + a_2 p_1^2 + a_3 p_1 + a_4 \tag{3.34}$$

Nonetheless, it is possible to further reduce the complexity of the model, employing a simpler curve which fits the data in a very similar manner, inside the operative range: **first order exponential** (green curve). Moreover it gives the important advantage of having an offset that can be set to a slightly positive value, keeping the coefficient from becoming negative for high pressures (which would lead to nonsense). This feature also helps the modelling of the coefficient for very high pressure values, which are not directly measurable with the available load range, but which behaviour is well predicted with the employed curve.

As a last remark, the exponential curve is not defined for negative pressures and it grows to infinity for zero pressure. This behaviour is acceptable, because the existence of negative pressures is impossible and the operative pressure varies in the range $3 \cdot 10^5 \div 105 \cdot 10^5$ Pa, where the critical part of the curve is not affecting the behaviour.

The equation for this particular curve is therefore given:

$$C_s = a\,(p_1)^b + c \tag{3.35}$$

with specific values:

$$a = 4,19 \cdot 10^{-9}, \quad b = -0,6589, \quad c = 1,07 \cdot 10^{-12}$$

It is worth noticing, the slip coefficient depends on the pressure, which is supposed to be an unknown value in the proposed control techniques. This issue must be solved deducing an estimation of the pressure. This topic will be investigated in Section 3.4.

3.3 Phisycal Model of the Load

The force generated by a standard load on the cylinder's piston, can be described according to the Laplace second order model:

$$F_c = A_c p_l = m_t s^2 x_c + B_v s x_c + K_l x_p + F_a \tag{3.36}$$

where $F_g =$ force generated or developed by the piston,
$m_t =$ total mass of the load referred to piston,
$B_v =$ viscous damping coefficient of the load,
$K_l =$ load spring gradient,
$F_a =$ arbitrary additional force on piston.

First of all it is necessary to model the physical configuration of the system, to evaluate the effect of the load weight on the piston. The physical description employed is depicted in Fig. 3.5.

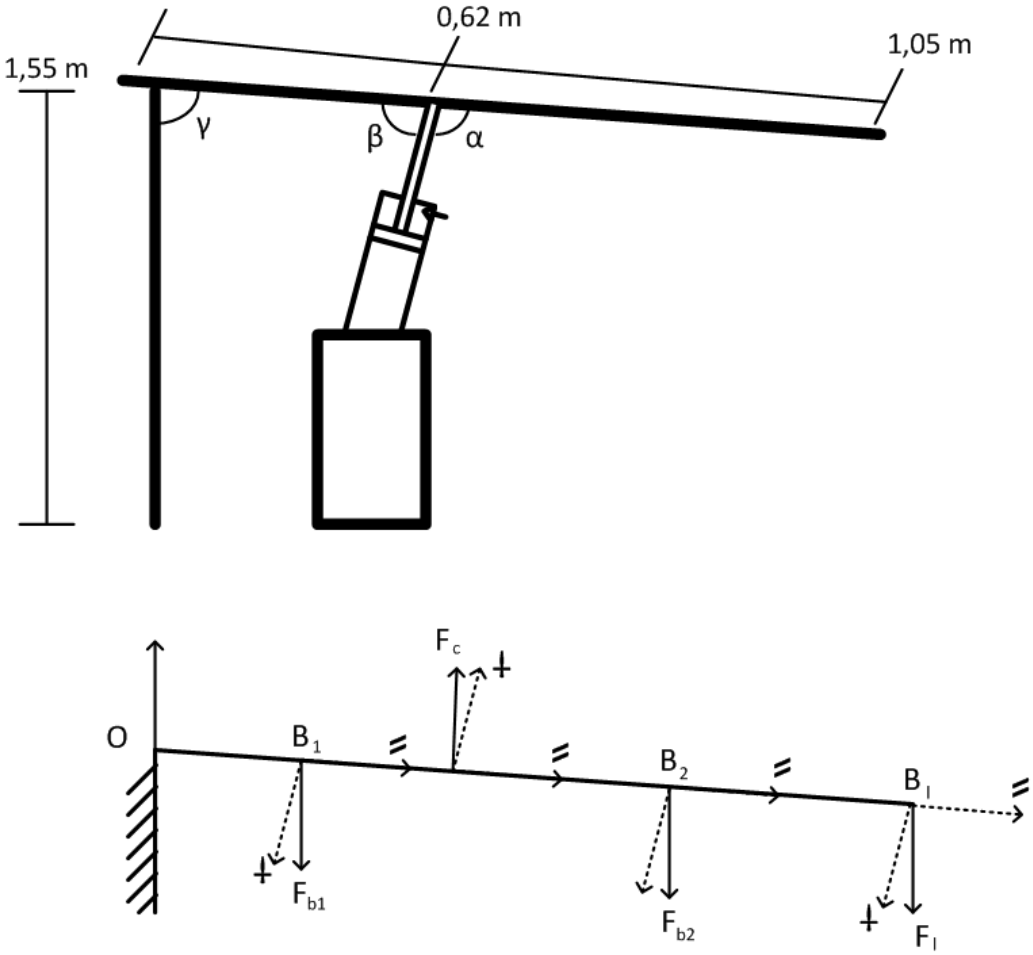

Figure 3.5: Physical schematic of sizes and forces

In order to determine the force that the piston has to develop in order to keep the load at a certain level, the conservation of momentum is applied with reference pole in O (main joint). The forces' components which are parallel to the arm do not contribute to the momentum, while only the orthogonal ones do. Moreover the crane boom is divided into two segments, which masses

are approximated as single dot-shaped and applied in the midpoints. The equation can be written as:

$$F_l^{\perp} B_l + F_{b1}^{\perp} B_1 + F_{b2}^{\perp} B_2 = F_c^{\perp} B_c \tag{3.37}$$

where $B_1 =$ arm of the application point of the first segment's mass force,
$B_2 =$ arm of the application point of the second segment's mass force,
$B_c =$ arm of the application point of the piston force,
$B_l =$ arm of the application point of the load's mass force,
$F_{b1} =$ force generated by the second segment's mass,
$F_{b2} =$ force generated by the first segment's mass,
$F_c =$ force generated or developed by the piston,
$F_l =$ force generated by the load's mass.

According to the angles naming in Fig. 3.5, the forces' orthogonal components are:

$$\begin{aligned} F_l^{\perp} &= F_l \, sin\gamma = m_l \, g \, sin\gamma \\ F_{b1}^{\perp} &= F_{b1} \, sin\gamma = m_{b1} \, g \, sin\gamma \\ F_{b2}^{\perp} &= F_{b2} \, sin\gamma = m_{b2} \, g \, sin\gamma \\ F_c^{\perp} &= F_c \, sin\beta \\ \beta &= 180^{\circ} - \alpha \end{aligned} \tag{3.38}$$

where $m_l =$ mass of the payload,
$m_{b1} =$ mass of the first boom segment,
$m_{b2} =$ mass of the second boom segment.

It is now easy to derive the equation for the force generated by the piston in equilibrium conditions:

$$\begin{aligned} F_c &= \frac{F_l B_l + F_{b1} B_1 + F_{b2} B_2}{B_c} \, \frac{sin\gamma}{sin\beta} \\ &= \frac{(m_l B_l + m_{b1} B_1 + m_{b2} B_2) g}{B_c} \, \frac{sin\gamma}{sin\beta} \end{aligned} \tag{3.39}$$

It remains to determine the magnitude of the acting forces and the variation range of the angles.

Payload For the purpose of testing different payloads for the setup, a variable weight is employed. The weight stack is composed by a variable number of discs (1 to 7) with a mass of $m = 25$ kg each, by the holder, $m_h = 5,5$ kg and by a supporting chain, $m_{ch} = 3$ kg. Therefore the payloads applied on the boom end are in the range:

$$m_l = 33,5 \div 183,5 \text{ kg}. \tag{3.40}$$

Boom Since there is not any datasheet available, the mass of the boom is unknown. Thus it is required to model it, in order to obtain an approximation of the mass.

As it is possible to see in Fig. 2.1 at page 8 the boom is composed by two metal rods of the same length, one inserted into the other. In order to simplify the model, the mass will be calculated according to the following approximations: the boom will be considered closed - i.e. the black rod is as long as the orange one and it is located along the whole length; the oblique shape of the orange rod will be approximated with the average along the whole length. The outcome of the approximations and a section of the boom is shown in Fig. 3.6.

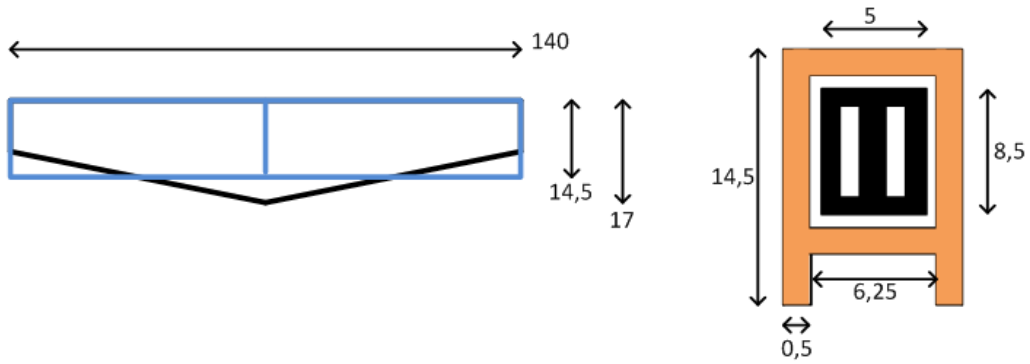

Figure 3.6: Schematic of the boom (measures in cm)

With the given measures, the area of a boom section and the total volume of each of the two halves result:

$$A_{\text{sec}} = 4 \cdot 10^{-3}\ m^2\,, \qquad V_{\text{boom}} = 2,8 \cdot 10^{-3}\ m^3 \tag{3.41}$$

Now, multiplying by the mass density of common steel ($\rho_s = 7820\ kg/m^3$), yields:

$$m_{b1} = m_{b2} = 21,9\ kg \tag{3.42}$$

Angles During the piston stroke, the joints' angles vary as follows:

$$\alpha = 85^\circ \div 120^\circ$$
$$\beta = 95^\circ \div 60^\circ$$
$$\gamma = 80^\circ \div 115^\circ$$

Finally, the values of acting force and required pressure (i.e., force divided by piston head area) in static conditions, during the whole movement are depicted in Fig. 3.7. Their averages are shown in Eq. (3.43) and Eq. (3.44).

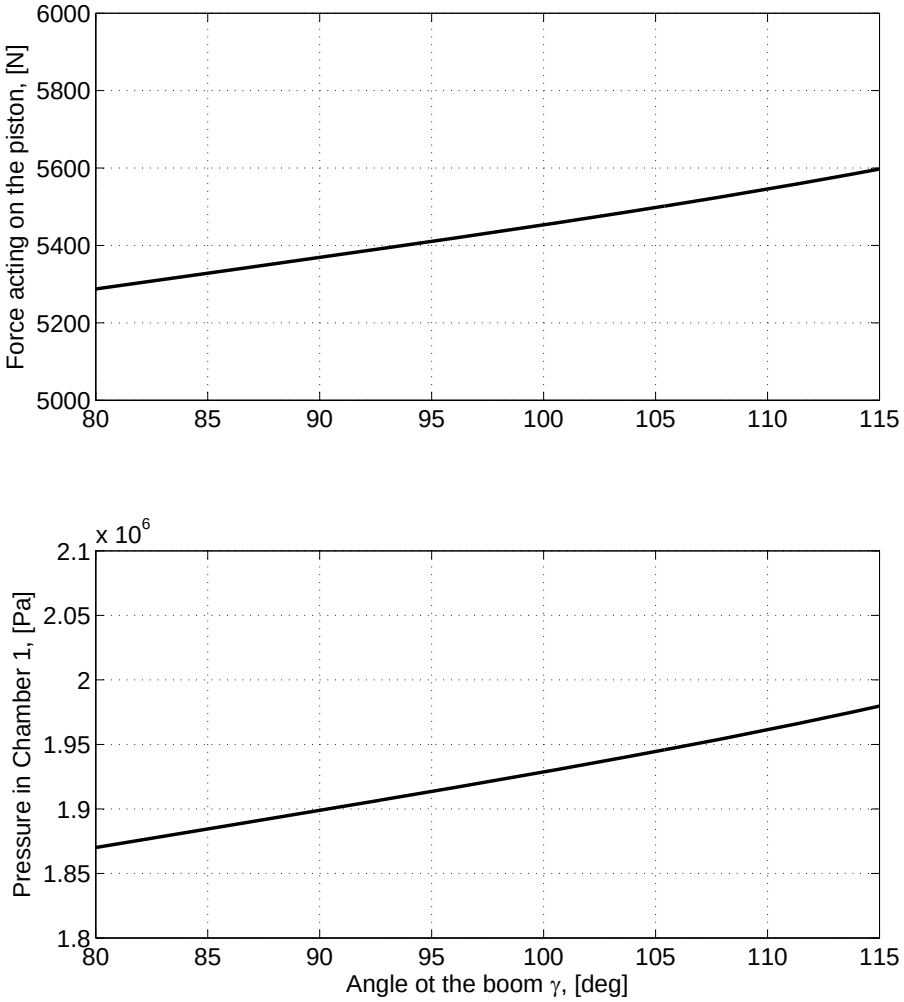

Figure 3.7: Values of acting force and required pressure ($m_l = 183,5$ kg)

$$F_{\mathrm{c,avg}} = 5,44 \cdot 10^3 \ N \tag{3.43}$$

$$p_{\mathrm{c,avg}} = 1,92 \cdot 10^6 \ Pa \tag{3.44}$$

It is worth noticing that the weight distribution during the whole movement is almost constant and the values barely deviate from the average.

3.3.1 Laplace Description of the Load

After obtaining the acting force, the second step would be to identify the parameters for the Laplace description of the load (3.36). Nonetheless, in the practice, this strategy has shown not to be applicable for this particular case. Actually, in the case pressure variation in both the lines is due to the elasticity of the system only, it could be assumed slowly variable (i.e., quasi-constant) during each movement. Then, the derivation of a control strategy, applying the Laplace transform, is straightforward and the second order model fits well the load. Therefore, it would be possible to relate the pressure in the system with the load movements according to the model.

Unfortunately, for the test setup, an unexpected phenomenon was noticed and it caused the necessity to follow a different strategy. The problem will be outlined in the following section and the alternative solution will be explained in Section 3.4. Anyhow, the physical model developed so far, will be used to precisely evaluate the variation of potential energy of the load for the efficiency calculation in Section 3.7.

3.3.2 Displacement Ratio and Pressure Peaks

The implemented test setup has manifested peculiar behaviours since the early beginning of the measurements. Especially during the lifting movement, some pressure peaks were noticed in the hydraulic lines. More precisely, the pressure appeared to grow quickly up to critical values in the case either a long movement or a fast one were required. The only possible explanation of this circumstance is that an opposing force dependent on velocity and displacement of the piston is generated in the system. Although this phenomenon could appear as a strongly marked damper-spring effect of piston and payload coupling, the values of the pressure turned out to be remarkably high and unpredictable to suit this model.

The reason of this unusual behaviour can be found analysing the phys-

ical dimensioning of hydraulic side of the system. In order to simplify the following deduction, all the formulas and relations will be given for the ideal components, without considering losses and friction. Nonetheless, the results remain valid for the practical system. Let us start the investigation, then, from the hydraulic cylinder, which is the conjunction point of the two sides of the system.

Eq. (3.24) and Eq. (3.25) at page 31 describe the volume in the two cylinder chambers at a certain time during each movement. Making the displacement the explicit quantity, yields:

$$\begin{cases} x_c(t) = \dfrac{V_1 - V_{01}}{A_1} \\ x_c(t) = -\dfrac{V_2 - V_{02}}{A_2} \end{cases} \tag{3.45}$$

The piston displacement $x_c(t)$ must be instantly the same as seen from both the chambers, so the two equations can be equated, yielding:

$$\frac{A_2}{A_1} = -\frac{V_2 - V_{02}}{V_1 - V_{01}} \simeq 0,75 \tag{3.46}$$

Equation 3.46 relates the piston head areas ratio with the volume ratio in the two chambers. Recalling (2.10) at page 19, for the test setup it corresponds to about 0,75.

Let us proceed finding a relation between the cylinder chambers volumes and the oil flow delivered by the pumps. In detail, the volume at a certain time during each movement is given by the sum of the initial volume and the amount of flow received at the chamber inlet since the movement started, in formulas:

$$\begin{cases} V_1 = V_{01} + \int_0^t Q_1(s)ds = V_{01} + D_1 \int_0^t \dot{\theta}_p(s)ds \\ V_2 = V_{02} - \int_0^t Q_2(s)ds = V_{02} - D_2 \int_0^t \dot{\theta}_p(s)ds \end{cases} \tag{3.47}$$

where the second equality comes from the definition of delivered flow for the ideal pump, recalling that the rotational speed $\dot{\theta}_p(t)$ of the two pumps is forced to be the same. In order to describe the flow, the equations can be written as:

$$\begin{cases} D_1 \int_0^t \dot{\theta}_p(s)ds = V_1 - V_{01} \\ D_2 \int_0^t \dot{\theta}_p(s)ds = -\left(V_2 - V_{02}\right) \end{cases} \tag{3.48}$$

Now, by substitution of the obtained relations (3.48), in the volume ratio equation (3.46), yields:

$$\frac{A_2}{A_1} = \frac{D_2 \int_0^t \dot{\theta}_p(s)ds}{D_1 \int_0^t \dot{\theta}_p(s)ds} \tag{3.49}$$

$$\frac{A_2}{A_1} = \frac{D_2}{D_1} \tag{3.50}$$

The obtained equality (3.50) states that the *piston head areas ratio* **must match** as closely as possible the *pump displacements ratio*, in order to guarantee a harmonic and functional behaviour of the system.

This condition is **not satisfied** for the particular implementation described. In the fact, recalling the pump displacements ratio already calculated in Eq. (2.3) at page 17:

$$0,75 \simeq \frac{A_2}{A_1} \neq \frac{D_2}{D_1} \simeq 0,63 \tag{3.51}$$

The **displacement sizing error** is therefore about 16%.

From this very first test setup, an important piece of information is then acquired: this error value is definitely too high to satisfy the system requirements. Its direct effect is to generate a flow difference between the two hydraulic lines, which engenders a breaking force opposed to the piston movement. This breaking force is the fundamental cause of the observed pressure peaks. In order to study the whole setup, it is hence necessary to rebuild it, keeping in consideration that the displacements ratio error must be kept remarkably lower.

Once the the issue has been identified and described, it is essential to figure out a solution to deal with this problem for the specific test setup. In this work it is decided to follow a *black-box approach*.

Black-box Approach The chosen way to deal with the described problem is to give up on modelling the load behaviour for control purposes. From now on, the combination of physical load and system side 2 will be assumed, altogether, as an unpredictably variable load. This strategy gives the possibility to define a control technique which takes advantage of the side 1 information only. It, moreover, evaluates the possibility to be applied on a one-sided

directly driven hydraulic system in common working condition. Actually, the presence of a variable load is quite usual in various applications, such as working machines, in which, for example, the weight of the load or the force required to dig the soil could be not known or predictable before the working cycle starts. Therefore, the results of this research could be applied in these fields and they could be even upgraded for a double-sided system, employing a well sized test setup.

In this scope, the pressure of line 1 remains the fundamental quantity which gives information about the unpredictable force acting against the piston movement. In the fact, the acting force is strictly linked to the pressure outcome generated. Nevertheless, the final aim is to keep the pressure as unknown quantity, for this aim, it is essential to find a relation between this value and another known physical measurement. The last available chance is to obtain an estimation of the chamber pressure from the torque feedback of the motor. The pursued procedure will be described in the following Section.

3.4 Pressure Estimation

For the sake of a uniformed description of the relation between the torque measured at the motor shaft and the pressure built in chamber 1, it is necessary to consider the torques which act in a hydraulic pump. The ideal torque pressure relation is:

$$T_p = D_1 p_1 \tag{3.52}$$

where $T_p =$ torque at the pump shaft,
$D_1 =$ displacement of pump 1,
$p_1 =$ pressure in chamber 1.

Remark 1: Torque input Equation (3.52) should employ the torque input measured at the pump shaft. Let us use, instead, the torque read at motor shaft. This simplification appears to be essential to model and control the test setup, because of an unpredictable behaviour of the torque in distribution shaft (described and commented in Remark 1 in Section 3.7). For this reason, for the control aim, the distribution shaft will be considered as a part of the pump itself and its power losses will be included in the final relation. However, the actual angular speed at the pump shaft could be obtained. Nonetheless, in order to uniform the quantities and to avoid the

introduction of the gear-box ratio, also for the speed, the one measured at electric motor shaft will be used.

In the practice, at least three sources of losses can be noticed ([29],[43]):

1. **Damping Torque:** It is proportional to the pump speed and it is required to shear the fluid in the small clearances between mechanical elements in relative motion. It can be written as:

$$T_d = B_d \dot{\theta}_m \tag{3.53}$$

where $T_d =$ damping torque,
$B_d =$ viscous damping coefficient,
$\dot{\theta}_m =$ angular speed at the motor shaft.

2. **Friction Torque:** It is due to friction originating at the contact of surfaces moving relative to each other. In particular, for a gear pump, the opposing forces are located at gear tooth tips, at gear sides, at seals, in bearings and on gear teeth. These surfaces can be generally identified as the load-supporting surfaces in a gear pump. This friction force is nearly independent from the relative speed of the surfaces, i.e., the angular speed of the pump. Nonetheless, it is directly proportional to the force normal to the surface which in turn is a function of the unbalanced pressure acting across the pump. At last, these forces are opposing to the motion direction, for this reason they have the same sign of the speed. The resulting torque can be summarized as:

$$T_f = \frac{\dot{\theta}_m}{|\dot{\theta}_m|} C_f p_1 \tag{3.54}$$

where $T_f =$ friction torque,
$C_f =$ internal friction coefficient.

3. **Seal Torque:** It is a small torque required to overcome seal friction (T_s), that is constant but reverses direction with speed. This torque can be written as:

$$T_s = \left(\dot{\theta}_m / |\dot{\theta}_m|\right) |T_s| \tag{3.55}$$

Summing up the previously explained terms, a more precise description

of the torque losses results:

$$T_p = D_1 p_1 + B_p \dot{\theta}_m + \frac{\dot{\theta}_m}{|\dot{\theta}_m|} C_f p_1 \tag{3.56}$$

where $T_p =$ is the torque applied to the pump shaft.

Now making pressure the explicit parameter:

$$p_1 = \frac{T_m - B_p \dot{\theta}_m - \left(\dot{\theta}_m / |\dot{\theta}_m|\right) |T_s|}{D_1 + \left(\dot{\theta}_m / |\dot{\theta}_m|\right) C_f} \tag{3.57}$$

This latter formula can be split into two equations, depending on the sign of shaft speed, both of them in the first order of torque and speed. In order to uniform this description, the different behaviour for negative and positive speed can be matched with a third order curve with different slope in initial and final part and with flat connection part around the zero speed. According to this idea, the equation finalized to estimate the pressure is researched among the two variables equations, in third power of T_1 and linearly in $\dot{\theta}_m$. In detail the speed acts as a offset moving the third order torque curve. Moreover, a constant parameter is kept to describe the seal torque. Therefore, the curve can be described according to the following model:

$$p_1 = A_{00} + A_{10} T_1 + A_{20} T_1^2 + A_{30} T_1^3 + A_{01} \dot{\theta}_m \tag{3.58}$$

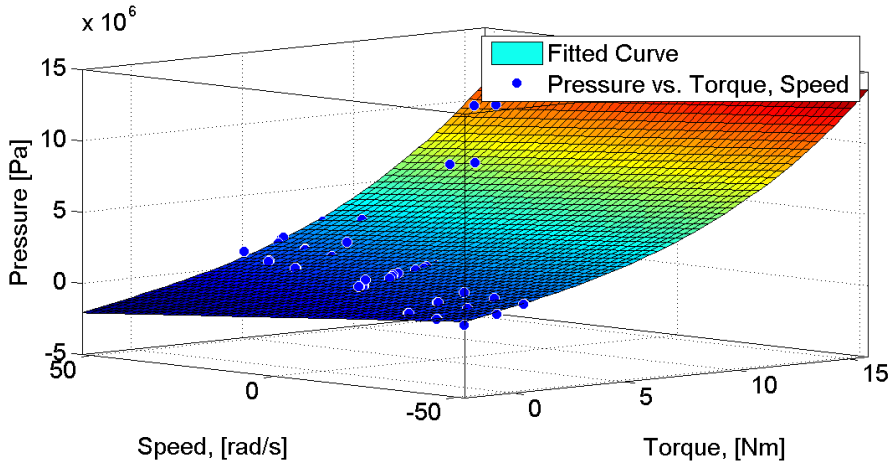

Figure 3.8: Determined pressure vs. torque, speed curve

Dedicated measurements were carried out with the aim of evaluating pressure vs. torque, speed in various operating conditions of the system. The results were analysed and used to obtain a valid estimation curve model which matches the requirements. The resulting curve is depicted in Fig. 3.8 and the numeric values of the parameters are:

$$A_{00} = -1,235 \cdot 10^5, \quad A_{10} = 3,338 \cdot 10^5, \quad A_{20} = 7,323 \cdot 10^3,$$
$$A_{30} = 1,363 \cdot 10^3, \quad A_{01} = -2,355 \cdot 10^4$$

3.5 Elasticity of the System

Interaction of the spring effect of a liquid and the mass of mechanical parts gives a resonance in nearly all hydraulic components. Resonance is often the main limitation to dynamic performances. The fluid spring is characterized by the value of the bulk modulus. The bulk modulus of a liquid can be substantially lowered by entrained air and/or mechanical compliance [29]. Nonetheless, for the scope of the current investigation, the dynamic performances are mostly not taken into account at all, since the aim is to analyse mainly the steady-state performances of the system.

Nevertheless the effective bulk modulus of the system was calculated, according to the theory outlined in [29], and employed in early versions of the control strategy. The result was not showing any relevant difference when compared to the version which neglects the elasticity phenomenon. The reason is attributed to the high value of this parameter which, appearing only at the denominator in the continuity equation (3.30), makes the contribution of this term negligible. Nevertheless, further studies in the field and improvement of the model could take in consideration also this aspect.

3.6 Final Control Equation

As a last step in the control equation deduction it is necessary to make the piston position the explicit variable from the continuity equation 3.30, obtained in the first part of this chapter, at page 33. The independent variables must be the angular speed of the pump shaft, which is computable as the motor speed feedback times the gear-box ratio, and the pressure in chamber 1, which can be estimated as explained in Section 3.4.

In order to make the calculations simpler, volume variation in chamber 1 is not considered. This assumption is justified by the fact the volume variation due to the piston movement is actually not relevant when compared with the volume of the whole forward chamber. Moreover, this quantity appears only divided by the bulk modulus, which numerical value, as stated in Section 3.5, overwhelms the small volume variations. Therefore Eq. (3.30) becomes:

$$D_{p1}\dot{\theta}_p - C_{s1}p_1 = A_1\frac{x_c}{dt} + \left(\frac{V_{01}}{\beta}\right)\frac{dp_1}{dt} \tag{3.59}$$

Moreover, the slip coefficient C_{s1}, as seen in Section 3.2.1, can be assumed quasi-constant for what concerns the operating pressures range. For this reason its variations will not be explicit. The application of Laplace transform to Eq. (3.30), yields:

$$D_{p1}\dot{\theta}_P(s) - C_{s1}P_1(s) = A_1X_c(s)s + \left(\frac{V_{01}}{\beta}\right)P_1(s)s \tag{3.60}$$

which gives, for $X_c(s)$:

$$X_c(s) = \frac{D_{p1}}{A_1}\frac{\dot{\theta}_P(s)}{s} - \frac{C_{s1}}{A_1}\frac{P_1(s)}{s} - \left(\frac{V_{01}}{\beta}\right)P_1(s) \tag{3.61}$$

Finally, the Laplace inverse transform of this latter equation yields:

$$x_c(t) = x_0 + \frac{D_{p1}}{A_1}\int_0^t \dot{\theta}_p(\tau)d\tau - \frac{C_{s1}}{A_1}\int_0^t p_1(\tau)d\tau - \left(\frac{V_{01}}{\beta}\right)p_1(t) \tag{3.62}$$

Therefore, Eq. (3.62) is the **final control equation** which is applied to predict the piston position during each movement. The integrals must be reinitialized to zero every time a single movement ends, while the previous condition is kept by means of the last reached position x_0. In the practice, the pressure is replace by its estimation from torque and speed. Moreover the last term concerning the elasticity of the system is barely relevant because of the overwhelming value of the bulk coefficient, hence it might be neglected without loss of precision. The slip coefficient varies according to the previously described model (Section 3.2.1).

3.7 Efficiency Equations

In order to evaluate the performance of the system during both the lifting and the lowering movement, it is necessary to introduce the basic equations over the energy balance. During the lifting movement, the test setup implements through the electric drive, the conversion from electric three-phase power, taken from the power line, to three-phase PWM power input to the motor. This machine, then, generates mechanical power and delivers it, by means of the gear box, to the two pumps. The pump rotation delivers oil flow, generating fluid power in the hydraulic lines, which is delivered to the piston. This last device converts it back into mechanical power, by way of linear movement, which final aim is to lift the load, increasing its potential energy. During the lowering movement, the power flow, following the same steps, goes in the other way round.

Therefore, it is possible to evaluate the efficiency of each power conversion dividing the system according to the scheme in Fig. 3.9.

Remark 1: Pumps efficiency Before starting the derivation of the equations, it is worth remarking it is not possible to analyse properly the efficiency of each pump on its own. This because, although torque and angular speed at the motor shaft are well known quantities, obtained from motor feedback, it is not possible to estimate, in this configuration, the amount of torque delivered to each pump. In other words, the splitting ratio of the generated torque is unknown. This ratio would depend on the loads on the two hydraulic lines, and could be estimated evaluating their pressure. Nonetheless, this idea does not fit to this particular system. In effect the pressure peaks which are generated in the lines because of the previously discussed displacement ratio error, make the system behaviour unpredictable. In particular, the raising pressure in hydraulic line 2, being the rotational speed imposed by the electric motor, force pump 2 to work as a motor, braking the natural oil flow. This situation introduces an assistive torque in the transmission shaft but, at the same time, the raising pressure in system chamber 1 increases the torque requirement to pump 1.

The final effect of this anomalous behaviour is to instil a hydraulic power loop between the pumps: while pump 2 acts as a motor introducing torque, the torque requirement for pump 1 raises. This situation transfers in a internal power consumption, due to the loop conversion between mechanical

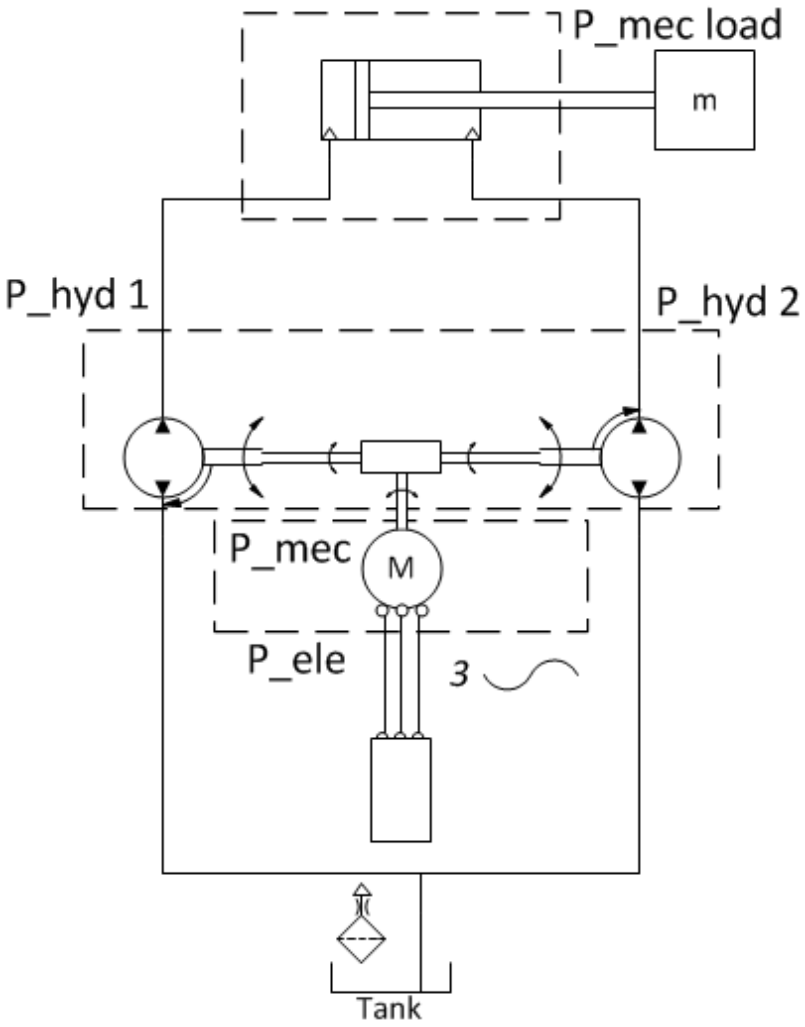

Figure 3.9: Schematic of the powers in the system

and fluid power. The outcome of this phenomenon is merely to waste part of the input energy, because of the internal losses in pumps, transmission and hoses.

For these reasons the ensemble of the transmission and the two pumps will be treated as a whole closed system with input/output terminal the motor shaft and the two hydraulic lines.

Remark 2: Electric Power As far as the electric power calculation is concerned, the efficiency of the frequency converter (electric drive) will not be taken into account since a measurement device was not available. Moreover the efficiency of this device is supposed to be considerably high, therefore the omission is not remarkably relevant.

The power measurements at the PWM electric motor input are acquired by means of Hioki 3390 power analyzer [47]. During the lifting movement, when the drive is delivering power to the electric motor, the active power is positive and the the measurements are carried out. Vice versa, during the lowering movement, when the regenerative torque at the motor shaft is the power source, this particular drive is not prepared to work in regenerative mode because of the absence of any braking resistor or accumulator device. For these reason, the drive is programmed to set the voltage and current vectors in the same direction, obtaining null power coefficient. Under this conditions the power is only reactive, and the measured power equals zero. For the motor efficiency were therefore kept the same values obtained during the lifting movement, in effect the brushless motor is supposed to present symmetrical efficiency during both motoring and regenerating. This approach can give an estimation of the percentage of energy which would be possible to recover introducing an accumulator device fitted.

First of all it is necessary to split the efficiency calculations for the lifting movement from the ones dedicated to the lowering one. Let us start from the first case.

3.7.1 Lifting Movement

The efficiency equations describing the lifting movement are quite straightforward. The input is the electrical power read at the electric motor terminals and the final output is the variation of potential energy applied to the load. Thus the overall efficiency is:

$$\eta_{\text{tot,up}} = \frac{\Delta E_{\text{pot}}}{E_{\text{ele}}} \tag{3.63}$$

where $E_{\text{ele}} =$ electric energy at motor terminals,
$\Delta E_{\text{pot}} =$ variation of load potential energy,
$\eta_{\text{tot,up}} =$ overall efficiency during lifting.

The electric energy is calculated as the time integral of the active power. The variation of potential energy as the space integral of force wielded by the payload, on the whole lifting. This force varies during the movement

according to the previously derived equation (3.39), at page 38. In formulas:

$$E_{\text{ele}} = \int P_{\text{ele}} dt = \int (V_1 I_1 + V_2 I_2 + V_3 I_3) dt \tag{3.64}$$

$$\Delta E_{\text{pot}} = \int_0^h F_c dx \tag{3.65}$$

where $F_c =$ force wielded by they payload,
$V_1,\ V_2,\ V_3 =$ phase voltages,
$I_1,\ I_2,\ I_3 =$ phase currents.

The efficiencies of the different system parts are:

$$\eta_{\text{mot,up}} = \frac{E_{\text{mec}}}{E_{\text{ele}}} = \frac{\int P_{\text{mec}} dt}{\int P_{\text{ele}} dt} \tag{3.66}$$

$$\eta_{\text{pumps,up}} = \frac{E_{\text{h,1}}}{E_{\text{mec}} + E_{\text{h,2}}} = \frac{\int P_{\text{h,1}} dt}{\int P_{\text{mec}} dt + \int P_{\text{h,2}} dt} \tag{3.67}$$

$$\eta_{\text{cyl,up}} = \frac{\Delta E_{\text{pot}} + E_{\text{h,2}}}{E_{\text{h,1}}} = \frac{\int F_c dx + \int P_{\text{h,2}} dt}{\int P_{\text{h,1}} dt} \tag{3.68}$$

where $E_{\text{h,1}} =$ hydraulic energy in line 1,
$E_{\text{h,2}} =$ hydraulic energy in line 2,
$P_{\text{mec}} =$ mechanical power at the motor shaft,
$P_{\text{h,1}} =$ hydraulic power in line 1,
$P_{\text{h,2}} =$ hydraulic power in line 2,
$\eta_{\text{mot,up}} =$ efficiency of the electric motor during lifting,
$\eta_{\text{pumps,up}} =$ efficiency of the ensemble of pumps and distribution line during lifting,
$\eta_{\text{cyl,up}} =$ efficiency of the hydraulic cylinder during lifting.

The employed powers are calculated as follows:

$$P_{\text{mec}} = T_m \dot{\theta}_m \tag{3.69}$$

$$P_{\text{h,1}} = p_1 Q_1 = p_1 A_1 \dot{x}_c \tag{3.70}$$

$$P_{\text{h,2}} = p_2 Q_2 = p_2 A_2 \dot{x}_c \tag{3.71}$$

where $T_m =$ torque at the motor shaft,
$p_1,\ p_2 =$ pressures in hydraulic lines,
$Q_1,\ Q_2 =$ flows in hydraulic lines,
$A_1,\ A_2 =$ piston head areas,
$\dot{x}_c =$ piston velocity.

As a remark, while the pressures values are directly read from sensors, the amounts of flow are estimated using the cylinder as a virtual flow sensor. Which means, according to the last term of (3.70) and (3.71), it is possible to estimate the flow in each line as piston speed times head area.

The numeric results for the investigated system will be given and analysed in Section 5.2.

3.7.2 Lowering Movement

During the lowering, the calculation of system efficiency requires more attention, in the fact, it is necessary to distinguish two different situations: *slow lowering* and *fast lowering*.

Remark 3: Free-fall speed Let us introduce the free-fall speed. This quantity has not to be interpreted as the speed the load would have when dropped, untrammelled from system constrains. Otherwise, it has to be understood as the **neutral lowering speed**, that is the velocity which the load would have when free-falling under the system constrains but without any input from the motor. This speed is given by the amount of pressure generated by the load weight in chamber 1. This hydraulic quantity, in the fact, would force the pump (working as a motor in this case) to rotate at a certain angular speed. This limit speed is given by the friction of the pump gears and transmission line.

Slow Lowering

In the case the payload is heavy and/or the lowering speed is slow the system acts against the natural free-fall, braking it. In this condition the system input is the potential energy acquired by the load during the previous lifting and the output is the mechanical energy at motor shaft, engendered by the regenerative torque. The evidence which allows to recognize this situation is given by the directions of angular speed and torque at the motor shaft. In

particular, to have regenerative torque, the latter must have opposite sign of the former. In detail, negative angular speed, i.e. lowering movement, and positive torque measurement. To summarize, this particular case occurs when the required lowering speed is lower than the previously defined free-fall speed.

Under these conditions, the calculations have just to be carried out in the other way round, if compared to the lifting movement. Thus the overall efficiency is:

$$\eta_{\text{tot,down}} = \frac{E_{\text{ele}}}{\Delta E_{\text{pot}}} = \eta_{\text{mot,down}} \frac{E_{\text{mec}}}{\Delta E_{\text{pot}}} \tag{3.72}$$

where $\eta_{\text{tot,down}} =$ overall efficiency while lowering,
$\eta_{\text{mot,down}} = \eta_{\text{mot,up}} =$ efficiency of the electric motor.

As already stated in Remark 2 of the current Chapter, it is not actually possible to measure the regenerative electric power, therefore, for the electric motor efficiency, the value calculated for the lifting movement is kept and the calculations are, in truth, carried out according to the formula in the last term of Eq. (3.72).

The efficiencies of the different system parts are:

$$\eta_{\text{cyl,down}} = \frac{E_{\text{h,1}}}{\Delta E_{\text{pot}} + E_{\text{h,2}}} \tag{3.73}$$

$$\eta_{\text{pumps,down}} = \frac{E_{\text{mec}} + E_{\text{h,2}}}{E_{\text{h,1}}} \tag{3.74}$$

where $\eta_{\text{cyl,down}} =$ efficiency of the hydraulic cylinder while lowering,
$\eta_{\text{pumps,down}} =$ efficiency of the ensemble of pumps and distribution line while lowering.

Fast Lowering

This case arises when the payload is light and/or the lowering speed is fast. The systems acts as a motor, speeding up the free-fall of the load. In this condition, the potential energy acquired by the load during the previous lifting, generates the free-fall speed, therefore, the energy is fully consumed and cannot be recovered. The system input is the mechanical energy at the motor shaft, while the output is the additional energy produced on the load to overcome the free-fall speed. The evidence which allows to recognize this situation is, again, given by the directions of angular speed and torque at

the motor shaft. In particular, the latter must have the same sign, hence both negative. To summarize, this particular case occurs when the required lowering speed is higher than the previously defined free-fall speed.

Under this state, the calculations become more involved. The overall efficiency is:

$$\eta_{\text{tot,down}} = \eta_{\text{mot,down}} \frac{E_{\text{load}}}{E_{\text{mec}}} \tag{3.75}$$

where $E_{\text{load}} =$ mechanical energy imparted to the load in order to overcome the free-fall speed.

It is possible to obtain an estimation of E_{load} considering the variation of mechanical power applied to the load during lowering and comparing it to the free-fall case. If only the gravitational force is acting, the work would be:

$$P_{\text{pot}} = \frac{\Delta E_{\text{pot}}}{t_f} \tag{3.76}$$

where $t_f =$ free-fall time,
$P_{\text{pot}} =$ work performed by the gravitational force only, on the load.

When, instead, also the additional force produced by the motor is acting, the time required for the movement is shorter and the global work of the two forces becomes:

$$P_{\text{pot+load}} = \frac{\Delta E_{\text{pot+load}}}{t_m} \tag{3.77}$$

where $t_m =$ measured time,
$P_{\text{pot+load}} =$ work performed by the sum of gravitational force and additional force, on the load.

The deduction of the additional power is then straightforward:

$$P_{\text{load}} = P_{\text{pot+load}} - P_{\text{pot}} = \frac{\Delta E_{\text{pot+load}}}{t_m} - \frac{\Delta E_{\text{pot}}}{t_f} \tag{3.78}$$

where $P_{\text{load}} =$ work performed by the additional force only, on the load.

Finally the energy contribution is obtained by time integral:

$$E_{\text{load}} = \int_0^{t_m} P_{\text{load}} dt \tag{3.79}$$

In order to calculate internal efficiencies, only the active load energy will be used. Inside the system, this energy is given by the sum of the integrals of hydraulic power in line 2, which pushes the piston head 2 downwards, and of the *effective hydraulic power* in line 1, i.e., the difference between the power calculated in free-fall conditions and the measured power. This latter quantity is different from the free-fall one because the pump 1 motion speeds up the flow in line 1, generating a pressure differential in the line, which supports the load in a weaker way, allowing the fast lowering. This quantity can be calculated as:

$$\Delta E_{\mathrm{h},1} = E_{\mathrm{h},1,\mathrm{f}} - E_{\mathrm{h},1,\mathrm{m}} = p_{1,\mathrm{f}} Q_{1,\mathrm{f}} - p_{1,\mathrm{m}} Q_{1,\mathrm{m}} \tag{3.80}$$

where
$\Delta E_{\mathrm{h},1}$ = hydraulic energy differential in line 1,
$E_{\mathrm{h},1,\mathrm{f}}$, $E_{\mathrm{h},1,\mathrm{m}}$ = hydraulic energies in line 1, calculated in free-fall condition and measurement condition,
$p_{1,\mathrm{f}}$, $p_{1,\mathrm{m}}$ = pressures in line 1, calculated in free-fall condition and measurement condition,
$Q_{1,\mathrm{f}}$, $Q_{1,\mathrm{m}}$ = flows in line 1, calculated in free-fall condition and measurement condition.

Specific measurements were carried out for the aim of measuring free-fall quantities in the system. Once these values are known, the efficiencies of the different system parts might be calculated as:

$$\eta_{\mathrm{cyl,down}} = \frac{\Delta E_{\mathrm{h},1}}{E_{\mathrm{load}} + E_{\mathrm{h},2}} \tag{3.81}$$

$$\eta_{\mathrm{pumps,down}} = \frac{\Delta E_{\mathrm{h},1} + E_{\mathrm{h},2}}{E_{\mathrm{mec}}} \tag{3.82}$$

Finally, as for the lifting movement, the reader is addressed to Section 5.2, where the results obtained from the setup will be analysed.

Chapter 4

Software Implementation

The current Chapter is finalized to describe and explain the software written for the practical part of this thesis work; three different tools are required. A general logic diagram is given in Fig. 4.1, to help the reader in understanding the relations between the parts of the system and the scope of each software.

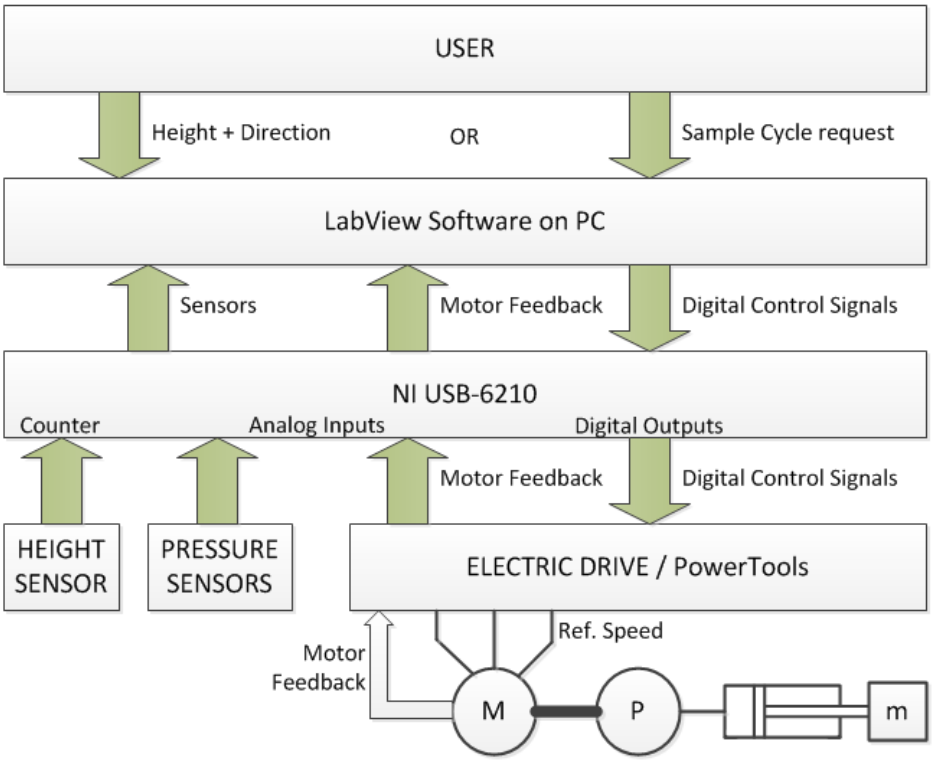

Figure 4.1: Logic diagram of the connections

First of all Emerson PowerTools software will be described. This tool is the basic interface in order to communicate directly with the drive, set up

basic input/output functions and drive parameters manage low level control command (such as move, move home, stop motion) and load the desired user programs.

Then National Instruments LabView is employed in order to manage higher level control strategy (such as flow control, position request, end-runs identification and sample cycles) and to read and write input/outputs of the system.

At last Matlab scripts are written in order to acquire data from LabView and Hioki Power Analyzer measurements, calculate efficiencies and model the load.

In the following, a section is devoted to each of these softwares.

4.1 PowerTools

In this Section, after the description of software features and their specific configuration, the user program designed in order to serve the control logic will be outlined.

4.1.1 Setup

- **Hardware Setup:** Simply by selecting the models of drive and motor used, PowerTools updates the related *Advanced Parameters* in the drive's memory. Those values are fundamental to obtain proper control and communication between drive and motor and, of course, to prevent critical damages. In the same window it is also possible to set the characteristics of the encoder inbuilt into the motor (Fig. 4.2).

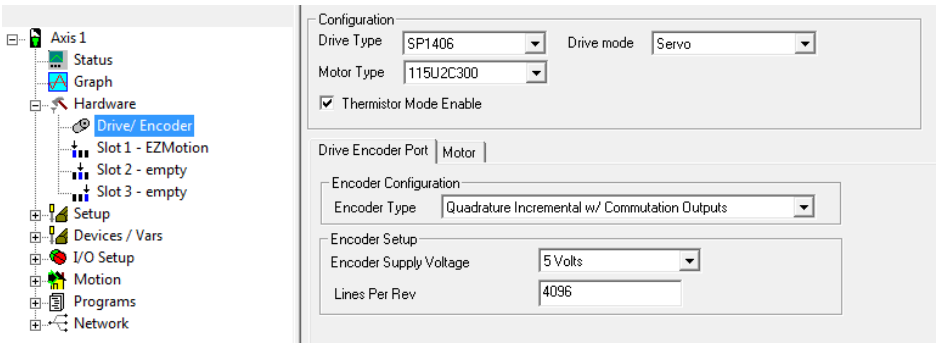

Figure 4.2: Hardware setup window

- **Analog outputs:** By means of this section it is possible to set up the parameters regarding output mode, scale and source; this is necessary to read the motor feedback. In Fig. 4.3 the employed configuration for speed and voltage is given.

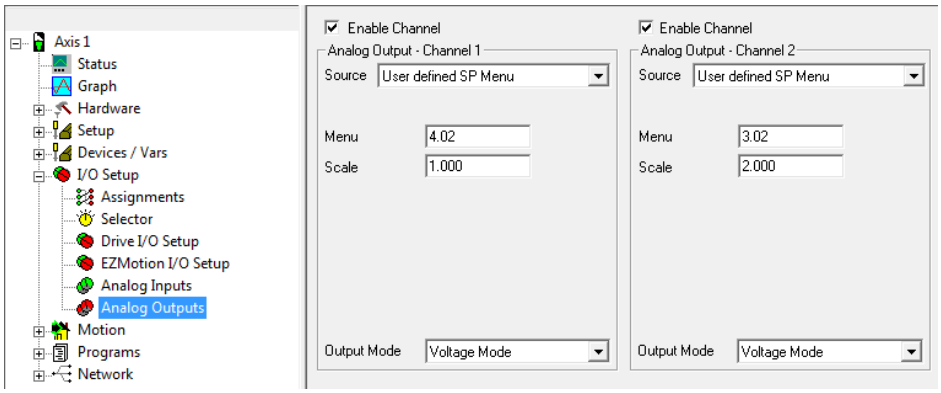

Figure 4.3: Analog Outputs

- **Setup NVM:** NVM values are all the parameter which can be modified at the start-up in the drive. For this application, for example, it is required to update the NVM regarding analog output configuration, in order to have speed and torque readings with the proper scale (Fig. 4.4).

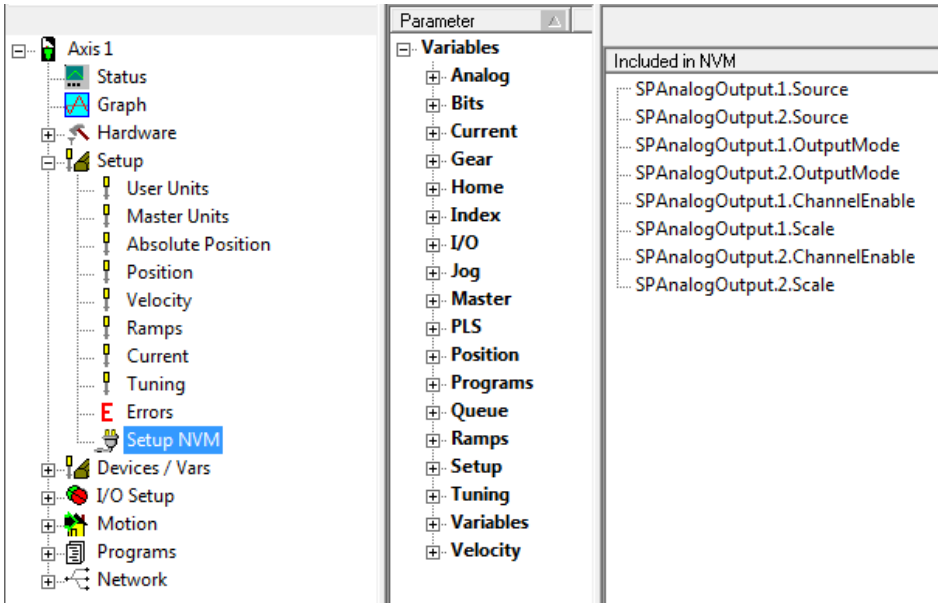

Figure 4.4: NMW values setup

- **Assignments:** In the assignment window it is possible to take advantage of any internal variable, status bit and input signal in order to enable other output or switches. In particular, as can be seen in Fig. 4.5, upon start-up the selector (see next paragraph) is enabled. As soon as the drive is active the user program starts its cycle and the digital inputs are sent to the selector.

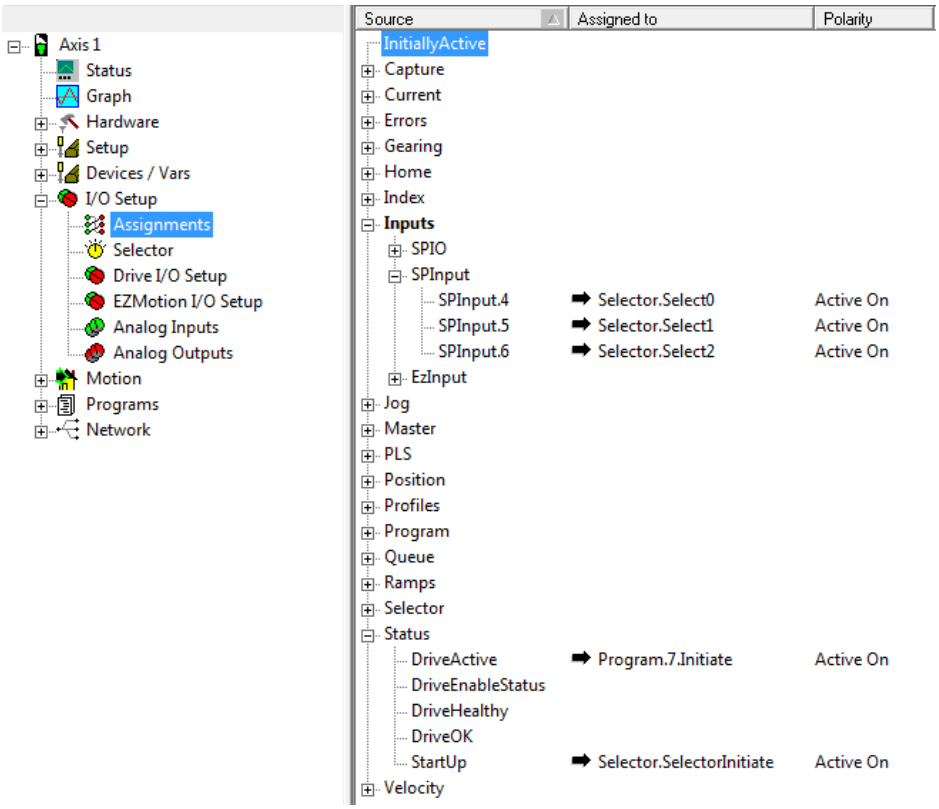

Figure 4.5: Assignments window

- **Selector:** It allows to implement a *Selector* for the digital inputs, which means working with combinations of them, instead of using each single signal on its own. This guarantees the possibility to have $2^{n_{bit}}$ virtual signals rather than only n_{bit} physical signals. This particular feature will be helpful for the implementation of the control logic, since the NI USB board offers only 4 digital outputs.

4.1.2 User Program

Even though the most demanding part of the control logic is managed through LabView (described in Section 4.2), the implementation of a small low-level user program was needed. Its purpose is to deal directly with the drive. It could be seen as an interpreter which translates high-level commands given by LabView in low-level action understandable for the drive. In detail, LabView elaborations produce variations on the digital signals read by the drive. The commutations of those signals, opportunely combined by the selector, induce different *states* of the user program, allowing the drive to initiate various movements.

A flow chart of the user program is depicted in Fig. 4.6 and the listing of the source code can be found in App. C.

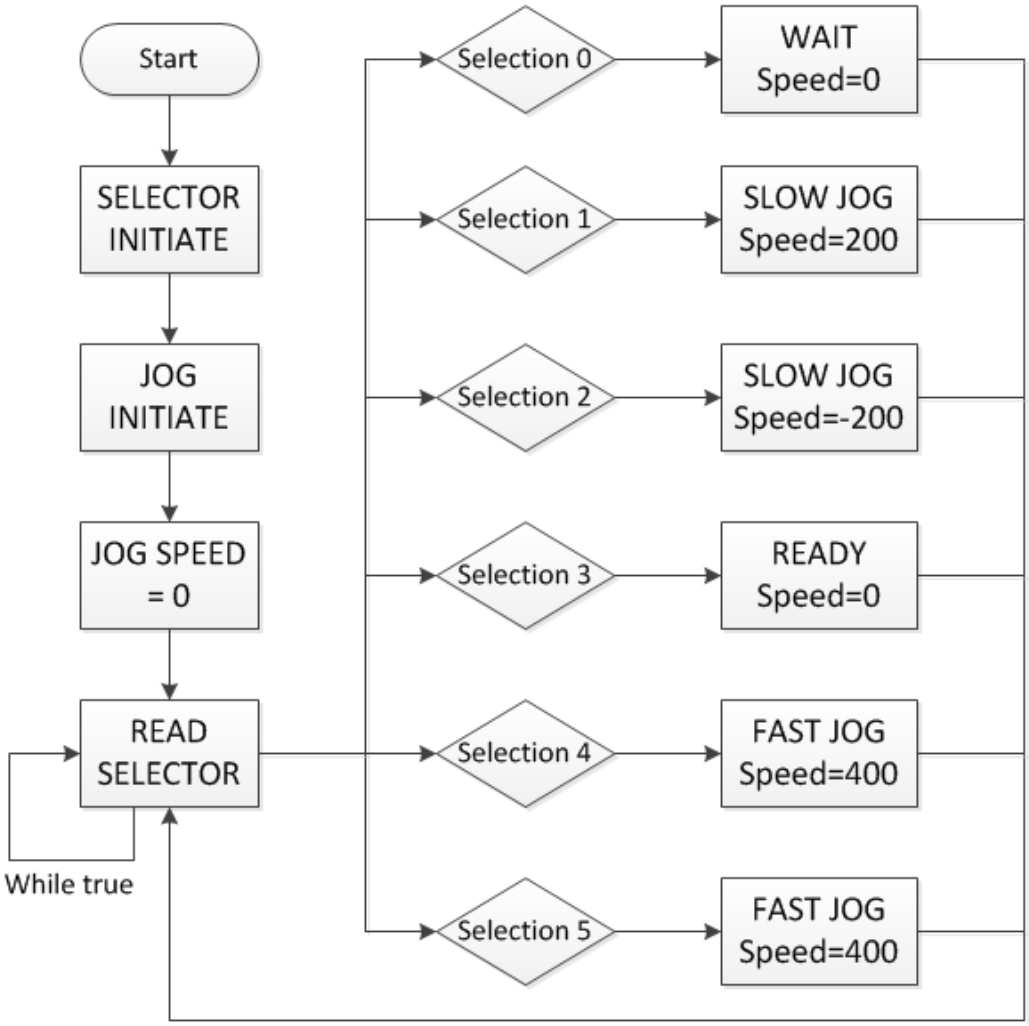

Figure 4.6: Flow chart of PowerTools user program.

In particular the user program is built to enable the motor movement (*jog*) on start up and then wait, on a *while-true loop*, until a changing in the selector status happens. For this software, 6 over the possible 8 combination of 3 bits are used:

- **Selection 0:** *Wait*, it is the first condition of the drive, before the real start of control logic. The drive waits for a variation on the selector. The software never cycle back to this status when left for the first time.
- **Selection 1, 2:** *Slow Jog*, they are slow positive and negative movements of the motor. They are used for initialization, homing procedures and reset after hitting the end-runs.
- **Selection 3:** *Ready*, the drive waits for the next input in a steady position. Differently from selection 0, this is the standard state in which the drive cycles after the first initialization.
- **Selection 4, 5:** *Fast Jog*, they are fast positive and negative movements of the motor. They are used for all the movements required by the user.

Remark: The speed of the fast jog movement is set to 400 rpm. For different tests the reference speed is changed in the user program, in order to make trials in various conditions.

4.1.3 Acceleration profiles

In hydraulics, the capability of the system to follow the reference in a smooth movement is often pursued. It is actually common, when operating with hydraulic actuators, to experience abrupt jerks especially in the first and in the last part of the movement. The tool given by Emerson to deal with this issue is the possibility to set up the acceleration profile according to different types: 5/8 S-Curve, 1/4 S-Curve, Linear, and S-Curve.

Once a curve is chosen, it works for all the motions. The "S-Curve" ramps offer the smoothest motion, but lead to higher peak acceleration/deceleration rates. "Linear" ramps have the lowest peak acceleration/deceleration rates but they are the least smooth ramp type. "5/8 S-Curve" ramps and "1/4 S-Curve" ramps use smoothing at the beginning and end of the ramp but have constant (linear) acceleration rates in the middle of their profiles. The

"5/8 S-Curve" is less smooth than the "S-Curve" but smoother than the "1/4 S-Curve".

S-Curve accelerations are very useful on machines where product slip is a problem. They are also useful when smooth machine operation is critical. Linear ramps are useful in applications where low peak torque is critical. Below there is a comparison of the 4 ramp types:

S-Curve:	Peak Acceleration =	2 x Average Acceleration
5/8 S-Curve:	Peak Acceleration =	1,4545 x Average
1/4 S-Curve:	Peak Acceleration =	1,142857 x Average Acceleration
Linear:	Peak Acceleration =	Average Acceleration

For the particular aim the **5/8 S-Curve** was chosen, with an acceleration of 4000 revs/min/s.

4.2 LabView

In this Section, the software written in order to accomplish the control strategy will be explained. Afterwards, particular examples of the code will be described in the details.

4.2.1 Software Structure

A flow chart of the user program is given in Fig. 4.7; the reader is advised to follow it during the explanation.

The software is organized in a case structure, containing different **states** (rectangular blocks in the flow chart) and it goes through them during the operations. When the program is launched, it automatically starts cycling in the **Wait** state. In this basic condition, LabView sets the Digital outputs to $[0, 0, 0]$ (Selection 0) and waits for user inputs.

In this state, the sole acceptable input is *Start* button which, when activated, transfers the system into **Initialize** state. Digital outputs are set to $[0, 0, 1]$ (Selection 1), the drive starts slow lifting mode, until the load is lifted up to 5 cm height.

When the fixed height is reached, ensuring the system is not in a end-run situation, the software automatically passes to **Move Home** state. Digital outputs are set to $[0, 1, 0]$ (Selection 2), the drive starts slow lowering mode, until low end-run is detected. Now the load is in home position, the estimated

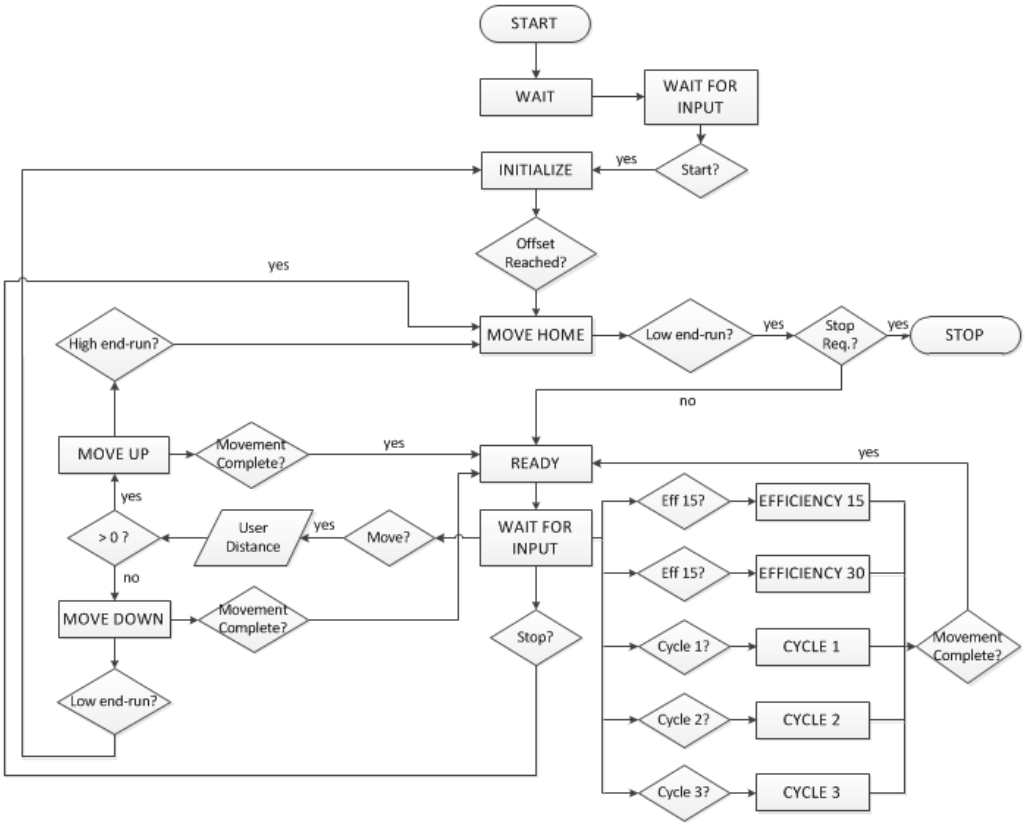

Figure 4.7: Flow chart of the software logic.
*Whenever a negative "if" returns to the asking process the branch it is not shown, for simplicity

position is set to 0 and system switches to **Ready** state (Digital outputs are set to $[0, 1, 1]$, Selection 3), where it waits for user inputs.

If a variation of the *Move* button is detected, the program verifies the required distance (reading the *Distance* entry in user panel) and start either a fast lifting (**Move Up** state, Dig. out. $= [1, 0, 0]$, Selection 4) or a fast lowering (**Move Down** state, Dig. out. $= [1, 0, 1]$, Selection 5). In this case, the movement continues until either the required distance is covered or one of the end-run condition arises.

If the movement is carried out properly, the system returns in **Ready** mode, waiting for a new input. Otherwise, if a *High end-run* occurs, the system is re-homed; else (*Low end-run* occurs) the system is re-initialized in order to drive off from the end-run, then, a homing procedure occurs.

If one of the *sample cycles* is required by pressing the relative button, the respective *timed structure* starts. Each timed structure is composed by various consecutive basic system operations, finalized to complete the more

complex cycle. Whenever a cycle ends, the system is pulled back to **Ready** state. The characteristics of each cycle will be described in Chap. 5.

If a variation of the *Stop* button is triggered, a particular case of homing procedure is required, in which, at the end, all the program variables are reset to the default state and the software is shut down.

In the following some chosen solutions will be discussed, supplying examples and figures from the software as well.

4.2.2 Sensors Readings

In order to get the real time measurements from the NI USB Board inputs, various input channels must be opened, and the readings must be converted from voltage values into meaningful engineering units.

Analog Channels (see Fig. 4.8)

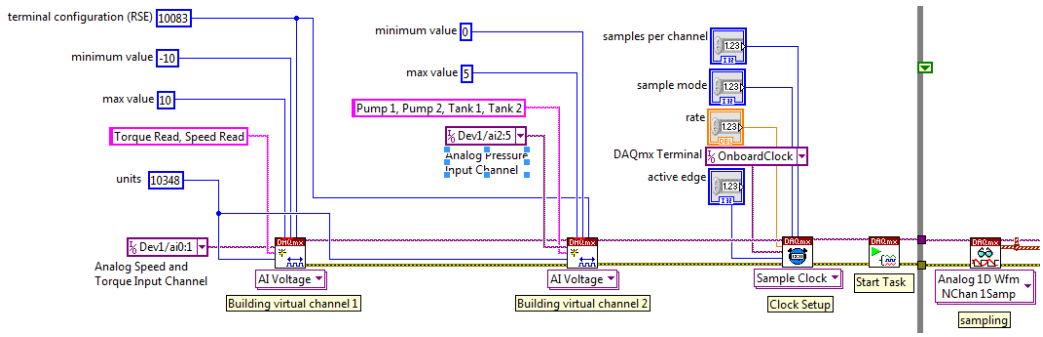

Figure 4.8: Initialization of analog input channels

In the same DaqMX task, the analog channels for speed, torque and pressure readings are opened. While torque and pressure can be in the same virtual channel, since they have the same voltage range, the four pressure sensors are conveyed in another virtual channel, with reduced input range. The clock for sampling is started and, inside the while true loop, one sample on each channel is acquired every cycle.

The conversion into engineering units is implemented, for each different measurement, with the appropriate multiplications and divisions.

Digital Channels (see Fig. 4.9)

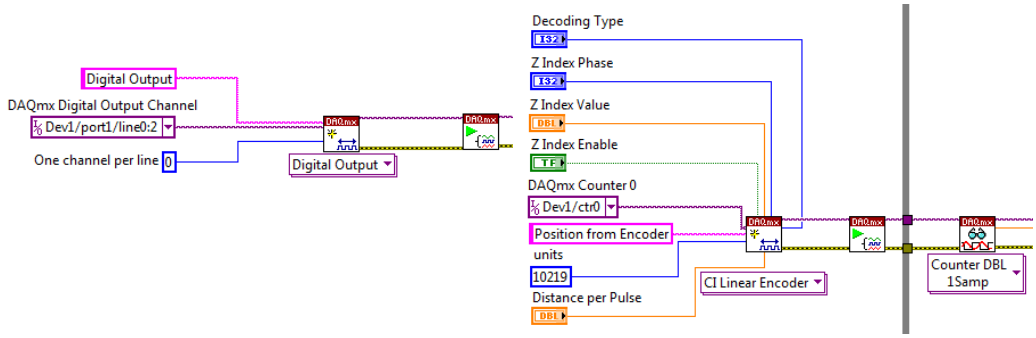

(a) Digital outputs (b) Counter for height sensor

Figure 4.9: Initialization of digital input/output channels

One DaqMX task is dedicated to write the digital outputs which control the status of drive's user program (Fig. 4.9a). The three physical channels are convoyed in one virtual channel and, during each iteration of the while true loop, the current output configuration is written into the channel. No conversion is needed, since these are logical values which can be either true (V_{OH}) or false (V_{OL}).

In a second DaqMX task, a counter is initialized Fig. 4.9b. It counts the digital pulses received from the height sensor, summing up them during lifting and subtracting them during lowering, in order to obtain the real position of the load. The conversion into engineering units is implemented inside the task, which receives as an input the distance per pulse covered by the sensor. The distance is read once each iteration of the while true loop.

4.2.3 Control Strategy

In order to implement the control equation (Fig. 4.10) described in Section 3.6, speed and pressure estimation are integrated. The integral period must be equal to the sampling period, otherwise the results would not be synchronous with the physical system. In the lower part of Fig. 4.10, the leakage coefficient is obtained, according to Eq. (3.31). The position component due to the leakage flow is subtracted from the component due to the ideal flow, the result gives the estimated covered distance. To get the position estimation, this value is continually summed up with the initial position, i.e. the estimated position when the motion begins. The movement ends when the covered distance equals the requested one.

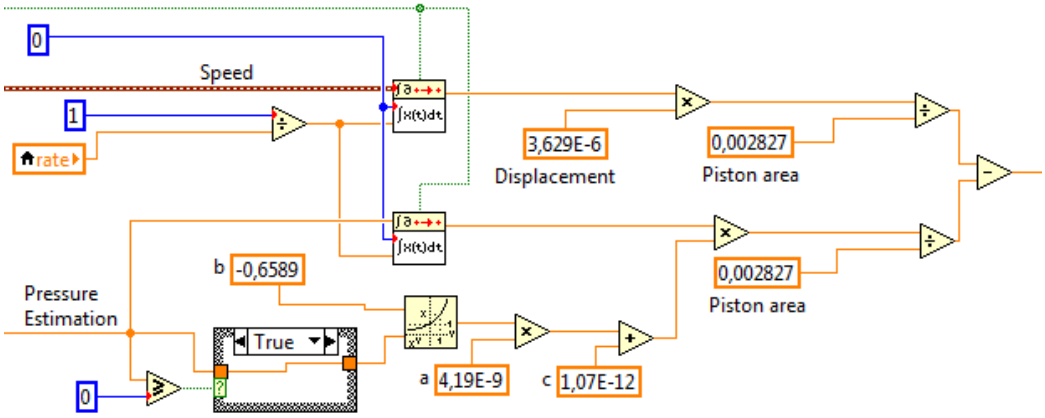

Figure 4.10: Implementation of the control strategy

As a remark, every time the system switches to a different state, it is essential to save the reached position (to have the initial condition of the next movement) and to reset the integrals. The integrals re-initialization is achieved setting to true the dedicated flag (green line in Fig. 4.10). Finally, the case structure (on the bottom) is needed to remove negative pressure values which could be generated because of the noise in the torque readings.

4.2.4 Pressure Estimation

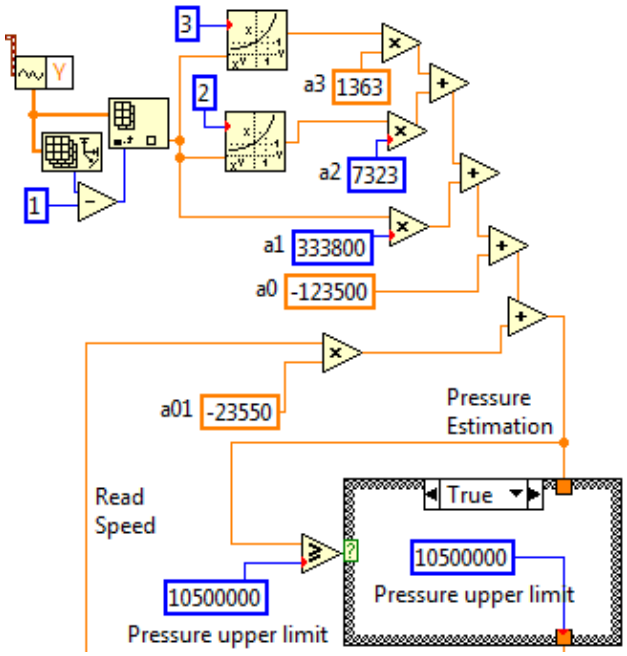

Figure 4.11: Implementation of the pressure estimation curve

In Fig. 4.11, the pressure estimation from torque and speed is implemented, according to Eq. (3.58). The case structure is needed to consider the pressure saturation. Actually, when the torque limit of the motor is reached, the maximum value of pressure is built in the chamber. Therefore, if the estimation overcomes $p_{\max} = 105$ bar, it is forced to saturate to this value.

4.2.5 End-runs Detection

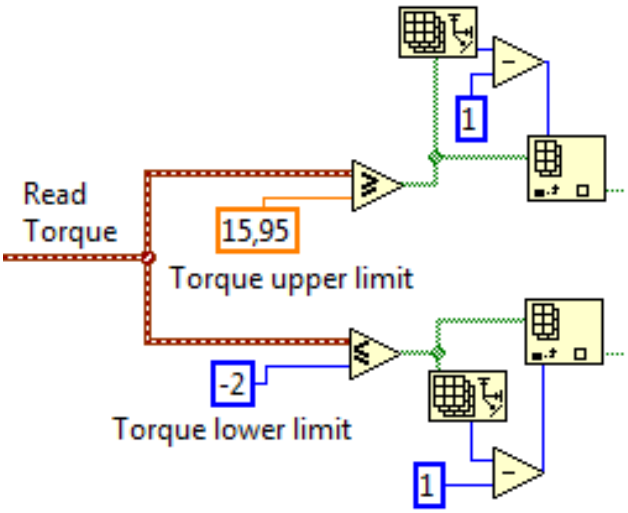

Figure 4.12: Implementation of the end-runs detection

The end-runs detection (Fig. 4.12) is implemented checking the torque feedback. In truth, whenever one of the end-run is hit, the torque quickly grows over the expected thresholds, because the system continues pushing against the hard stop. Stopping the motion, it is possible to avoid potential damages to the system in the case "out of limits" movement requests.

4.3 Matlab

Various Matlab scripts were written in order to analyse the data, make calculations, derive the slip coefficient and define the pressure estimation functions. The most interesting features will be briefly outlined in the following.

4.3.1 Weight Distribution

The weight distribution function implements Eq. (3.39), obtained by means of physical modelling of the load at page 38. This function allows to estimate the force acting on the piston during a lifting movement, which height and payload are given as input parameters. It is used to obtain an accurate value for variation of potential energy of the payload, for the efficiency calculations.

4.3.2 Data Acquisition

The first essential procedure in order to analyse the measurements data is the acquisition. LabView's data is saved in Excel spreadsheets (.tdms), the import is easily implementable with the *xslsread* command. Each variable is then saved in a dedicated location of a cell array. When all the measurements for an experiment are imported, they are stored in a master cell array, containing all the data series.

Hioki Power Analyzer's data is stored in text files (.csv); this data is imported with text file parsing, directly in table structures. One column in the table corresponds to a variable.

The data import works in a similar manner for all the experiments, in the fact, when the measurements are imported, it is possible to conduct different operations on them.

4.3.3 Leakage Coefficient

The leakage coefficient is obtained following the directions given in Section 3.2.1. Particularly, pressure and payload drop velocity are extracted from the data and, for each measurement, a data point is obtained through Eq. (3.33). Once the amount of measurements is sufficient, it is possible to divide the data set into an identification and a validation set. The former set is fitted with the *curve fitting tool* and the obtained model is validated with the latter set.

The LMS error appears to be very similar employing the two different curves proposed in Section 3.2.1, but Eq. (3.35) has less parameters and works better for high pressures, where the curve is supposed to decrease slowly but remaining always positive.

4.3.4 Pressure Estimation Function

For the pressure estimation curve, sample cycles of lifting and lowering at various speeds, loads and height are measured. From the acquired data, values for instantaneous pressure, torque and speed are saved for: lifting, stop motion, lowering and peak conditions. The data is again split into an identification and a validation set. At last, it is fitted with the *curve fitting tool*.

As a remark, trying to fit the data without the inclusion of the peak values, the LMS error becomes small and the presence of *outliers* is barely observable. The obtained pressure estimation curve is very precise and, if applied to the system, behaves well in the *comfort zone* (i.e. where the effect of pressure peaks is not relevant), giving a small position error. Nonetheless, if this function is employed outside of the *comfort zone*, whenever a pressure peak arises, the estimated value is sensibly lower than the pressure readings and the position error grows quickly.

For this latter reason, it is necessary to include the pressure peaks in the curve fitting data and to adjust the fitting in order to have either more precision in the low pressure range or in the high pressure one.

4.3.5 Efficiency Calculation

For this part, sample cycles composed just by lifting and lowering motions are measured. The data is split between lifting and lowering part, triggering the digital inputs. The synchronization of power analyzer's and LabView's measurements is obtained setting the same sample period (50 ms) and triggering the power analyzer data series when the phase voltage varies sensibly. This condition identifies the beginning of the motion.

During both lifting and lowering the energies in the system are calculated as integrals of the powers (*trapz* function); the efficiencies, as ratio of these powers (according to the Equations in Section 3.7) and the resulting values are stored in a table.

Chapter 5

Results and Discussion

This Chapter is finalized to describe the measurements carried out in order to analyse the performances of the setup and outline the numerical results obtained. First of all the control precision, then the efficiency of the system, will be evaluated. Measurements were taken in various conditions of payload, speed and position, for the sake of a general analysis.

For position control, the main performance indicators are: *position error*, which states the difference between the estimated position and the real one during each cycle; *final position error*, which states the difference between the estimated position and the real one at the end of each cycle. The analysis of these values will give clues about control precision and repeatability of the movements, that states how many cycles could be done before a homing procedure is required.

For efficiency calculations, powers and energies at different system nodes are read and compared. They give an accountable description of the overall efficiency of the whole setup and, for what is possible, of each component. The calculations are carried out according to the theory deduced in Section 3.7. The analysis of their results will allow the discussion about effectiveness and applicability of this novel approach.

Data is collected employing the control software described in Section 4.2; calculations and analysis are done using the Matlab scripts explained in Section 4.3.

5.1 Control Precision

In order to evaluate the precision of the implemented control strategy, three different *sample cycles* were defined (Fig. 5.1).

5.1.1 Sample Cycles

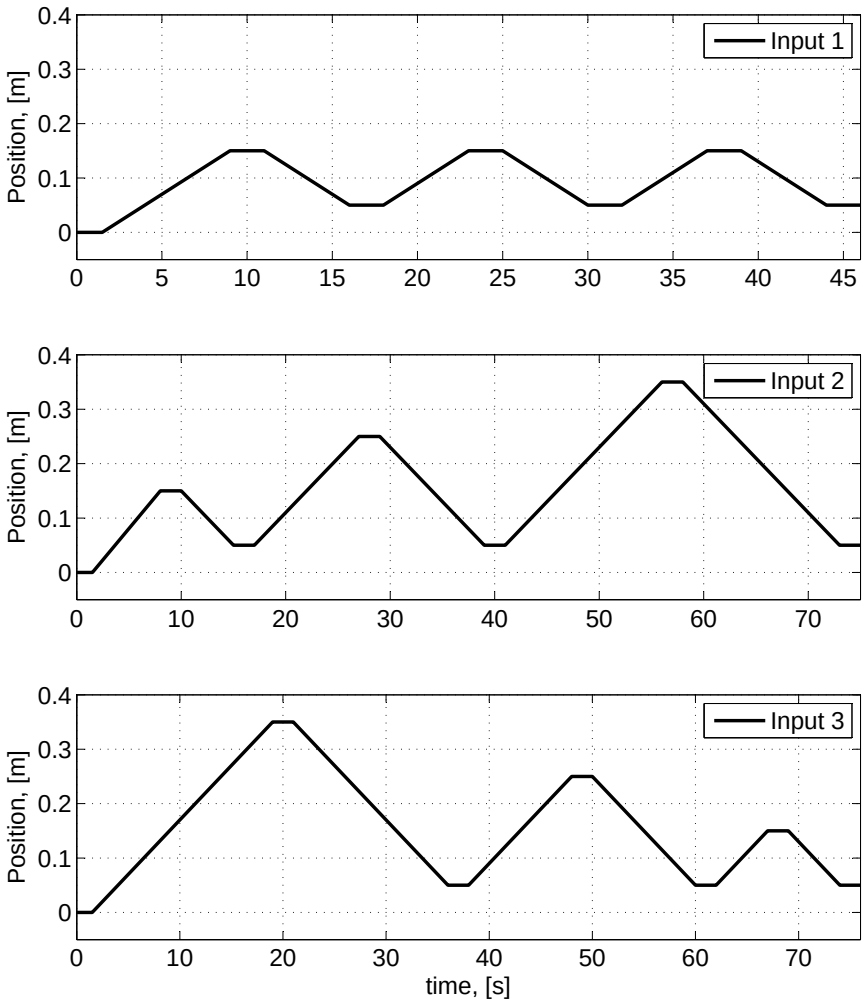

Figure 5.1: Employed sample cycles

The aim of the first cycle (Input 1) is to check the repeatability of the system, by means of requesting three times the same movement. The setup is controlled to operate inside a range of heights where the effect of pressure

peaks is not very relevant. This region will be called *comfort zone* in the following. The other two, instead, are important to give information about the capability of the control strategy to deal with the pressure peaks generated by displacement ratio error. In these two cases, the effect of what is modelled as a *variable load* is analysed. Particularly, by requesting the higher lifting either in the last part (Input 2) or in the first part (Input 3) of the cycle, it is possible to compare how much the peaks influence the average position error. In the fact, if the effect of the peak is strongly relevant, the average position error should drop from Input 2 to Input 3, while the final error should be approximately the same.

It is worth remarking that the inputs require the setup to cover a certain distance, not to move up to a defined absolute position. This configuration will turn out in a visible slope in the resulting movements, given by the leakage flow during stop motion. Nonetheless, being the leakage flow predicted by the model, the position estimation should follow the real one.

For each of the inputs, measurements were carried out at three different speeds and with three different payloads. In detail these values are:

$$\dot{\theta}_1 = 300\ rpm \qquad \dot{\theta}_2 = 400\ rpm \qquad \dot{\theta}_3 = 500\ rpm$$
$$m_1 = 33,5\ kg \qquad m_2 = 108,5\ kg \qquad m_3 = 183,5\ kg$$

5.1.2 Results and Analysis

The resulting errors are listed in Table 5.1, and calculated as:

$E_{\text{avg}} =$ average position error during the cycle,
$E^{\%}_{\text{avg}} =$ average percent position error, compared to the piston full stroke,
$E_{\text{fin}} =$ final position error at the end the cycle,
$E^{\%}_{\text{fin}} =$ final percent position error, compared to the piston full stroke.

From a general observation of Table 5.1, it is possible to point out the main features of the results obtained.

The average position error fluctuates around 0,60 cm (1,51 %). It is always enclosed in the range $[0,30; 1,00]$ cm, with the only exception of the last test (Test 27), that is affected by a peculiar issue which will be described in the last part of the current Section.

Furthermore, the position error slowly grows during each cycle, resulting in a final gap of about 1,25 cm (3,10 %). The final error is always contained

Test	**Configuration**			E_{avg}, [cm]	$E^{\%}_{\text{avg}}$	E_{fin}, [cm]	$E^{\%}_{\text{fin}}$
1	33,5 kg	300 rpm	Input 1	0,31	0,77	0,73	1,82
2			Input 2	0,80	2,00	1,88	4,69
3			Input 3	0,95	2,38	1,81	4,53
4		400 rpm	Input 1	0,43	1,07	1,08	2,70
5			Input 2	1,12	2,79	2,55	6,39
6			Input 3	1,00	2,49	1,99	4,97
7		500 rpm	Input 1	0,50	1,26	1,14	2,85
8			Input 2	0,69	1,73	1,70	4,25
9			Input 3	0,69	1,73	1,65	4,13
10	108,5 kg	300 rpm	Input 1	0,58	1,46	1,22	3,06
11			Input 2	0,93	2,31	2,30	5,75
12			Input 3	0,96	2,39	2,00	4,99
13		400 rpm	Input 1	0,51	1,28	1,24	3,10
14			Input 2	0,70	1,74	1,81	4,52
15			Input 3	0,61	1,53	1,55	3,87
16		500 rpm	Input 1	0,50	1,24	1,03	2,58
17			Input 2	0,66	1,66	1,54	3,84
18			Input 3	0,61	1,51	1,35	3,37
19	183,5 kg	300 rpm	Input 1	0,45	1,12	1,10	2,75
20			Input 2	0,54	1,34	1,49	3,72
21			Input 3	0,71	1,77	1,69	4,22
22		400 rpm	Input 1	0,42	1,05	0,98	2,46
23			Input 2	0,63	1,57	1,83	4,58
24			Input 3	0,55	1,39	1,43	3,57
25		500 rpm	Input 1	0,52	1,29	0,69	1,74
26			Input 2	0,60	1,51	1,03	2,56
27			Input 3	1,31	3,29	0,57	1,42

Table 5.1: Position errors

in the range $[0,60; 2,55]$ cm.

From these performance indexes, as desired, it is not possible to recognize a clear dependence either on the speed or on the payload, which means the performance of the control strategy is load and speed independent. Nonetheless, the tests carried out in *comfort zone* (Input 1) result usually in decisively lower error, compared to the other two inputs. This observation confirms the negative effect of pressure peaks. As a last remark, comparing the results of Input 2 and Input 3, it is noticeable that the position of the peak does not influence the performances strongly.

Let us go more deeply in the test results. Test 24 (Fig. 5.2) is a basic test example. It shows the performances of the control strategy in average conditions.

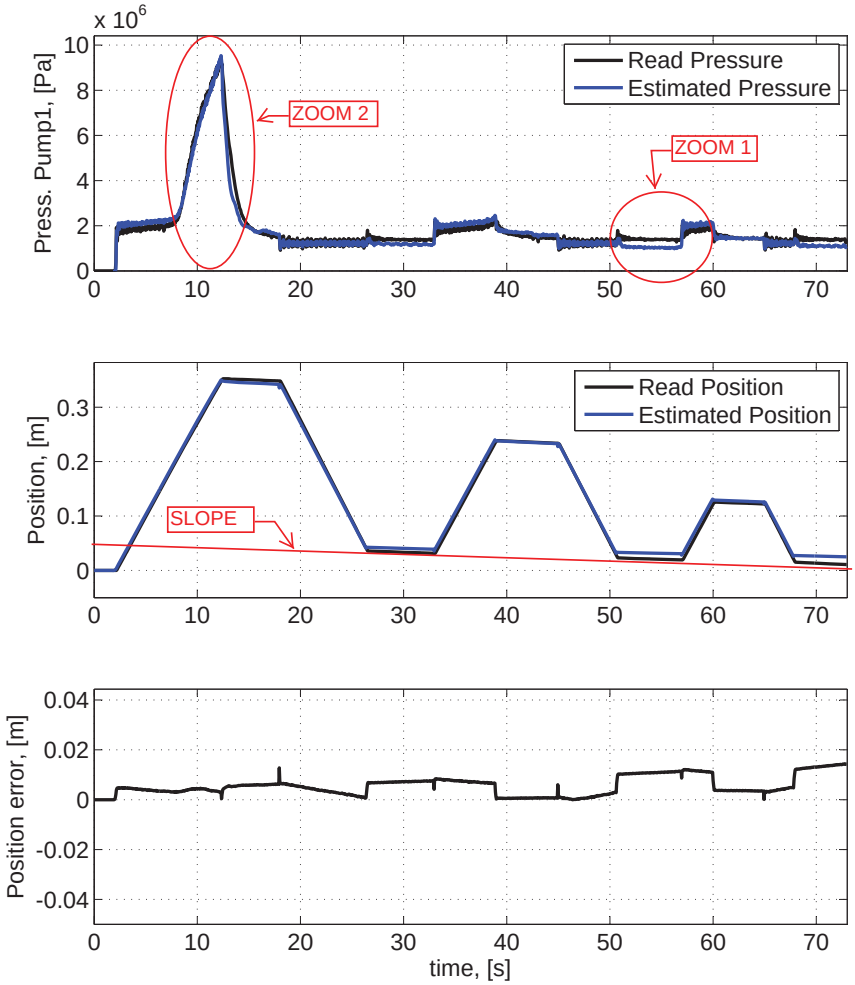

Figure 5.2: Test 24: 183,5 kg, 400 rpm, Input 3

First of all, it is possible to notice that the position (graph 2) is affected by a constant slope during the whole cycle. This slope is due to the effect of leakage flow in stop motion, i.e. when the payload is hold at a certain level. The load slowly drops because of the slip flow, which is not stopped by any valve in this system. For this research it was decided to keep this effect, without compensating it. In any case, the position estimation decreases in the same manner as the real position, which means the leakage estimation is quite precise. Therefore, being the drop of the load predicted properly, it would be possible to compensate it, if needed. For example extra-rotations could be added or absolute position reference, instead of relative movement, could be used for the control.

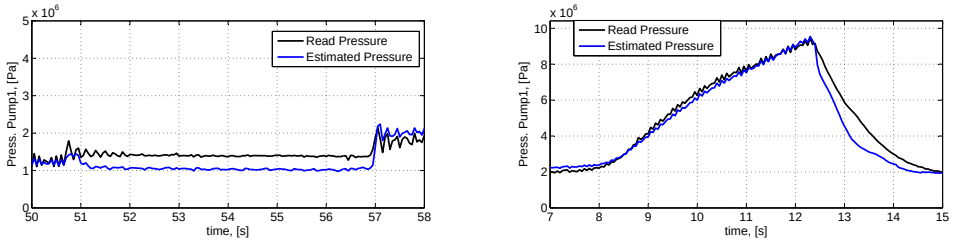

(a) Estimation inaccuracy (b) Estimation of the peak

Figure 5.3: Details of pressure estimation of Fig. 5.2

On the one hand, the position error slowly increases during the cycle (graph 3 in Fig. 5.2), ending in a final error of 1,43 cm. The most relevant contribution to the error increase is due to the inaccuracy of the pressure estimation obtained from torque and speed. This phenomenon is observable in the pressure comparison graph (graph 1) in Fig. 5.2. Actually, in order to fit properly the behaviour of the system when exposed to pressure peaks, the estimation function is less precise for low pressure. This turns out in a certain gap (as an example, see the detail 1 in Fig. 5.3a) between the real pressure and the estimated one. This latter gap generates a slightly different leakage flow estimation and the error, as a consequence.

On the other hand, the pressure peak is predicted well by the function (see detail 2 in Fig. 5.3b) and its effect on the position estimation is not very relevant, because the position error does not grow remarkably.

As a last remark, the average position error along the cycle is 0,55 cm, which can be considered a pretty worth result for mobile working machine applications.

In the following, some particular cases will be analysed and the reasons of performance differences will be discussed. In order to keep the text flowing, the reference Figures are located in App. D (referenced by D.x).

Fig. D.1 depicts the results for the same input (Input 3), in condition of smallest payload and speed. In this situation the peaks are modelled less well, and they are the bigger source of position error. On the other hand, the pressure estimation curve has better performances for low pressures. This is due to the fact that, in this case, the lowering is not regenerative. That means both the read torque and the read speed are negative and the system is operating in a different part of the pressure estimation curve, where it fits well the data. From graph 2 in Fig. D.1, it is observable that after the peaks the position error remains roughly constant and the load drop is not very sensible, because of the small load applied. In this case the average error appears to be slightly higher (0,95 cm) and it grows up to a final error of 1,81 cm.

Let us, now, analyse the results for medium load and high speed. Test 18 is shown in Fig. D.2, and a detail given in Fig 5.4.

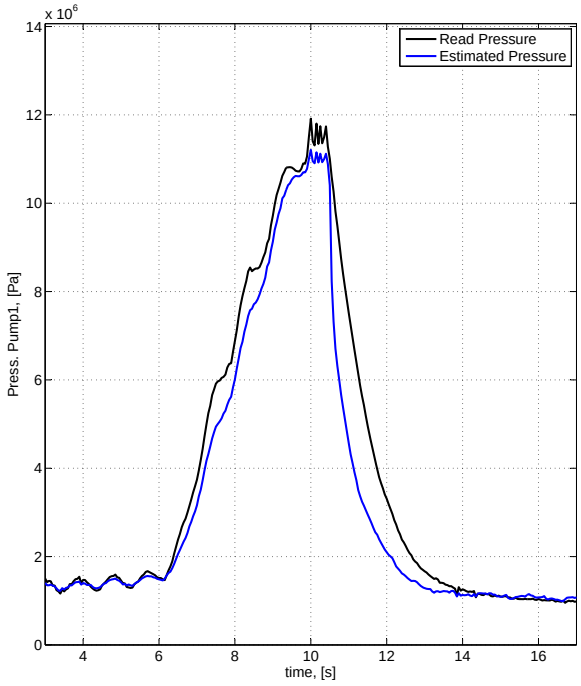

Figure 5.4: Test 18: 108,5 kg, 500 rpm, Input 3; detail of Fig. D.2

Under these conditions, an oscillation in the pressure read is observable; it is due to the fast lifting. The pressure estimation follows well the peak, but returns a less fluctuating signal, if compared to the read pressure. This behaviour can actually be useful for the control strategy, because the estimation works, somehow, as a filter generating a more continuous signal. This feature helps the control system to get a better estimation of the leakage flow, which is not affected by dynamic transients due to the oscillations. The general performances in the cycle are satisfactory; the pressure estimation is very similar to the real one. The results can be read from Table 5.1.

A very particular situation is noticed in Test 27 (Fig. D.3), in this case also the motor speed is shown. A detail for the relevant part of the movement is depicted in Fig. 5.5.

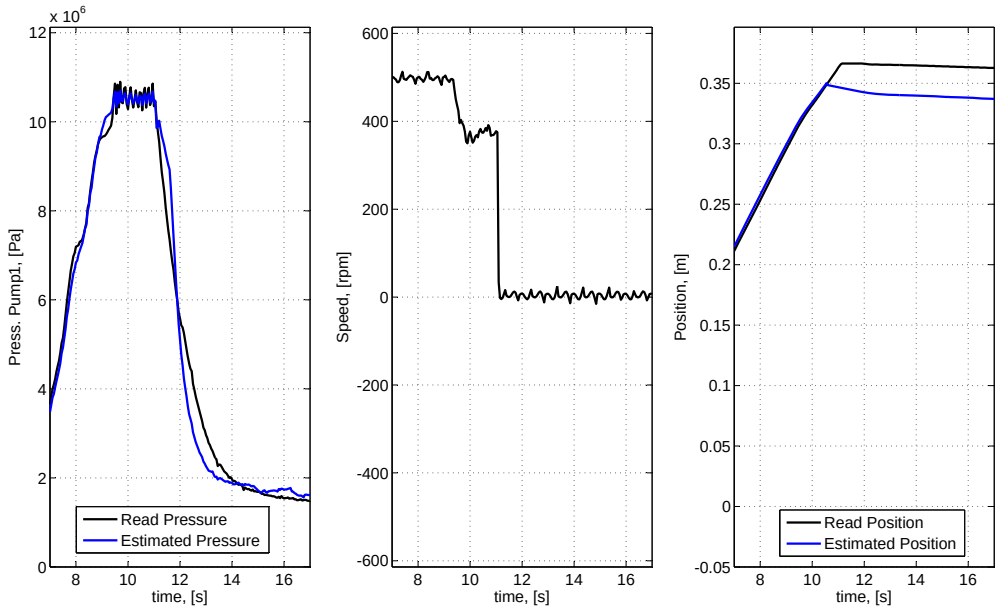

Figure 5.5: Test 27: 183,5 kg, 500 rpm, Input 3; detail of Fig. D.3

When the speed requested to the motor is too high, with long movement and heavy load, the braking effect of Pump 2 becomes strongly relevant. The motor can reach the maximum output torque and the pressure saturate at the maximum (105 bar) obtainable with this torque level. When this condition lasts, the opposing braking overwhelm the available motor torque, slowing down the movement. The control strategy suffers of this unusual situation and a relevant position error arises. This error is slightly reduced during the

cycle, but kept until the end of it. It is worth noticing that the pressure estimation saturates following the same behaviour of the read one. The average error is slightly higher than in the other common cases (1,31 cm), while the final error has actually a acceptable magnitude (0,57 cm).

As a comparison, Test 23 is depicted in Fig. D.4. This test employs the second input. No particular differences are noticed in the system behaviour. The main sources of error can be attributed to the peaks and, especially, to the estimation in the low pressure phases. The obtained results are in the average range.

Repeatability

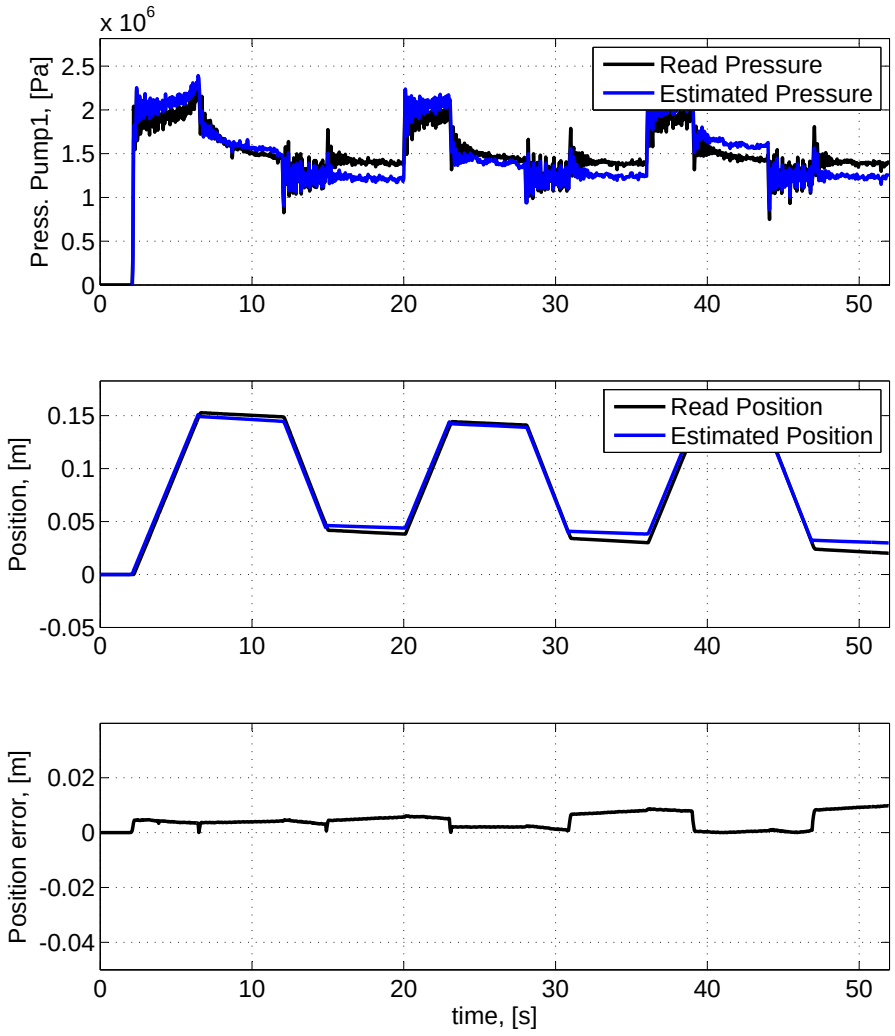

Figure 5.6: Test 22: 183,5 kg, 400 rpm, Input 1

In order to analyse the system repeatability, Input 1 was employed. The same lifting and lowering cycle is required three times to the setup. In this case, the main error is introduced by the pressure estimation imprecisions for low pressures and the error slowly grows in the low pressure region. Fig. 5.6 depicts test 22, as a typical example.

The position error grows of 0,3 cm after each lifting/lowering cycle, up to 0,9 cm at the end of the third one. The average error is 0,42 cm. Depending on the specific application, the position error has to be kept below a certain value and the system needs to be homed when the threshold is overcame. For example, for an average working machine, 1 cm error could be considered an acceptable margin. If this is the case, this setup would need to be homed every about 60 seconds.

5.2 Efficiency

In order to analyse the efficiency of the test setup, two basic *sample cycles* were defined. The cycles are lifting/lowering cycles and the only difference is the required height: either 15 cm or 30 cm. The tests were carried out for various speeds and payloads, according to the basic idea of generality followed for the position control as well. In detail the values are:

$$\dot{\theta}_1 = 300\ rpm \qquad \dot{\theta}_2 = 400\ rpm \qquad \dot{\theta}_3 = 500\ rpm$$
$$m_1 = 33,5\ kg \qquad m_2 = 108,5\ kg \qquad m_3 = 183,5\ kg$$

In these situations the system is required to work in different operative points and, depending on speed and load, the lowering movement can be either regenerative or not.

In particular, for m_1, the free-fall speed is almost null, because the small payload does not generate pressure enough to move the system. Therefore, almost all the mechanical energy acting on the load is generated by the motor. Thus, the condition of regenerative slow lowering was never observed.

For m_2 instead, the free-fall condition is reached with an angular speed of the shaft of about 310 rpm. Thus, $\dot{\theta}_1$ is a critical speed value, for which the powers in the system are small and the efficiencies are high, but the actual regeneration is almost negligible. For $\dot{\theta}_2$ and $\dot{\theta}_3$, instead, the electric motor performs more mechanical work in order to accelerate the lowering.
Summarizing, for speed $\dot{\theta}_1$ the system behaves in a slightly regenerative manner (slow lowering); otherwise, for $\dot{\theta}_2$ and $\dot{\theta}_3$, the system is not regenerative (fast lowering).

For m_3 the free-fall speed is higher than the maximum speed in this tests ($\dot{\theta}_3$), therefore, the fast lowering was never observed. In this condition the lowering movement is always regenerative and it is theoretically possible to obtain energy back from the system.

The following section presents measurement results and their analysis.

5.2.1 Results and Analysis

The overall efficiency results are depicted in Fig. 5.7 for the lower sample cycle (15 cm) and in Fig. 5.8 for the higher one (30 cm). Lifting is on the right (positive motor speed), while lowering is on the left (negative speeds).

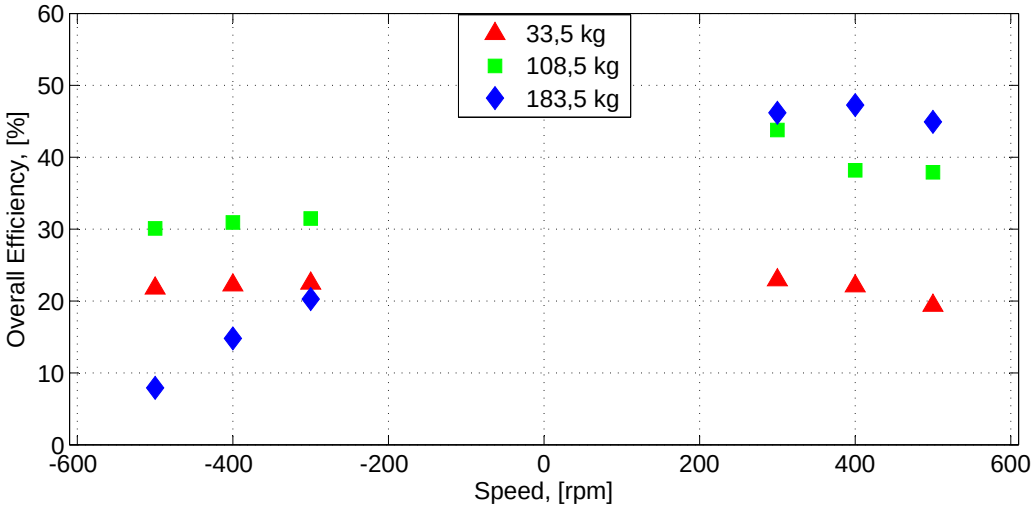

Figure 5.7: Overall efficiency, height = 15 cm

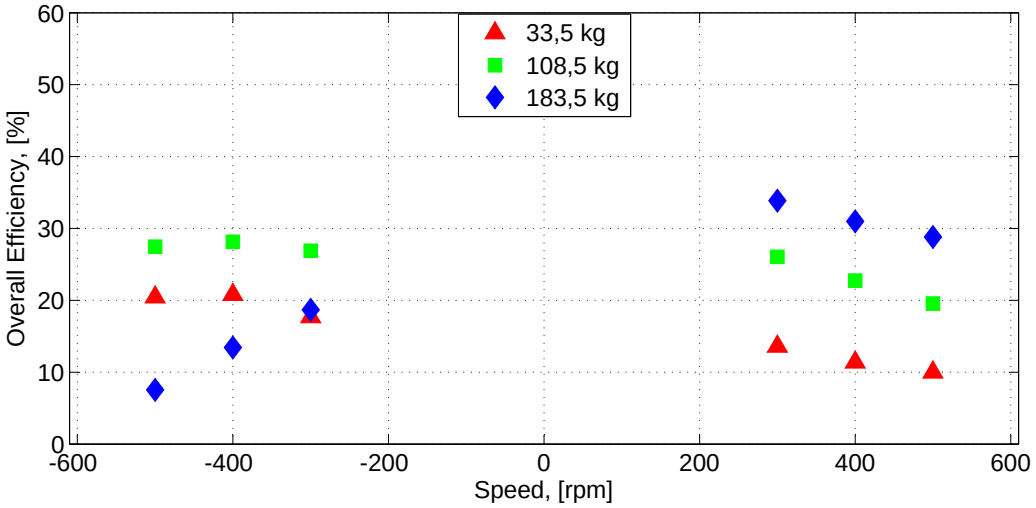

Figure 5.8: Overall efficiency, height = 30 cm

As shown in Fig. 5.7, for the 15 cm cycle, the overall lifting efficiency varies with from 48 to 20 %; while for the 30 cm cycle (Fig. 5.8), the overall lifting efficiency varies from 35 to 10 %. During lowering, the overall efficiency is in the range of 9 to 36 % and the behaviour does not depend significantly on the height.

The relevant reduction of lifting efficiency observed while raising the height is due to the effect of pump size ratio error. In Fig. 5.7, when the motion is short, this phenomenon is not very sensible, thus the setup shows higher efficiency; otherwise, for longer movements (Fig. 5.8) the peaks become more relevant, reducing the overall efficiency. During the lowering

movement, instead, the energy behaviour remains the same for both the sample cycles. In this case, the effect of the size ratio is to reduce the amount of flow delivered by pump 2. Nonetheless, this does not affect sensibly the overall efficiency, because the reference chamber is still the first one and pump 2 becomes simply for the motion aim.

On the one hand, during lifting, the system is more efficient when a heavier payload is employed, since the pumps and transmission line losses become less relevant, if the required amount of power is bigger.

On the other hand, during lowering the efficiency with m_3 is strongly lower when compared to the other two cases. This is due to the fact that, actually, only in the former condition (m_3) the lowering is regenerative. Therefore, even if the efficiency is small, the system energy balance is positive, because some potential energy could be recovered. In the latter cases (m_1 and m_2), instead, the efficiency expresses how effective is the motor in accelerating the free-fall, therefore the energy balance is negative and there is power consumption. As a last remark, the lowering efficiency with m_2 is higher than with m_1, since the system is closer to the free-fall speed, thus the acceleration required is smaller and the amount of consumed energy less relevant.

Figure 5.9 shows the results concerning the electric machine efficiency.

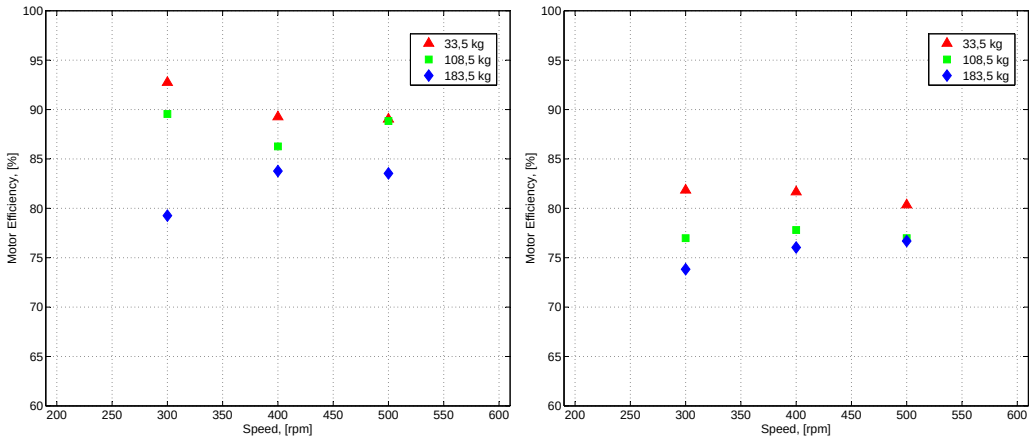

(a) Height = 15 cm (b) Height = 30 cm

Figure 5.9: Electric motor efficiency

According to the test results, increasing the payload degrades the motor efficiency. The maximum motor efficiency is reached with the smaller values of speed and payload ($\dot{\theta}_1$ and m_1) and it is 92 %.

Comparing Fig. 5.9a and Fig. 5.9b, it can be noticed that the motor efficiency slightly reduces ($\simeq$5 % degradation) when the height grows. That is because, whenever a pressure peak arises, overrated torque is required to the motor, up to the maximum limited torque for the case $\dot{\theta}_3$ and m_3. This requirement compels the motor in a low performance operative point.

Figure 5.10 shows a comparison between examples of measured data (speed, torque, pressure and position) for motor speed $\dot{\theta}_1$. In Fig. 5.10a, the condition is slow lowering (m_3), while fast lowering (m_1) in In Fig. 5.10b.

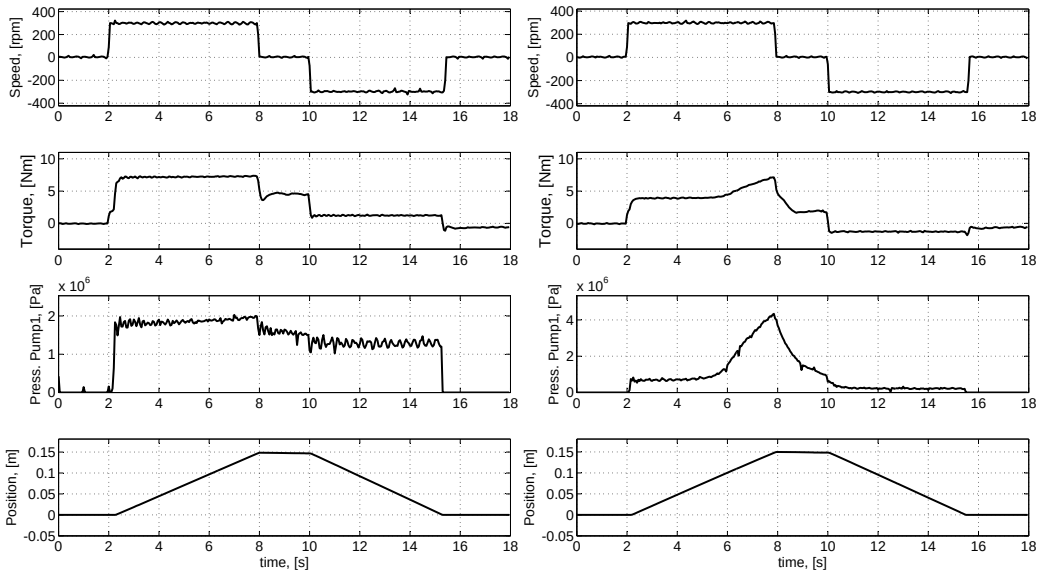

(a) Regenerative cycle (183,5 kg) (b) Non regenerative cycle (33,5 kg)

Figure 5.10: Motor speed, torque, pressure in line 1, cylinder's rod position

A summary of the experimental values, obtained from Fig. 5.10b, is given in Table 5.2. As a remark, a pressure peak is noticeable from second 6 to 8.

	Torque, $[Nm]$		**Pressure,** $[Pa]$	
	Lifting	**Lowering**	**Lifting**	**Lowering**
Regen. Cycle	7	1	$20 \cdot 10^5$	$10 \cdot 10^5$
Non-Regen. Cycle	4	-1	$1 \cdot 10^5$	$0,5 \cdot 10^5$

Table 5.2: Motor torque and the pressure in line 1, from Fig. 5.10

It is relevant to observe the difference between the two conditions, concerning the lowering motion: in the first case speed and torque have opposite signs, in the second one, these quantities are both negative. This is the key evidence which distinguish between regenerative and not regenerative cycle.

Concerning the efficiency of the single components of the system, Fig. 5.11 shows the Sankey's diagrams for the sample case previously introduced (in Fig. 5.10a). The picture on the left illustrate the lifting motion, while the one on the right the lowering movement.

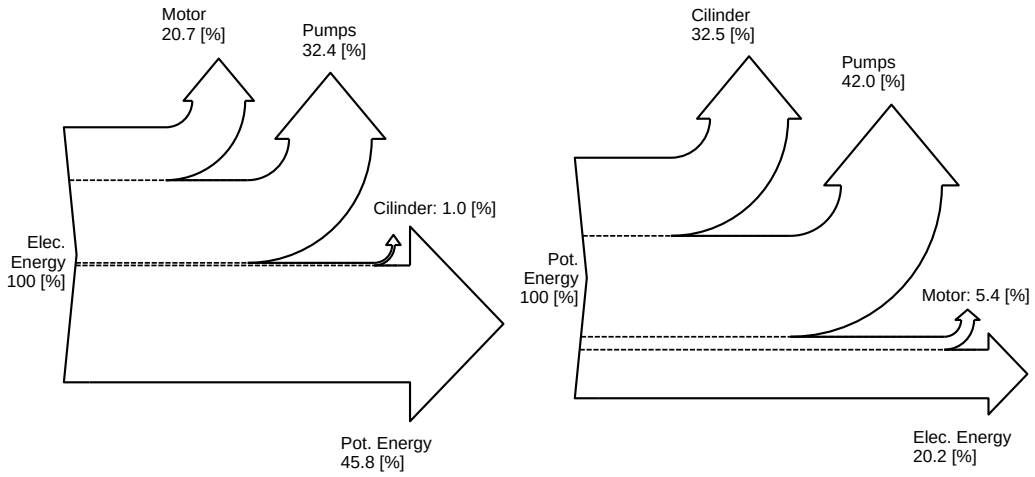

(a) Lifting (b) Lowering

Figure 5.11: Sankey's diagrams for regenerative cycle (183,5 kg)

The losses division follows the scheme introduced in Fig. 3.9 at page 50. To recall, the pump losses concern the ensemble of the transmission and the two pumps, while the cylinder losses regards the hoses and the cylinder. These two contributions, together, describe the losses of the hydro-mechanical part of the system. They amount to 33.4 % of the total losses during lifting, and to 74.4 % during lowering. It can be observed that the hydro-mechanical losses are predominant during both lifting and lowering.

The apparent inefficiency of the cylinder, during lowering, is due to the operating condition of the system. Actually, the fixed speed of the pumps brakes the fluid flow in the hoses. This condition reduces the hydraulic power in the line. The fluid power is the cylinder's output, therefore its power conversion results less efficient, nonetheless this effect is mainly imposed by the controlled lowering.

Finally, for the case of regenerative lowering (*slow lowering*), in addition to the efficiency equations, it is possible to estimate how much energy could be theoretically recovered, employing a regenerative electric drive. By observation of a sample cycle (e.g., Fig. 5.11): during lifting, the input electric energy is stored - reduced because of the losses - as potential energy; during lowering the same amount of potential energy plays the role of input for the system and - decreased by the efficiency - generates a regenerative electric power output. Assuming the possibility to store this latter output (losses of the power converter excluded), a certain amount of energy could be recovered. In order to obtain an estimation of this quantity, the Cycle Efficiency η_{cycle} is defined:

$$\eta_{\text{cycle}} = \eta_{\text{lifting}} \cdot \eta_{\text{lowering}} \tag{5.1}$$

where η_{cycle} is the product of the efficiencies for the lifting and lowering motion; it shows the percentage of input energy which could be recovered and stored (besides power converter losses) after a complete sample cycle.

By calculating Eq. (5.1) for the regenerative sample cycles (m_3), yields the results in Fig. 5.12.

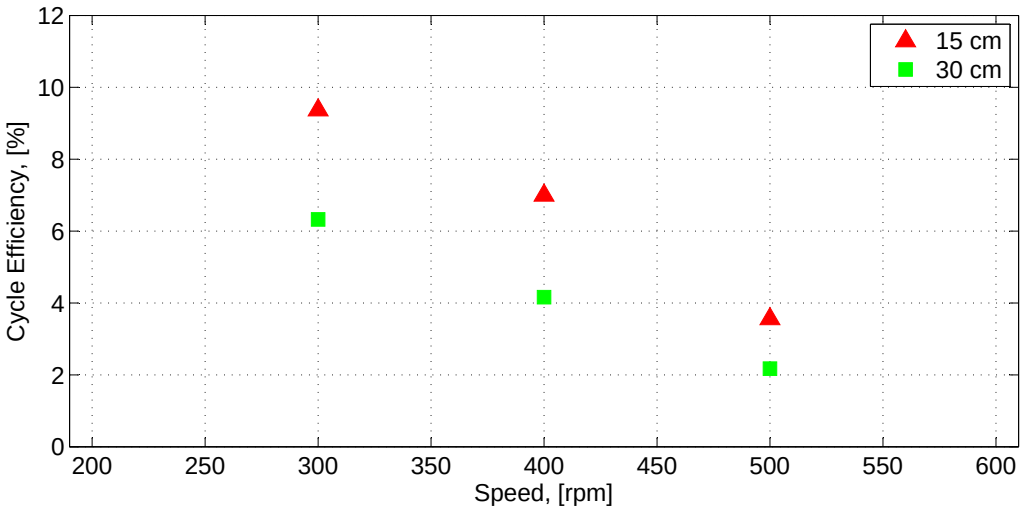

Figure 5.12: Cycle efficiency η_{cycle}

The cycle efficiency is in the range 10 % to 2 %. The best result is obtained with the lower speed, where the effect of the pressure peaks is less sensible. With the raising speed the theoretical recoverable energy becomes very small since the internal losses predominate in the system.

Chapter 6

Conclusions

The aim of this master's thesis is to study direct driven hydraulic systems, from position control and efficiency point of view. All the components of such kind of hydraulic lifting system are studied and modelled. The interaction between electric and hydraulic part is also analysed and employed for control purposes. The measurements are carried out with a test setup, which is a small electro-hydraulic crane. In this thesis a control strategy for this type of novel system is defined and the possibilities of energy recovery are studied.

The key findings of this work are:

1. A model for the DDH system is proposed, in order to link electric, hydraulic and mechanical part. Power conversions along the system and control quantities are defined. The critical issues concerning the design of this type of system are pointed out.

2. A pump leakage flow model is derived from theory and particularized for the system by empirical results.

3. A pressure estimation function is deduced studying the torque losses in the hydraulic pumps and identified basing on measurements.

4. A flow control strategy is implemented directly varying the speed of the servo motor.

5. A sensorless implementation of the position control is given, employing only the feedback from the servo motor.

6. Control precision and repeatability of the system are analysed by means of empirical measurements on the test setup.

7. Efficiency of the system is analysed and the potential energy recovery is estimated.

The results of this thesis are strongly affected by the pump sizing error, which compelled the investigation in uncommon application conditions. Thus, the first relevant information obtained from the work is a dimensioning rule for future system design.

Nonetheless, the control strategy proposed can be applied to various types of DDH setup and employed in practical system implementations. The test results show a discrete control precision, which could be acceptable for NRMM applications, but they also point out which are the bigger causes of error and what could be done to improve them.

From the efficiency point of view, the test results are comparable to the case of a standard hydraulic system. Nevertheless, the particular test setup employed demonstrated to have internal losses due to design imprecision. Thus, with investigation on a well sized system, relevant enhancements could be reached.

6.1 Future Developments

From a practical point of view, this work could be extended to other type of working machines, such as mine loaders, industrial lifts and forklifts. The key point to keep in consideration is the proper dimensioning of the pumps for each particular system.

A similar investigation is suggested to be carried out for a new, well-sized setup; in order to get results for control precision and efficiency in a more common situation. Particularly, concerning the efficiency part, a system implementation with a regenerative drive and some kind of energy storage (e.g., a battery), could be employed in order to confirm the theoretical energy recovery estimations calculated in the thesis. In this case, the efficiency of the power converter and possible inverter should be kept in consideration.

Furthermore, hydraulic accumulators could be used to absorb the pressure peaks. Simulations and tests could be carried out in order to evaluate the effect of hydraulic accumulators insertion in the pump lines. The possibility of introducing such devices in place of the tank could also be investigated. The resulting setup would be a closed-loop hydraulic system, with additional size reduction.

The sensorless strategy opens the way for various cheap and efficient practical applications. Investigation is suggested in order to evaluate the implementation of a fault sensitive system, which, reading the motor feedback, could get clues about the health of the components in a automated manner. This idea comes from the observation that the relation "setup status versus speed and torque levels" is quite univocal, therefore, unexpected readings of the feedback in a standard cycle could represent an evidence of a physical problem.

For the control quality, most of the imprecisions derive from the pressure estimation function. For this reason, further studies and improvements are recommended. A more precise model of the torque losses could lower the positioning error.

At last, different implementations with other types of hydraulic pumps could be analysed, in order to evaluate the generality of the results.

Appendices

Appendix A

Electric Drive Details

A.1 Parameters

Those are stored in the *Advanced menus*, divided by type. The menus are listed in Fig. A.1.

Menu number	Description
0	Commonly used basic set up parameters for quick / easy programming
1	Frequency / speed reference
2	Ramps
3	Slave frequency, speed feedback and speed control
4	Torque and current control
5	Motor control
6	Sequencer and clock
7	Analog I/O
8	Digital I/O
9	Programmable logic, motorised pot and binary sum
10	Status and trips
11	General drive set-up
12	Threshold detectors and variable selectors
13	Position control
14	User PID controller
15, 16, 17	Solutions Module set-up
18	Application menu 1
19	Application menu 2
20	Application menu 3
21	Second motor parameters

Figure A.1: Advanced menus (Emerson [30])

The setting of the parameters can be done either directly form the drive's

display or from the dedicated section in the drive's software (PowerTools, discussed in sec. 4.1). Mostly the second option was chosen, because it appears to be faster and more immediate. The most useful parameters can be found in the first menu (*Commonly used*), a quick overview is given in Fig. A.2, A.3, and a deeper explanation is given in the following for most interesting ones. For all the others and further details the reader is addressed to the user manual [30].

Parameter			Range(⇳)			Default(⇨)			Type					
			OL	VT	SV	OL	VT	SV						
0.00	**xx.00**													
0.01	Minimum reference clamp	{**1.07**}	±3,000.0Hz	±Speed_limit_max rpm		0.0			RW	Bi			PT	US
0.02	Maximum reference clamp	{**1.06**}	0 to 3,000.0Hz	Speed_limit_max rpm		EUR> 50.0 USA> 60.0	EUR> 1,500.0 USA> 1800.0	3,000.0	RW	Uni				US
0.03	Acceleration rate	{**2.11**}	0.0 to 3,200.0s/ 100Hz	0.000 to 3,200.000 s/1,000rpm		5.0	2.000	0.0200	RW	Uni				US
0.04	Deceleration rate	{**2.21**}	0.0 to 3,200.0s/ 100Hz	0.000 to 3,200.000 s/1,000rpm		5.0	2.000	0.0200	RW	Uni				US
0.05	Reference select	{**1.14**}	A1.A2 (0), A1.Pr (1), A2.Pr (2), Pr (3), Pad (4), Prc (5)			A1.A2 (0)			RW	Txt		NC		US
0.06	Current limit	{**4.07**}	0 to Current_limit_max %			165.0	175.0		RW	Uni		RA		US
0.07	OL> Voltage mode select	{**5.14**}	Ur_S (0), Ur (1), Fd (2), Ur_Auto (3), Ur_I (4), SrE (5)			Ur_I (4)			RW	Txt				US
	CL> Speed controller P gain	{**3.10**}		0.0000 to 6.5335(1/rad s^{-1})			0.0100		RW	Uni				US
0.08	OL> Voltage boost	{**5.15**}	0.0 to 25.0% of motor rated voltage			3.0			RW	Uni				US
	CL> Speed controller I gain	{**3.11**}		0.00 to 653.35 (1/rad)			1.00		RW	Uni				US
0.09	OL> Dynamic V/F	{**5.13**}	OFF (0) or On (1)			0			RW	Bit				US
	CL> Speed controller D gain	{**3.12**}		0.00000 to 0.65336 (s)			0.00000		RW	Uni				US
0.10	OL> Estimated motor speed	{**5.04**}	±180,000 rpm						RO	Bi	FI	NC	PT	
	CL> Motor speed	{**3.02**}		±Speed_max rpm					RO	Bi	FI	NC	PT	
0.11	OL & VT> Drive output frequency	{**5.01**}	±Speed_freq_max Hz						RO	Bi	FI	NC	PT	
	SV> Drive encoder position	{**3.29**}			0 to 65,535 ($1/2^{16}$ths of a revolution)				RO	Uni	FI	NC	PT	
0.12	Total motor current	{**4.01**}	0 to Drive_current_max A						RO	Uni	FI	NC	PT	
0.13	OL & VT> Motor active current	{**4.02**}	±Drive_current_max A						RO	Bi	FI	NC	PT	
	SV> Analog input 1 offset trim	{**7.07**}			±10.000 %			0.000	RW	Bi				US
0.14	Torque mode selector	{**4.11**}	0 to 1	0 to 4		Speed control mode (0)			RW	Uni				US
0.15	Ramp mode select	{**2.04**}	FASt (0) Std (1) Std.hV (2)	FASt (0) Std (1)		Std (1)			RW	Txt				US
0.16	OL> F5 and F6 auto-selection disable	{**8.39**}	OFF (0) or On (1)			0			RW	Bit				US
	CL> Ramp enable	{**2.02**}		OFF (0) or On (1)			On (1)		RW	Bit				US
0.17	OL>F6 digital input destination	{**8.26**}	Pr **0.00** to Pr **21.51**			Pr **6.31**			RW	Uni	DE		PT	US
	CL> Current demand filter time constant	{**4.12**}		0.0 to 25.0 ms			0.0		RW	Uni				US
0.18	Positive logic select	{**8.29**}	OFF (0) or On (1)			On (1)			RW	Bit			PT	US
0.19	Analog input 2 mode	{**7.11**}	0-20 (0), 20-0 (1), 4-20tr (2), 20-4tr (3), 4-20 (4), 20-4 (5), VOLt (6)			VOLt (6)			RW	Txt				US
0.20	Analog input 2 destination	{**7.14**}	Pr **0.00** to Pr **21.51**			Pr **1.37**			RW	Uni	DE		PT	US
0.21	Analog input 3 mode	{**7.15**}	0-20 (0), 20-0 (1), 4-20tr (2), 20-4tr (3), 4-20 (4), 20-4 (5), VOLt (6), th.SC (7), th (8), th.diSp (9)			VOLt (6)			RW	Txt			PT	US
0.22	Bipolar reference select	{**1.10**}	OFF (0) or On (1)			OFF (0)			RW	Bit				US
0.23	Jog reference	{**1.05**}	0 to 400.0 Hz	0 to 4000.0 rpm		0.0			RW	Uni				US
0.24	Pre-set reference 1	{**1.21**}	±Speed_limit_max rpm			0.0			RW	Bi				US
0.25	Pre-set reference 2	{**1.22**}	±Speed_limit_max rpm			0.0			RW	Bi				US
0.26	OL> Pre-set reference 3	{**1.23**}	±Speed_freq_ max Hz/rpm			0.0			RW	Bi				US
	CL> Overspeed threshold	{**3.08**}		0 to 40,000 rpm			0		RW	Uni				US
0.27	OL> Pre-set reference 4	{**1.24**}	±Speed_freq_ max Hz/rpm			0.0			RW	Bi				US
	CL> Drive encoder lines per revolution	{**3.34**}		0 to 50,000			2048	4096	RW	Uni				US
0.28	Keypad fwd/rev key enable	{**6.13**}	OFF (0) or On (1)			OFF (0)			RW	Bit				US

Figure A.2: Commonly used parameters 1 (Emerson [30])

Parameter			Range(⇳)			Default(⇨)			Type					
			OL	VT	SV	OL	VT	SV						
0.29	SMARTCARD parameter data	{**11.36**}	0 to 999			0			RO	Uni		NC	PT	US
0.30	Parameter cloning	{**11.42**}	nonE (0), rEAd (1), Prog (2), AutO (3), boot (4)			nonE (0)			RW	Txt		NC		*
0.31	Drive rated voltage	{**11.33**}	200 (0), 400 (1), 575 (2), 690 (3) V						RO	Txt		NC	PT	
0.32	Drive rated current	{**11.32**}	0.00 to 9999.99A						RO	Uni		NC	PT	
0.33	OL> Catch a spinning motor	{**6.09**}	0 to 3			0			RW	Uni				US
	VT> Rated rpm autotune	{**5.16**}		0 to 2			0		RW	Uni				US
0.34	User security code	{**11.30**}	0 to 999			0			RW	Uni		NC		PS
0.35	Serial comms mode	{**11.24**}	AnSI (0) rtu (1)			rtU (1)			RW	Txt				US
0.36	Serial comms baud rate	{**11.25**}	300 (0), 600 (1), 1200 (2), 2400 (3), 4800 (4), 9600 (5), 19200 (6), 38400 (7), 57600 (8) Modbus RTU only, 115200 (9) Modbus RTU only			19200 (6)			RW	Txt				US
0.37	Serial comms address	{**11.23**}	0 to 247			1			RW	Uni				US
0.38	Current loop P gain	{**4.13**}	0 to 30,000			All voltage ratings: 20	200V drive: 75 400V drive: 150 575V drive: 180 690V drive: 215		RW	Uni				US
0.39	Current loop I gain	{**4.14**}	0 to 30,000			All voltage ratings 40	200V drive: 1000 400V drive: 2000 575V drive: 2400 690V drive: 3000		RW	Uni				US
0.40	Autotune	{**5.12**}	0 to 2	0 to 3		0			RW	Uni				
0.41	Maximum switching frequency	{**5.18**}	3 (0), 4 (1), 6 (2), 8 (3), 12 (4), 16 (5) kHz			3 (0)		6 (2)	RW	Txt		RA		US
0.42	No. of motor poles	{**5.11**}	0 to 60 (Auto to 120 pole)			0 (Auto)			RW	Txt				US
0.43	OL & VT> Motor rated power factor	{**5.10**}	0.000 to 1.000			0.850			RW	Uni				US
	SV> Encoder phase angle	{**3.25**}			0.0 to 359.9º				RW	Uni		NC	PT	
0.44	Motor rated voltage	{**5.09**}	0 to AC_voltage_set_max V			200V drive: 200 400V drive: EUR> 400 USA> 480 575V drive: 575 690V drive: 690			RW	Uni		RA		US
0.45	OL & VT> Motor rated full load speed (rpm)	{**5.08**}	0 to 180,000 rpm	0.00 to 40,000.00 rpm		EUR> 1,500 USA> 1,800	EUR> 1,450.00 USA> 1,770.00		RW	Uni				US
	SV> Motor thermal time constant	{**4.15**}			0.0 to 400.0			20.0	RW	Uni				US
0.46	Motor rated current	{**5.07**}	0 to Rated_current_max A			Drive rated current [**11.32**]			RW	Uni		RA		US
0.47	Rated frequency	{**5.06**}	0 to 3,000.0 Hz	0 to 1,250.0 Hz		EUR> 50.0 USA> 60.0			RW	Uni				US
0.48	Operating mode selector	{**11.31**}	OPEn LP (1), CL VECt (2), SErVO (3)			OPEn LP (1)	CL VECt (2)	SErVO (3)	RW	Txt		NC	PT	
0.49	Security status	{**11.44**}	L1 (0), L2 (1), Loc (2)						RW	Txt			PT	US
0.50	Software version	{**11.29**}	1.00 to 99.99						RO	Uni		NC	PT	

Figure A.3: Commonly used parameters 2 (Emerson [30])

- **Pr 0.01 - 0.02:** Set Pr 0.01 and Pr 0.02, respectively, at the required minimum and maximum motor speed for both directions of rotation. The drive speed reference is scaled between Pr 0.01 and Pr 0.02.

- **Pr 0.03 - 0.04:** Used to shape the control curve. Set Pr 0.03 and Pr 0.04, respectively, at the required rate of acceleration and deceleration. Note that larger values produce lower acceleration. The rate applies in both directions of rotation.

- **Pr 0.05:** Limits the maximum output current of the drive (and hence maximum motor torque) to protect the drive and motor from overload.

- **Pr 0.10:** Indicates the value of motor speed that is obtained from the speed feedback.

- **Pr 0.11:** Displays the position of the encoder in mechanical values of 0 to 65,535. There are 65,536 units to one mechanical revolution.

- **Pr 0.13:** When the motor is being driven below its rated speed, the torque is proportional to Pr 0.13. The conversion factor depends on the K_t constant of the driven motor and the scale is described in sec. 2.3.
- **Pr 0.27:** Enter the number of lines per revolution of the drive encoder. Has to be fitted to the encoder characteristics of the driven motor (sec. 2.3).
- **Pr 0.32:** Indicates the maximum continuous Heavy Duty current rating (which will allow for an overload of 150%).
- **Pr 0.42 - 0.47:** Basic description of the driven motor. Must be set to properly fit the driven motor. These ratings are reported in sec. 2.3.

A.2 Control Connections

The drive is equipped with a 32 terminals, their characteristics and standard configuration are briefly explained in Fig. A.4.

In the following will be described the terminal configuration employed in the test setup:

- **Term. 1 - 2:** Negative and Positive power supply (24 VDC).
- **Term. 9:** Motor active current analog output, used, after proper conversion, to read the instantaneous torque delivered to the shaft.
- **Term. 10:** Speed output, reading of the instantaneous speed of the shaft.
- **Term. 11:** Common reference for the RSE readings of the analog outputs.
- **Term. 27 - 28 - 29:** Digital inputs employed to control the flow of the drive's software. Each combination of these digital signals yield a different movement speeds and direction. The control logic is explained in cap. 4.
- **Term. 41 - 42:** Terminals which give information about the motor status, in case of unexpected behaviour or actuation of the security button the drive would stop the motion.

4.13 Control connections

4.13.1 General

Table 4-10 The Unidrive SP control connections consist of:

Function	Qty	Programmability	Terminal number
Differential analog input	1	Destination, offset, offset trim, invert, scaling	5,6
Single ended analog input	2	Mode, offset, scaling, invert, destination	7,8
Analog output	2	Source, mode, scaling,	9,10
Digital input	3	Destination, invert, logic select	27,28,29
Digital input / output	3	Input / output mode select, destination / source, invert, logic select	24,25,26
Relay	1	Source, invert	41,42
Drive enable (Secure Disable)	1		31
+10V User output	1		4
+24V User output	1	Source, source invert	22
0V common	6		1, 3, 11, 21, 23, 30
+24V External input	1		2

Key:

Destination parameter: indicates the parameter which is being controlled by the terminal / function

Source parameter: indicates the parameter being output by the terminal

Mode parameter: analog - indicates the mode of operation of the terminal, i.e. voltage 0-10V, current 4-20mA etc.

digital - indicates the mode of operation of the terminal, i.e. positive / negative logic (the Drive Enable terminal is fixed in positive logic), open collector.

All analog terminal functions can be programmed in menu 7.

All digital terminal functions can be programmed in menu 8.

The setting of Pr **1.14** and Pr **6.04** can cause the function of digital inputs T25 to T29 to change. For more information, please refer to section 10.20.1 *Reference modes* on page 154 and section 10.20.7 *Start / stop logic modes* on page 159.

WARNING

The control circuits are isolated from the power circuits in the drive by basic insulation (single insulation) only. The installer must ensure that the external control circuits are insulated from human contact by at least one layer of insulation (supplementary insulation) rated for use at the AC supply voltage.

WARNING

If the control circuits are to be connected to other circuits classified as Safety Extra Low Voltage (SELV) (e.g. to a personal computer), an additional isolating barrier must be included in order to maintain the SELV classification.

CAUTION

Ensure the logic sense is correct for the control circuit to be used. Incorrect logic sense could cause the motor to be started unexpectedly.
Positive logic is the default state for Unidrive SP.

Figure 4-29 Default terminal functions

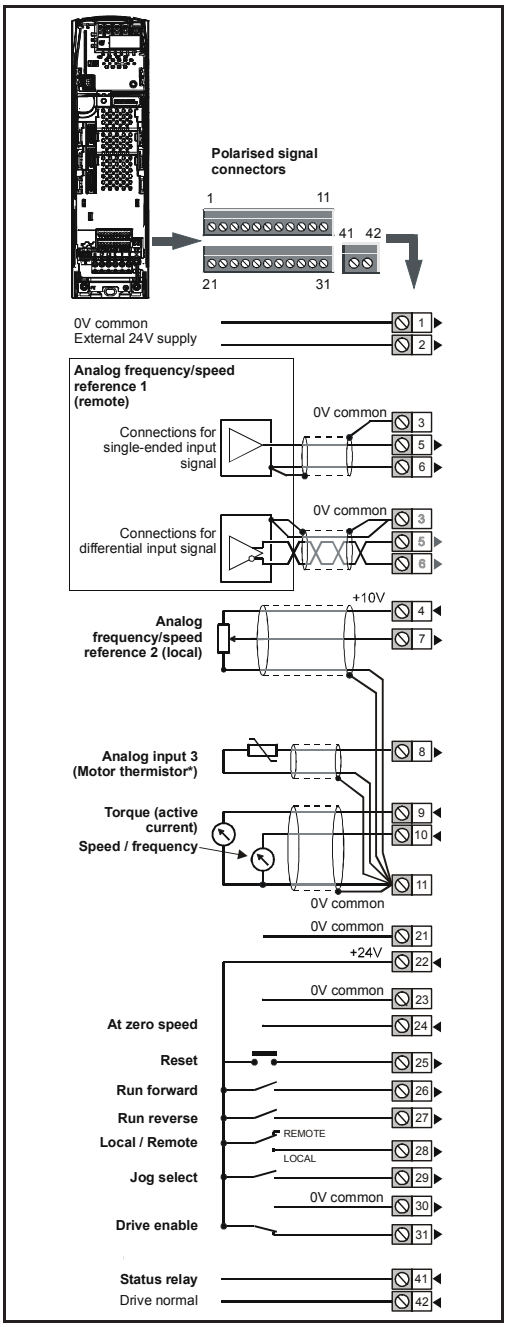

Figure A.4: Control Connections (Emerson [30])

A.3 Scales I/O

An excerpt of the User Manual [30, p. 118] with description of the parameters which deal with these issues is given in Fig. A.5. It is easy to see that the first parameter of each triplet sets the source from which the parameter is taken (in the particular case one would be speed, while the other active current),

the second one applies a multiplying factor to the reading (1 was chosen for the active current, while 2 for the speed) and the third decides the mode (always 0 to have voltage mode).

7.19	T9 analog output 1 source	Pr **0.00** to **21.51**	Pr **5.01**	Pr **3.02**	RW	Uni			PT	US
7.20	T9 analog output 1 scaling	0.000 to 4.000	1.000		RW	Uni				US
7.21	T9 analog output 1 mode	VOLt (0), 0-20 (1), 4-20 (2), HSPd (3)	VOLt (0)		RW	Txt				US
7.22	T10 analog output 2 source	Pr **0.00** to **21.51**	Pr **4.02**		RW	Uni			PT	US
7.23	T10 analog output 2 scaling	0.000 to 4.000	1.000		RW	Uni				US
7.24	T10 analog output 2 mode	VOLt (0), 0-20 (1), 4-20 (2), HSPd (3)	VOLt (0)		RW	Txt				US

Figure A.5: Speed and active current outputs parameters (Emerson [30])

To understand how the output scale is built it is necessary to consult the Advanced User Manual [31, p. 150] as well.

Speed The definition of the maximum output value involves couple of fundamental parameters. $SPEED\_FREQ\_MAX$ is the first one which has to be taken into account, it stand for the maximum allowable speed in closed-loop (or frequency in open-loop, where frequency control is used instead of speed control). Its value is set by the advanced parameter **Pr. 1.06** (or equally **Pr. 0.02** of the commonly used parameters) and its value is set to 4000rpm. Then:

$$SPEED\_FREQ\_MAX = 4000 \text{ rpm} \tag{A.1}$$

The second parameter involved is $SPEED\_MAX$, to allow headroom for overshoot and similar behaviours, is calculated as twice the maximum speed reference.

$$SPEED\_MAX = 2 * SPEED\_FREQ\_MAX = 8000 \text{ rpm} \tag{A.2}$$

This last parameter corresponds to the maximum of the voltage speed feedback output, but, keeping in mind the presence of the scaling factor (**Pr. 7.20** in Fig. A.5) the feedback output must be multiplied by it. As previously said, this factor was chosen at a value of 2, since the maximum working speed of the setup is definitely under 1000 rpm in the carried out tests, therefore it is preferable to reduce the full-swing value in order to obtain more precision and robustness to noise as a counterpart. This latest reasoning yields the full-swing value of the speed feedback output:

$$SPEED\_fs = \frac{SPEED\_MAX}{2} = 4000 \text{ rpm} \tag{A.3}$$

Equalling it to the maximum value of the voltage output (10V) it is possible to obtain a proper scale for the readings, following a linear relation:

$$s_{\text{rpm}} : 4000 \text{ rpm} = V_{\text{out,speed}} : 10 \text{ V} \tag{A.4}$$

$$s_{\text{rpm}} = \frac{4000 \cdot V_{\text{out,speed}}}{10} \text{ rpm} \tag{A.5}$$

Active current The active current is the part of the total current which actually produces torque. For the computation of its scale, first of all it is necessary to find K_c, which is the current scaling factor for the drive, it depends on the drive size and its characteristics. K_c is the conversion between the speed controller output and the torque producing current. A value of unity at the output of the speed controller gives a torque producing current equal to K_c. The drive automatically compensates the torque producing current for flux variations in field weakening, and so K_c can be assumed to have a constant value even in field weakening. Consulting the table of drive ratings [31, p. 22] the value $K_c = 9,5$ Amp is found.
Hence the full-swing value for the active current output is given by the relation ([31, p. 150]):

$$10.0V = K_c/0.45 \tag{A.6}$$

To convert the reading in proper value of torque expressed in Nm, it is necessary to multiply the value by K_t. K_t is the torque constant of the motor (i.e. torque in Nm per amp of torque producing current), and it obviously depends on the motor itself. As seen in sec. 2.3, for the employed one its value is $K_t = 1,6$, that yields a full-swing torque of:

$$T_{fs} = \frac{9,5 * 1,6}{0,45} = 33,8 \text{ Nm} \tag{A.7}$$

In this case the scaling factor for the output is chosen to 1 since the overrated torque limit is fixed at 15,95 Nm for this particular motor and application.
Finally the relation between measured voltage and torque results to be:

$$T_{\text{Nm}} : 33,8 \text{ Nm} = V_{\text{out,torque}} : 10 \text{ V} \tag{A.8}$$

$$T_{\text{Nm}} = \frac{33,8 \cdot V_{\text{out,torque}}}{10} \text{ Nm} \tag{A.9}$$

Appendix B

NI USB-6210 Specifications

- 16 single endend (or 8 differential) **analog inputs**, with ADC resolution 16 bits, maximum sampling rate 250 kS/s and maximum input range ± 10 V.
- No **analog outputs**.
- 4 **digital inputs**, with output signal thresholds in voltage mode $V_{IL} = 0 \div 0,8$ V and $V_{IH} = 2 \div 5,25$ V.
- 4 **digital outputs**, with output signal thresholds in voltage mode $V_{OL} = 0,6$ V and $V_{OH} = 3,8$
- 2 **counters**, with resolution 32 bits and a buffer of 1023 samples.

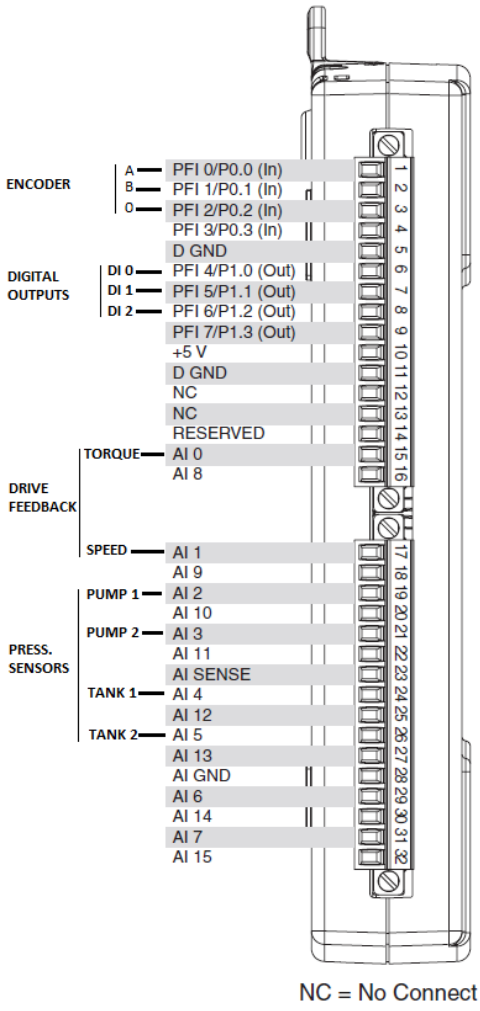

Figure B.1: NI USB-6220 board pinout and wiring scheme

Appendix C

PowerTools listings

```
Jog.1.PlusInitiate
Jog.1.Vel = 0

Do While true
    If Selector.Selection0  Then
        Jog.1.Vel = 0
    Endif
    If Selector.Selection1  Then
        Jog.1.Vel = 200
    Endif
    If Selector.Selection2  Then
        Jog.1.vel = -200
    Endif
    If Selector.Selection3  Then
        Jog.1.Vel = 0
    Endif
    If Selector.Selection4  Then
        Jog.1.Vel = 400
    Endif
    If Selector.Selection5  Then
        Jog.1.Vel = -400
    Endif
Loop
```

Appendix D

Position Control measurement samples

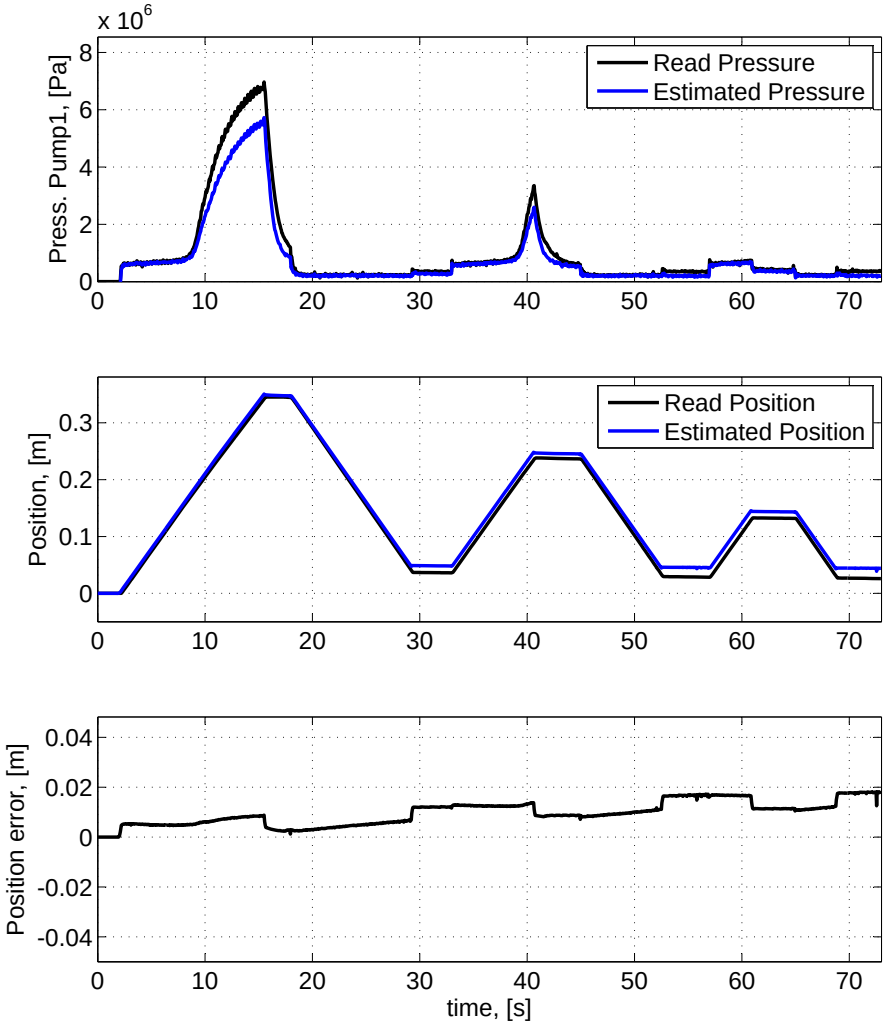

Figure D.1: Test 3: 33,5 kg, 300 rpm, Input 3

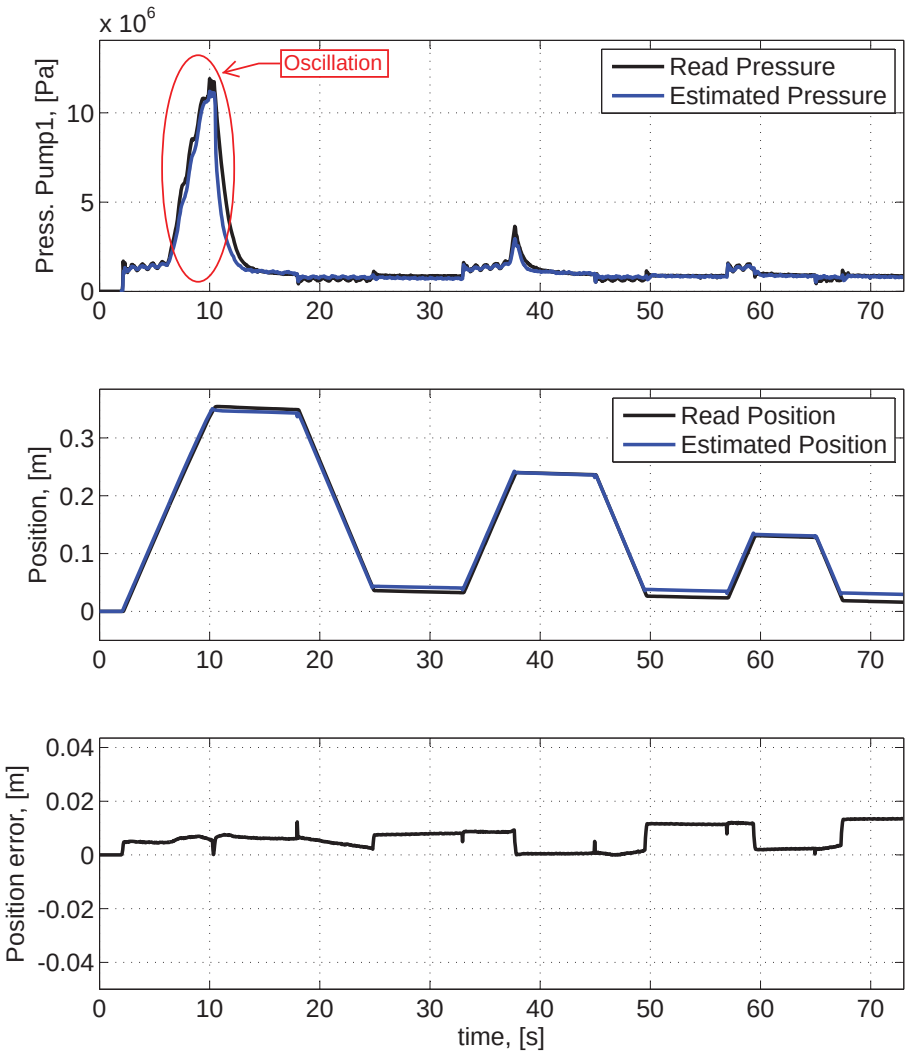

Figure D.2: Test 18: 108,5 kg, 500 rpm, Input 3

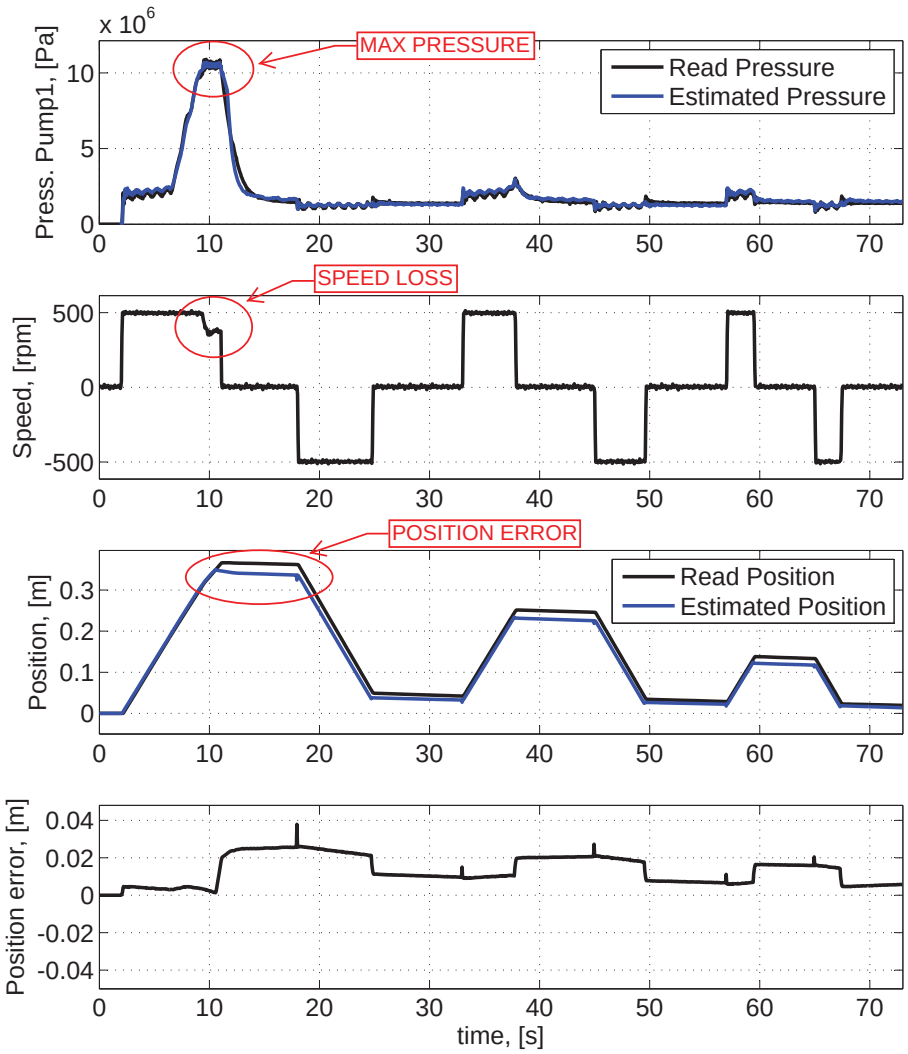

Figure D.3: Test 27: 183,5 kg, 500 rpm, Input 3

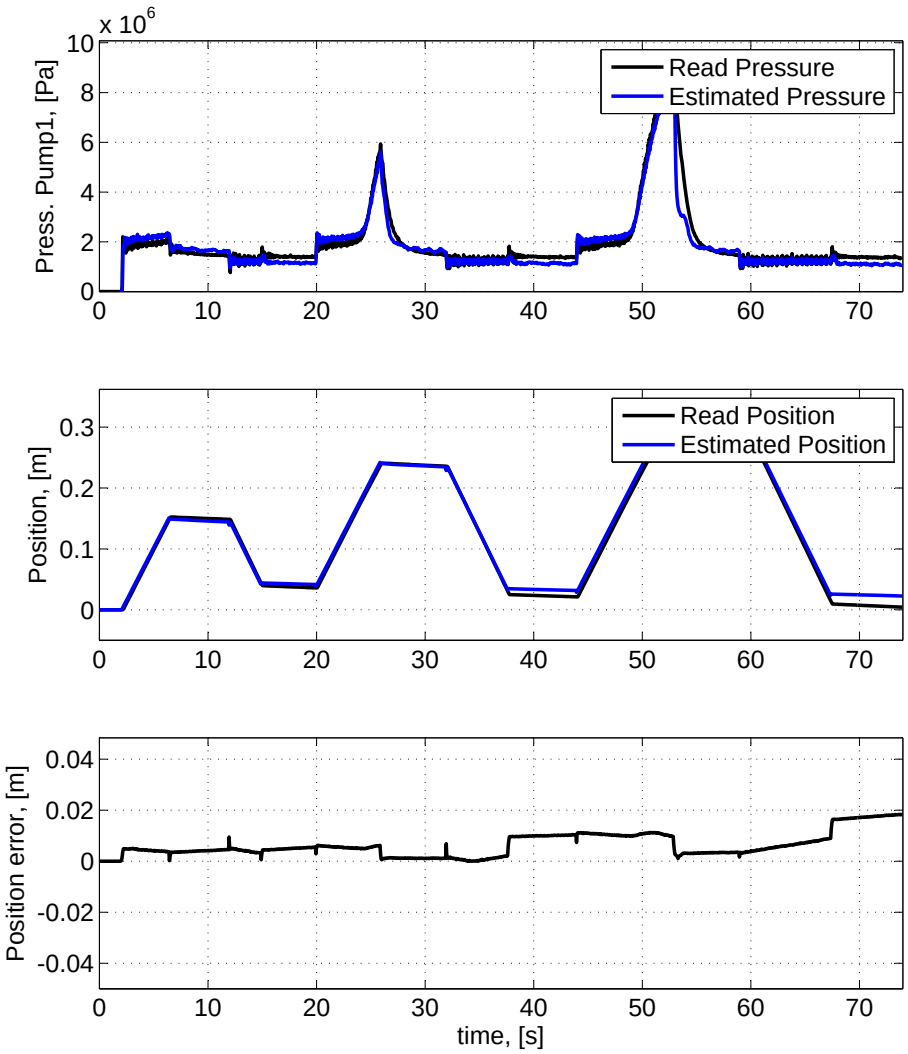

Figure D.4: Test 23: 183,5 kg, 400 rpm, Input 2

Bibliography

[1] T. Minav. "Electric-drive-based control and electric energy regeneration in a hydraulic system". Doctoral Dissertation. Lappeenranta University of Technology, Faculty of Technology, Electrical Engineering, Electrical Drives Technology, Aug. 2011.

[2] S. Majumdar. *Oil Hydraulic Systems: Principles and Maintenance*. McGraw-Hill professional engineering. McGraw-Hill Education, 2003. ISBN: 9780071406697. URL: http://books.google.fi/books?id=Eyc4uLwFwsMC.

[3] W. H. Matthaeus G. P. Zank. "The equations of nearly incompressible fluids. I - Hydrodynamics, turbulence, and waves". In: *Physics of Fluids A Fluid Dynamics* (1991).

[4] W. Anderson. *Controlling Electrohydraulic Systems*. Fluid Power and Control. Taylor & Francis, 1988. ISBN: 9780824778255. URL: http://books.google.fi/books?id=vIgZJGd3rPwC.

[5] R.H. Frith and W. Scott. "Control of solids contamination in hydraulic systems — an overview". In: *Wear* 165.1 (1993), pp. 69 –74. ISSN: 0043-1648. DOI: http://dx.doi.org/10.1016/0043-1648(93)90374-U. URL: http://www.sciencedirect.com/science/article/pii/004316489390374U.

[6] D. Summers-Smith. "Contamination control in hydraulic systems". In: *Tribology International* 18.1 (1985), pp. 55 –56. ISSN: 0301-679X. DOI: http://dx.doi.org/10.1016/0301-679X(85)90014-3. URL: http://www.sciencedirect.com/science/article/pii/0301679X85900143.

[7] In-Sek Rhee, Carlos Velez, and Karen Von Bernewitz. *Evaluation of Environmentally Acceptable Hydraulic Fluids.* Tech. rep. DTIC Document, 1995.

[8] K.V.J. Jokinen et al. *Hydraulic fluids*. US Patent 4,783,274. Nov. 1988. URL: http://www.google.com/patents/US4783274.

[9] R. Doddannavar, A. Barnard, and J. Ganesh. *Practical Hydraulic Systems: Operation and Troubleshooting for Engineers and Technicians: Operation and Troubleshooting for Engineers and Technicians*. Practical professional books from Elsevier. Elsevier Science, 2005. ISBN: 9780080455488. URL: http://books.google.fi/books?id=VhVUa997dbwC.

[10] K. E. Rydberg. "Hydrostatic drives in heavy mobile machinery-new concepts and development trends". In: *SAE transactions* 107 (1998), pp. 232–238.

[11] B.F.P. Andrews. *Electrohydraulics*. Coxmoor Publishing Company, 2008. ISBN: 9781901892208. URL: http://books.google.fi/books?id=2wBAJgAACAAJ.

[12] Joeri Van Mierlo, Gaston Maggetto, and Ph Lataire. "Which energy source for road transport in the future? A comparison of battery, hybrid and fuel cell vehicles". In: *Energy Conversion and Management* 47.17 (2006), pp. 2748–2760.

[13] EPA. *Clean Air Nonroad Diesel - Tier 4 Final Rule*. 2011. URL: http://www.epa.gov/nonroaddiesel/2004fr.htm.

[14] Wagner. *Tier IV emissions regulations: Knowing the facts*. 2010. URL: http://www.wagnerequipment.com.

[15] K. E. Rydberg. "Design of Energy Efficient Hydraulic Systems - System Concepts and Control Aspects". In: *Proceedings of the 5th International Symposium on Fluid Power Transmission and Control, Beidaihe, China*. 2007.

[16] Kazmin E. V. Gysen B. L. J. Paulides J. J. H. and E. A. Lomonova. "Hybrid Vehicle System Analysis Using an In-Wheel Motor Design". In: *Proceedings of the IEEE Vehicle Power and Propulsion Conference (VPPC)*. (Harbin, China). Sept. 2008.

[17] Quan Long. "Current State, Problems and the Innovative Solution of Electro-hydraulic Technology of Pump Controlled Cylinder". In: *Chinese Journal of Mechanical Engineering* (Nov. 2008). Ed. by Taiyuan University of Technology Institute of Mechatronic Engineering.

[18] Lian Zhanghua et al. "Fluid field analysis of high pressure throttle valve and it's structure improvement". In: *PHOENICS user* (2004).

[19] M Sc Arto Laamanen and Matti Vilenius. "Is It Time for Digital Hydraulics?" In: *The Eighth Scandinavian International Conference on Fluid Power, SICFP'03*. (Tampere, Finland). May 2003.

[20] M. Jelali and A. Kroll. *Hydraulic Servo-systems: Modelling, Identification and Control*. Advances in Industrial Control. Springer London, 2003. ISBN: 9781852336929. URL: http://www.google.fi/books?id=s1EVyLn5GT0C.

[21] Li Yilei et al. "A novel energy regeneration system for emulsion pump tests". English. In: *Journal of Mechanical Science and Technology* 27.4 (2013), pp. 1155–1163. ISSN: 1738-494X. DOI: 10.1007/s12206-013-0223-7. URL: http://dx.doi.org/10.1007/s12206-013-0223-7.

[22] Tatiana A. Minav, Lasse I.E. Laurila, and Juha J. Pyrhönen. "Analysis of electro-hydraulic lifting system's energy efficiency with direct electric drive pump control". In: *Automation in Construction* 30.0 (2013), pp. 144 –150. ISSN: 0926-5805. DOI: http://dx.doi.org/10.1016/j.autcon.2012.11.009. URL: http://www.sciencedirect.com/science/article/pii/S092658051200204X.

[23] Pietola M. Hänninen H. "Analysis on the Adaptability of Two Different Hydraulic Energy Recovery Circuits on Various MachineTypes and Work Cycles". In: *ASME/BATH 2013 Symposium on Fluid Power and Motion Control*. Sarasota, Florida, Oct. 2013.

[24] Monika Ivantysynova. "Innovations in pump design-what are future directions". In: *Proceedings of the International symposium on fluid power*. 2008.

[25] Ohtsu K. Sato H. Oda H. and K. Kanehiro. "Designing advanced rudder roll stabilization system - Using High Power with Small Size Hydraulic System". In: *7th JFPS International Symposium on Fluid Power*. Toyama, Japan, Sept. 2008.

[26] Jian-ming Zheng, Sheng-dun Zhao, and Shu-guo Wei. "Fuzzy iterative learning control of electro-hydraulic servo system for SRM direct-drive volume control hydraulic press". English. In: *Journal of Central South University of Technology* 17.2 (2010), pp. 316–322. ISSN: 1005-9784.

DOI: 10.1007/s11771-010-0048-9. URL: http://dx.doi.org/10.1007/s11771-010-0048-9.

[27] Zheng Jian-ming, Zhao Sheng-Dun, and Wei Shu-guo. "Adaptive Fuzzy PID Control for Switched Reluctance Motor Direct Drive Servo Hydraulic Press". In: *Measuring Technology and Mechatronics Automation, 2009. ICMTMA '09. International Conference on.* Vol. 1. Apr. 2009, pp. 771–774. DOI: 10.1109/ICMTMA.2009.62.

[28] Shuguo Wei, Shengdun Zhao, and Jianming Zheng. "Self-Tuning Fuzzy Control of Switched Reluctance Motor Directly-driven Hydraulic Press". In: *Software Engineering, 2009. WCSE '09. WRI World Congress on.* Vol. 2. May 2009, pp. 461–465. DOI: 10.1109/WCSE.2009.164.

[29] H.E. Merritt. *Hydraulic Control Systems.* John Wiley and Sons, Inc., 1967. URL: http://books.google.fi/books?id=Imu-v-6lzwYC.

[30] Emerson. *User Guide Unidrive SP, Universal Variable Speed AC Drive for induction and servo motors.* 2002. URL: http://www.emersonindustrial.com/en-US/controltechniques/downloads/userguidesandsoftware.

[31] Emerson. *Advanced User Guide Unidrive SP, Universal Variable Speed AC Drive for induction and servo motors.* 2011. URL: http://www.emerson-ct.cn/pdf/English/Unidrive%20SP/drive%20manuals/Unidrive%20SP%20Advanced%20User%20Guide.pdf.

[32] Omron. *Surface-mounting Relay G6J-Y.* 2002. URL: www.omron.com/ecb/products/pdf/en-g6j_y.pdfâĂŰ.

[33] Emerson. *Unimotor FM Product Data, 055 to 250 Frames, 0.72 Nm to 136 Nm.* 2013. URL: http://www.emersonindustrial.com/en-US/controltechniques/downloads/userguidesandsoftware.

[34] Vivoil Oleodinamica Vivolo s.r.l. *Reversible Motor - XV Series.* 2009. URL: www.vivoil.com/files/xm_en/xm217.pdfâĂŰ.

[35] Pikapaja Oy. *Hydarulisilinterit.* 2009. URL: http://www.pikapaja.fi/MIRO_cylinders_FIN+SWE.pdf.

[36] Gems Sensors and Control. *3100 Series and 3200 Heavy Duty Series, Compact OEM Pressure Transmitters.* URL: http://intl.gemssensors.com/uploadedFiles/Literature/Spec_Sheets/3200_HiPressTrans_Web.pdf.

[37] SIKO GmbH. *Wire actuated encoders SGW/SGI*. URL: www.siko-global.com/adbimage/asset/a6-a64a5c0f1dd9b5e6/data-sheet-sgw-sgi.pdf.

[38] SIKO GmbH. *Magnetic incremental encoder IV58M*. URL: www.siko-global.com/adbimage/asset/a0-a0d1407288ca6fc1/data-sheet-iv58m.pdf.

[39] MS-Graessner GmbH & Co. *Power Gear, the high performance bevel gearbox*. 2010. URL: http://www.graessner.at/upload/3760263-Download-Katalog-Kegelradgetriebe-PowerGear-englisch.pdf.

[40] National Instruments Corp. *NI USB-621x Specifications*. 2006. URL: www.ni.com/pdf/manuals/371932f.pdf.

[41] National Instruments Corp. *DAQ M Series, NI USB-621x User Manual*. 2009. URL: www.ni.com/pdf/manuals/371931f.pdf.

[42] W.E. Wilson. "Performance criteria for positive-displacement pumps und fluid motors". In: *Trans ASME* 71.2 (1949).

[43] W.E. Wilson. *Positive-displacement Pumps and Fluid Motors*. Pitman Pub. Corp., 1950. URL: http://books.google.fi/books?id=cFlEAAAAMAAJ.

[44] W.E. Wilson. "Rotary-pump theory". In: *Trans ASME* 68.4 (1946).

[45] Yoshiharu Inaguma. "A practical approach for analysis of leakage flow characteristics in hydraulic pumps". In: *Proceedings of the Institution of Mechanical Engineers. Part C: Journal of Mechanical Engineering Science* vol. 227.no. 5 (May 2013), pp. 980–991.

[46] Xu Hong; Yang Lijuan; Jing Baode; Tao Zhiliang. "Research of Internal Leakage Theory Model in the Exterior Meshing Gear Pump". In: *International Conference on Intelligent Human-Machine Systems and Cybernetics. IHMSC '09* vol. 2 (Aug. 2009), pp. 331–334.

[47] Hioki E. E. Corporation. *Hioki 3390 Power Analyzer Instruction Manual*. 2009.